In vitro-Untersuchungen zur Eignung nanofibrillärer Peptid-Hydrogele für die Behandlung von Parodontitis

Kumulative Dissertation
zur
Erlangung des akademischen Grades
Doktor der Medizinwissenschaften (Dr. rer. hum.)
der Universitätsmedizin Rostock

vorgelegt von
Franziska Koch
geboren am 02.05.1988 in Schmalkalden

Rostock, 2019

Universitätsmedizin Rostock

Universität Rostock

Traditio et Innovatio

https://doi.org/10.18453/rosdok_id00003010

Gutachter 1

PD Dr. Kirsten Peters, Abteilung für Zellbiologie, Universitätsmedizin Rostock

Gutachter 2

Prof. Dr. Oliver Germershaus, Institut für Pharma Technologie, Fachhochschule Nordwestschweiz

Gutachter 3

Prof. Dr. Hermann Lang, Poliklinik für Zahnheilkunde und Parodontologie, Universitätsmedizin Rostock

Datum der Einreichung: Juli 2019

Datum der Verteidigung: Februar 2021

In der vorliegenden kumulativen Dissertation werden die Forschungsergebnisse in verkürzter und zusammengefasster Form dargestellt. Die detaillierten Ergebnisse sind bereits in den folgenden Artikeln des Journals Royal Society Open Science, International Journal of Nanomedicine und Advanced Healthcare Materials veröffentlicht.

Studie I

Koch F, Müller M, König F, Meyer N, Gattlen J, Pieles U, Peters K, Kreikemeyer B, Mathes S, Saxer S. Mechanical characteristics of beta sheet-forming peptide hydrogels are dependent on peptide sequence, concentration and buffer composition. *Royal Society Open Science*. 2018; 5(3):171562

Studie II

Koch F, Wolff A, Mathes S, Pieles U, Saxer S, Kreikemeyer B, Peters K. Amino acid composition of nanofibrillar self-assembling peptide hydrogels affects responses of periodontal tissue cells *in vitro. Journal of International Nanomedicine*. 2018; 13: 6717-6733

Studie III

Koch F, Ekat K, Kilian D, Hettich T, Germershaus O, Lang H, Peters K, Kreikemeyer B. A versatile biocompatible antibiotic delivery system based on self-assembling peptides with antimicrobial and regenerative potential. *Journal of Advanced Healthcare Materials*. 2019, 1900167

Inhaltsverzeichnis

1 Einleitung

Das häufigste Krankheitsbild in der Zahnheilkunde ist neben der Zahnkaries die Entzündung des Zahnhalteapparates (Parodontitis). Die Parodontitis wird hauptsächlich durch bakterielle Ablagerung am Zahnhals (auch bekannt als Zahnbelag) hervorgerufen und wird heutzutage aufgrund ihrer hohen Prävalenz als Volkskrankheit eingestuft. Statistisch gesehen erkranken 20-50 % der Weltbevölkerung an mindestens einem Zahn in ihrem Leben an Parodontitis [1]. Aufgrund des steigenden Lebensalters und der negativen Auswirkungen der Parodontitis auf weit verbreitete Allgemeinerkrankungen wie Herz-Kreislauf-Erkrankungen oder Typ 2 Diabetes, gewinnt diese zunehmend an Bedeutung für die Mundgesundheit sowie für die allgemeine Gesundheit [2]. Daher besteht ein zunehmendes Interesse an der Entwicklung geeigneter Therapien und Biomaterialien zur Behandlung der Parodontitis im Frühstadium dieser Erkrankung.

1.1 Aufbau des Zahnhalteapparates

Der Zahnhalteapparat ist ein hochkomplexes Konstrukt, welcher einzigartige architektonische Eigenschaften besitzt. Der Zahnhalteapparat stellt das umgebende Gewebe des Zahnes dar, dass hauptsächlich aus zwei Hartgeweben (Zement und Alveolarknochen) und zwei Weichgeweben (Gingiva und Wurzelhaut) aufgebaut ist [3]. Die Wurzelhaut, auch bezeichnet als Desmodont, besteht aus strukturell ausgerichteten Kollagenfasern (Sharpey-Fasern) sowie Fibroblasten, Epithelzellen, Osteoblasten, Zementoblasten und mesenchymalen Stammzellen (MSC) und fungiert als Anker, um den Zahn am Alveolarknochen zu befestigen [4] .

1.2 Die Parodontitis

Die Parodontitis ist eine bakterielle, multifaktorielle und dynamische Erkrankung, welche zu einer Entzündungsreaktion und Zerstörung des Zahnhalteapparates führt [5]. Im Falle einer gesunden Mundflora, besteht ein Gleichgewicht zwischen symbiotischen Bakterien wie z. B. *Streptococcus sanguinis* und Pathobionten wie z. B. *Porphyromonas gingivalis.*

Aufgrund einer schlechten Mundhygiene sowie durch Stress, Rauchen, falsche Ernährung, Alterung, Medikamenteneinnahme, hormonellen Veränderungen und Immunodefiziten kann diese Hämostase der symbiotischen Mikrobiota gebrochen und auf überwiegend gram-negative Pathobionten verlagert werden (dysbiotische Mikrobiota) [6, 7]. Dieser Zusammenbruch führt in erster Linie zu einer verstärkten bakteriellen Invasion in das Zahnfleischgewebe (Gingiva), die wiederum eine Infiltration von Entzündungszellen (z. B. dendritische Zellen (DC), Makrophagen, Lymphozyten (B-Zellen und T-Zellen)) auslöst (Abb. 1A) [8]. Durch die Freisetzung von pro-inflammatorischen Mediatoren wie Interleukin-(IL-)1β, IL-17, Tumornekrosefaktor (TNF) wird daraufhin eine serielle Immunantwort ausgelöst (Abb. 1B) [9]. Diese Mediatoren können mit dem angeborenen Immunsystem und auch mit Bindegewebszelltypen wie Neutrophilen, Fibroblasten und Osteoblasten interagieren und die Freisetzung gewebedegradierender Moleküle induzieren [10, 11].

So ist beispielsweise bekannt, dass die Interaktion von Fibroblasten mit IL-17, die Produktion und Freisetzung von Matrix-Metalloproteinasen sowie die Bildung reaktiver Sauerstoff-Spezies induziert. Diese Prozesse können schlussendlich zu einem Abbau des Weichgewebes führen [12]. Darüber hinaus erhöht IL-17 die Expression des kB-Liganden (RANKL), der die Reifung von Osteoklasten-Vorläufer Zellen (OCP) induziert und schließlich zu einem Abbau des Alveolarknochens durch reife Osteoklasten (OCL) führt (Abb. 1B) [13].

Der Abbau spezifischer Gewebestrukturen führt zur Bildung einer Zahnfleischtasche, die als Reservoir für Bakterien, bakterielle Antigene und andere entzündungsfördernde Mediatoren fungieren kann [14, 15]. Bakterien aus der Mundflora können nicht nur lokale Entzündungsreaktionen hervorrufen, sondern auch durch den Eintritt in die Blutbahn systemisch zirkuliert werden. Daher ist die Parodontitis u.a. auch mit Herz-Kreislauf-Erkrankungen, Diabetes mellitus, Schwangerschaftskomplikationen, Osteoporose und rheumatoider Arthritis verbunden [16].

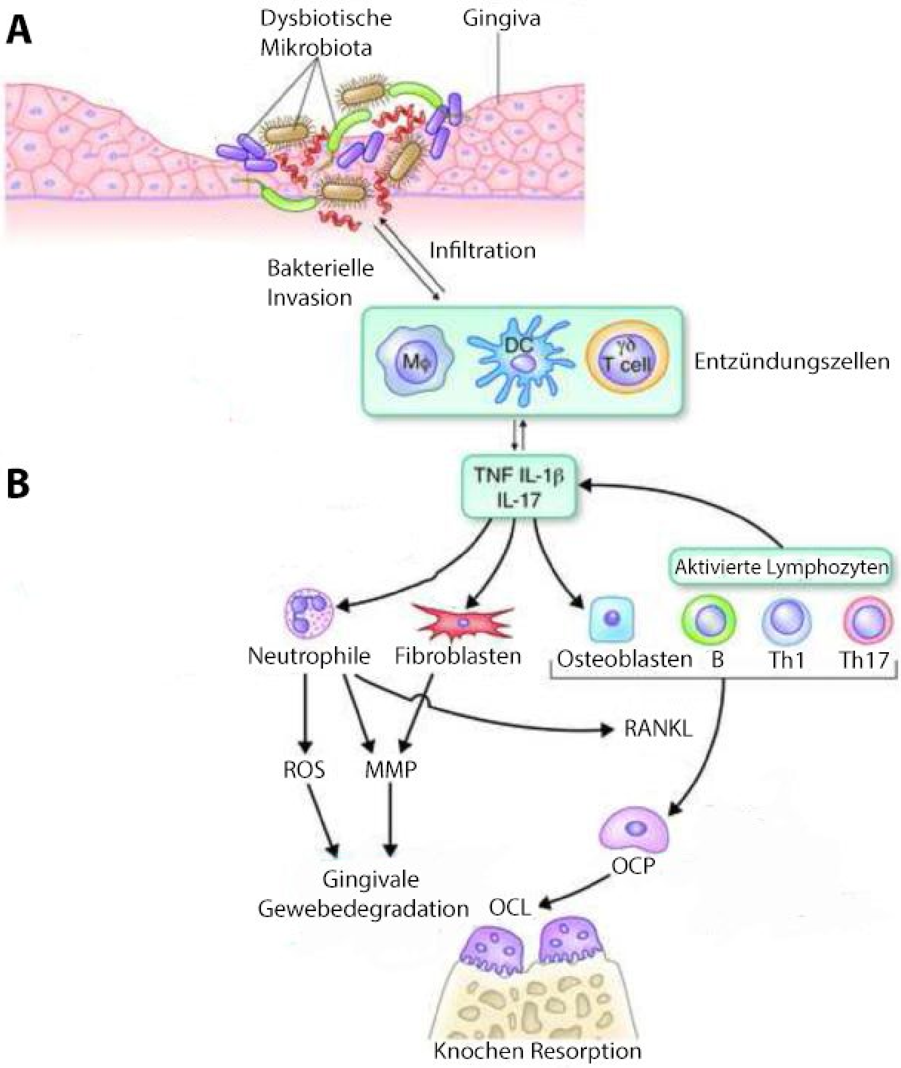

Abb. 1. Schematische Darstellung der Pathogenese der Parodontitis (A) und der damit verbundenen Zell-vermittelten immunologischen Reaktionen (B). *Angepasst von George Hajishengallis, Trends in Immunology 2014* [8].

1.3 Strategien zur Regeneration des Zahnhalteapparates

Konventionelle Therapieansätze

Das Ziel einer konventionellen Therapie im Bereich Parodontitis umfasst die Beseitigung von entzündetem Gewebe und bakteriellen Verunreinigungen. Durch den Einsatz verschiedener chirurgischer Eingriffe, werden bakterielle Biofilme von der Wurzeloberfläche entfernt und die Taschentiefe durch die Umlagerung des Zahnfleisches reduziert. Diese Art der Behandlung ist oft nur mit einem kurzzeitigen Therapieerfolg assoziiert, da die Regeneration des Zahnhalteapparates ohne den Einsatz eines zusätzlichen Biomaterials nur zu einem bestimmten Grad erfolgen kann [17].

Regenerative Therapieansätze unter Einsatz von verschiedenen Biomaterialien

In den letzten Jahrzehnten wurden verschiedene Arten von Behandlungsstrategien und Biomaterialien entwickelt, um zerstörtes Hartgewebe (Alveolarknochen) und Weichgewebe (Desmodont) wiederherzustellen [18].

Als Biomaterial für die Regeneration des Alveolarknochens werden z. B. bioaktive Gläser, Calciumphosphat- oder Sulfatformulierungen verwendet [19]. Diese Transplantatmaterialien funktionieren meist als osteogene, osteoinduktive und/oder osteokonduktive Gerüste [20]. Um das Weichgewebe des Desmodonts zu regenerieren, werden Hydrogele verwendet, die entweder natürlichen (Chitosan, Kollagen) oder synthetischen (Poly(L-Milchsäure), Polyglykolsäure) Ursprunges sind [19]. Beide Arten von Materialien weisen verschiedene Vor- als auch Nachteile auf. Beispielsweise sind Naturprodukte, wie z. B. Kollagen, Chitosan und Gelatine bekannt für ihre hohe Biokompatibilität, Bioabbaubarkeit und geringe Toxizität [21]. Zugleich sind diese aber auch mit Immunreaktionen und Chargen-abhängigen Variationen in ihrer Zusammensetzung verbunden [22].

Im Gegensatz zu Naturprodukten können synthetische Biomaterialien in einem großen Umfang hergestellt und in verschiedenen Formen mit unterschiedlichen chemischen Funktionsgruppen und mechanischen Eigenschaften produziert werden [23]. Im Falle von synthetischen Polylaktiden können abbauende Prozesse zu einem frühzeitigen Verlust der mechanischen Eigenschaften und zu zellunverträglichen Abbauprodukten führen [22]. Daher sollten bei der Auswahl des geeigneten Biomaterials immer alle Vor- und Nachteile in Hinsicht auf die spezifische Applikation berücksichtigt werden.

Selbst-Strukturierende Peptide

Ein synthetisches Material, welches sich bereits für die Regeneration unterschiedlicher Gewebe bewährt hat, ist die Klasse der Selbst-Strukturierenden Peptide (SSP), englisch bezeichnet als Self-Assembling-Peptides (SAP) [24]. Die meisten Sequenzen der SSP stammen von natürlich vorkommenden Molekülen ab und wurden für einen regenerativen Einsatz weiterentwickelt [25].

Die fibrilläre Netzwerkstruktur von SSP ähnelt der nativen extrazellulären Matrix (EZM) [26]. Dieser Aspekt ist von großer Bedeutung, da die Topographie der EZM das Zellverhalten und damit wiederum auch das regenerative Potential positiv beeinflussen kann [27]. Auf der Grundlage natürlicher Moleküle sind innerhalb der letzten Jahre eine Vielzahl von SSP entstanden. Diese können aufgrund ihrer vielfältigen Kombinierbarkeit als Bausteine für die Entwicklung einer variierbaren Hydrogel-Plattform fungieren. SSP-Hydrogele sind aufgrund ihrer einfachen Herstellung mit vergleichsweise niedrigen Kosten, ihrer Architektur und ihrer vielseitigen mechanischen sowie physikochemischen Eigenschaften für eine regenerative Anwendung von großem Interesse [28]. Durch nichtkovalente Wechselwirkungen, (d.h. Wasserstoffbrückenbindungen und elektrostatische hydrophobe und Van-der-Waals Wechselwirkungen) können SSP höhere hierarchische Strukturen wie Nanosphären, Nanoröhren, Mizellen und Nanofibrillen ausbilden (Abb. 2) [29, 30].

Die Hydrogelbildung findet durch die Verwendung von 2 Komponenten statt. Somit wird eine minimal invasive Applikation z. B. mit einer 2-Komponenten-Spritze und schliesslich eine fibrilläre Netzwerkausbildung ermöglicht. Im Rahmen dieser Promotionsarbeit wurden antiparallele β-Faltblattbildende P11-SSP ausgewählt, welche aus 11 natürlichen Aminosäuren bestehen [25, 26, 31]. Die sogenannten P11-SSP können hierarchische Strukturen wie Fibrillen und Fasern in Abhängigkeit des pH-Wertes, der Ionenstärke und der Peptidkonzentration ausbilden (Abb. 2). Bei höheren Konzentrationen (typischerweise höher als ≥ 10 mg/ml) können diese supramolekularen Strukturen durch Wassereinlagerungen fibrilläre Hydrogele bilden [32]. Die Zusammenlagerung von P11-SSP basiert auf den günstigen intermolekularen Seitenkettenwechselwirkungen (z. B. durch Arginin- und Glutamat-Reste) und der kooperativen intermolekularen Wasserstoffbindung des Peptidrückrates (z. B. durch terminale Glutamin-Reste), was schließlich zur Bildung von β-Faltblättern führt [26].

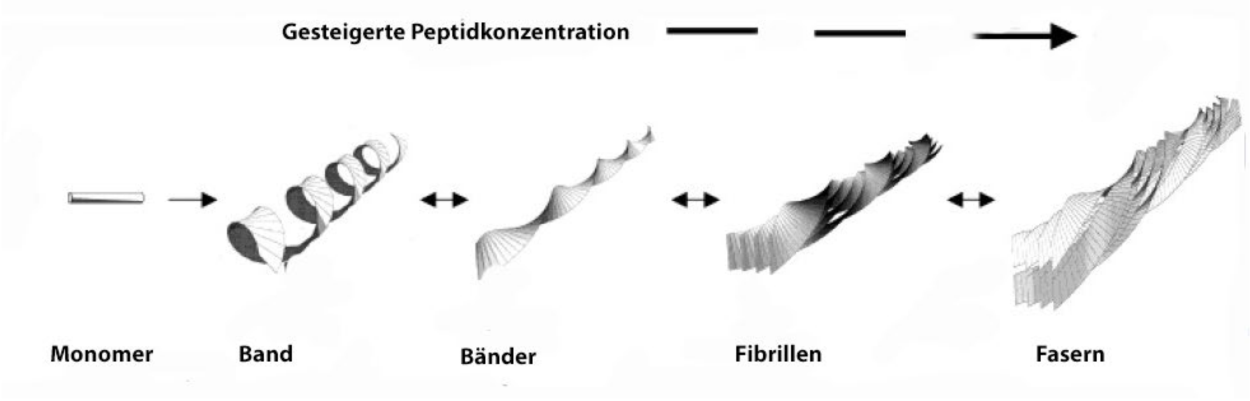

Abb.2. Theoretisches Modell der hierarchischen Zusammenlagerung von P11-SSP, angepasst von Aggeli et al [31].

Durch den systematischen Austausch einzelner Aminosäuren innerhalb der Peptidprimärstruktur, konnte eine breite P11-SSP Bibliothek entwickelt werden [25, 33]. Einhergehend mit dem Austausch der Aminosäuren kommt es zu einer veränderten Anzahl an z. B. Carboxyl- oder Amid-Gruppen, welche zu unterschiedlichen physikochemischen Eigenschaften der Hydrogele führen [32]. Aus dieser Peptidbibliothek wurden für die vorliegende Promotionsarbeit vier P11-SSP-Systeme ausgewählt, welche keine Immunreaktion induzieren und zugleich biokompatibel und injizierbar sind [34-37]. Des Weiteren konnte in mehreren Studien gezeigt werden, dass die ausgebildete fibrilläre Struktur und ihre physikochemischen Eigenschaften zu einer Einlagerung von Kalzium und Phosphat aus dem Speichel führt und somit eine Remineralisierung des harten Zahngewebes, wie z. B. dem Zahnschmelz, erlaubt [38]. Somit könnten diese vier P11-SSP-Hydrogele auch für die parodontale Regeneration geeignet sein.

2 Fragestellung

Die Parodontitis ist aufgrund der hohen Prävalenz, der verminderten Lebensqualität und der Assoziation mit systemischen Erkrankungen ein großes Anliegen der öffentlichen Gesundheit [1]. Daher besteht großes Interesse an der Entwicklung geeigneter Biomaterialien zur Regeneration von zerstörtem Gewebe des Zahnhalteapparates. Für eine Behandlung im Frühstadium der Parodontitis sollte ein geeignetes Biomaterial einfach applizierbar sein (z. B. durch die Verwendung einer Spritze). Ziel der vorliegenden Dissertation war es daher, das Potenzial von Selbst-Strukturierenden Peptiden (SSP) als injizierbares Biomaterial für die parodontale Geweberegeneration *in vitro* zu untersuchen. Dabei wurden die folgenden Fragen adressiert:

1) Welchen Einfluss hat die P11-SSP Aminosäuresequenz auf die physikalisch-chemischen und mechanischen Eigenschaften der daraus resultierenden Hydrogele?

2) Wie wirken sich die unterschiedlichen SSP-Hydrogele auf parodontale Gewebezellen aus?

3) Verfügen SSP über eine intrinsische antimikrobielle Aktivität?

4) Können SSP-Hydrogele als lokale Antibiotika-Verabreichungssysteme verwendet werden?

3 Eingesetzte Methoden

Die folgenden Beschreibungen der Methoden werden in verkürzter und zusammengefasster Form dargestellt. Eine detaillierte Beschreibung aller verwendeten Methoden ist in den veröffentlichten Artikeln enthalten.

3.1 Herstellung der SSP-Hydrogele

Für jedes Peptidsystem wurde die Pufferzusammensetzung aufgrund ihrer spezifischen physikalisch-chemischen Eigenschaften angepasst. P11-4 und P11-8 Hydrogele wurden hergestellt, indem zunächst das lyophilisierte Peptidpulver in 100 µl von Puffer A (z. B. H_2O, pH 6) gelöst wurde, um eine Peptidmonomerlösung zu erhalten. Zur Induktion des fibrillären Prozesses wurden 100 µl des Puffers B (z. B. 55 mM Tris, 236 mM NaCl, pH 7) zugesetzt. Komplementäre Peptidsysteme (wie z. B. P11-13/14 und P11-28/29) wurden separat mit 100 µl ihres peptidspezifischen Puffers gelöst und anschließend 1:1 gemischt, um ein Endvolumen von 200 µl zu erhalten. Im Allgemeinen wurden die folgenden Peptidkonzentrationen angewandt: 15 mg/ml für P11-4, P11-8 und 10 mg/ml für P11-13/14/ P11-28/29.

3.2 Analyse der Eigenschaften von SSP-Hydrogelen

Analyse der fibrillären Netzwerk-Architektur

Zur Untersuchung einzelner Fibrillen wurde eine Transmission-Elektronen-Mikroskopie (TEM) durchgeführt. SSP-Hydrogele wurden mit Wasser verdünnt, auf ein TEM-Kupfergitter (Electron Microscopy Sciences, USA) transferiert und mit 10 µl Uranylacetat (2 %, Electron Microscopy Sciences, USA) gefärbt. Die Bilder wurden mit einem Transmissions-Elektronenmikroskop (Zeiss EM900, Deutschland) aufgenommen, welches mit einer AMT XR280 sCMOS-Kamera (AMT - Advanced Microscopy Techniques, USA) ausgestattet ist. Um das endgültige Faserkonstrukt zu untersuchen, wurde eine Raster-Elektron-Mikroskopie (REM)-Analyse durchgeführt. Hierfür wurden SSP-Hydrogele hergestellt, mit einer 4 % Glutaraldehyd-Lösung fixiert und mit einer Ethanol-Lösung dehydriert.

Anschliessend wurden die Netzwerkstrukturen kritisch Punkt getrocknet (Balzers Union, CPD020) und mit 2,5 nm Gold-Palladium (Thermo VG Scientific, Polaron, SC7620) gesputtert. REM-Aufnahmen wurden mit einem Zeiss SUPRA® 40VP angefertigt.

Analyse der physikochemischen Eigenschaften von SSP-Hydrogelen

Zeta-Potentialmessungen wurden durchgeführt, um die Fibrillen-Oberflächenladung zu bestimmen. Hierfür wurde ein Zeta-Sizer (Malvern, UK) verwendet. P11-SSP-Lösungen (3 mg/ml) wurden in 0,001 M NaCl-Puffer hergestellt. Die Messungen wurden bei Raumtemperatur direkt nach der pH-Einstellung mit 0,1 M NaOH und 0,1 M HCl durchgeführt. Um das Quellverhalten von P11-SSP-Hydrogelen zu bestimmen, wurden Proben mit 15 mg/ml in 55 mM Tris-Puffer vorbereitet. Die Proben wurden vor und nach dem 24 stündigen Quellvorgang gewogen und schließlich über Nacht mit einem Christ Lyophilisator (Christ® Gefriertrockner alpha 1-4 LSC, Deutschland) bei -50 °C und $1{,}0\times10^{-3}$ Pa lyophilisiert.

Mechanische Eigenschaften von SSP-Hydrogelen

Rheologie-Messungen wurden durchgeführt, um die Steifigkeit, die Sprödigkeit und die Geliergeschwindigkeit von P11-SSP-Hydrogelen mit einem Anton Paar MCR301-Rheometer zu untersuchen. Zur Bestimmung der Hydrogel-Steifigkeit wurden oszillatorische Amplituden-Tests bis zu 150 % durchgeführt, bei denen die Speichermodule (G') innerhalb des linearen viskoelastischen Bereichs (LVR) gemessen wurden. Die Sprödigkeit wurde mit MATLAB basierend auf den Gelbrechpunkten aus den Amplituden-Tests berechnet. Zur Untersuchung der Geliergeschwindigkeit wurde das Speichermodul (G') über 150 Minuten gemessen.

Protein Adsorption an P11-SSP-Hydrogelen

P11-SSP-Hydrogele wurden mit Fibronektin (300 µg/ml aus Rinderplasma, Sigma-Aldrich, Schweiz) für 1 Stunde bei 37 °C inkubiert. Die Hydrogele wurden zweimal gewaschen, bevor sie mechanisch mit einem Branson Sonifikator 250 (Heinemann, Deutschland) zerstört wurden. Um die Menge an Fibronektin zu bestimmen, wurden die Proben mit dem Qubit® Protein Assay (Thermo Fisher Scientific, Schweiz) gemessen.

3.3 Zellkultur-Experimente mit P11-SSP-Hydrogelen

Verwendete Zelltypen und ihre Kultivierung

Humane Peridontal-Ligament-Fibroblasten (HPDLF) und humane Kalvaria-Osteoblasten (HCO) wurden von ScienCell, USA, bezogen. Die dentalen Stammzellen (humane dentale Follikel Stammzellen (hDFSC)) wurden freundlicherweise von der Gruppe von Prof. H. Lang (Klinik für Restaurative Zahnheilkunde und Parodontologie, Universitätsmedizin Rostock) zur Verfügung gestellt. Die Isolierung und Charakterisierung der hDFSC wurde von Chatzivasileiou et al.[39] beschrieben. Die Zellen wurden bis zu 80-90 % Konfluenz in ihrem jeweiligen Expansionsmedium kultiviert und mit 0,5 % Trypsin-EDTA-Lösung (Gibco™ von Life Technologies, Deutschland) passagiert. Eine Passage dauerte 5 Tage. Alle Zelltypen wurden in 75 cm^2 Kulturflaschen (CELLSTAR®, Greiner bio-one) kultiviert und expandiert und in den Passagen 4 bis 6 für die verschiedenen Experimente verwendet.

Zytotoxizität der Extraktionsprodukte von P11-SSP-Hydrogelen

Die Untersuchung der Zytotoxizität von P11-SSPHydrogel-Extrakten auf HPDLF und HCO Zellen wurde nach dem Standardtestprotokoll ISO 10993-5 durchgeführt. Die Zytotoxizität wurde schlussendlich mit einem Laktatdehydrogenase (LDH) Zytotoxizitätstest (Roche, Deutschland) nach dem Protokoll des Herstellers bestimmt.

Bestimmung der metabolischen Aktivität

P11-SSP-Hydrogele wurden bis zu 14 Tage mit HPDLF oder HCO Zellen kultiviert und mit einem PrestoBlue®Viability Reagent (Invitrogen-Life Technologies, Deutschland) auf ihre metabolische Aktivität, wie vom Hersteller beschrieben, analysiert.

Untersuchung der Zellmorphologie

Nach 24 Stunden Inkubation auf P11-SSP-Hydrogelen wurden die Zellen mit PBS gewaschen und mit 4 %iger Paraformaldehydlösung (Sigma-Aldrich, Deutschland) fixiert. Um die Zellmembranen zu permeabilisieren, wurde 0,1 % Triton-X100-PBS (Fluka, Deutschland) hinzugefügt.

Die Zellen wurden dann gewaschen und mit 1 %iger Rinderserumalbumin-Lösung (Cell Signaling Technology, Deutschland) inkubiert. Für die Färbung des F-Aktin-Zytoskeletts wurde Rhodamin-konjugiertes Phalloidin (Thermo Fisher Scientific, Schweiz) 1:40 (Bestand 1:1000 in Methanol) in PBS hinzugefügt. Abschließend wurden die Zellen mit einem konfokalen Laser-Scanning-Mikroskop (LSM 780, Zeiss, Deutschland) visualisiert.

Osteogene Differenzierung auf P11-SSP-Hydrogelen

Die osteogene Differenzierung von HCO Zellen wurde durch die Messung osteogener Marker, wie die alkalische Phosphatase (ALP), Osteocalcin, Osteoprotegerin und der extrazellulären Kalziummenge bestimmt. Zur Quantifizierung der ALP-Aktivität wurde der kolorimetrische ALP-Assay (Abcam, UK) durchgeführt. Zelllysate wurden auf Osteocalcin und Osteoprotegerin mit einem Milliplex MAP Human Bone Magnetic Bead Kit (Merck Milipore, Deutschland) analysiert. Zur Quantifizierung des extrazellulären Kalziums wurden die Zellen nach 30 Tagen Kultur fixiert und mit einer Kresolphthaleinlösung (Sigma-Aldrich Chemie GmbH) inkubiert. Nach Zugabe von 2-Amino-2-methyl-1-propanol (Sigma-Aldrich, Chemie GmbH) wurde die Absorption der Überstände bei 580 nm mit einem Mikroplattenleser (anthos Mikrosysteme GmbH) gemessen.

3.4 Mikrobiologische Untersuchungen

Verwendete Bakterienspezies und ihre Kultivierung

Porphyromonas gingivalis W83 wurde freundlicherweise von Jan Potempa und Patrick J. Venables [40] zur Verfügung gestellt und auf Columbia-Blutagarplatten (5 % Schafblut, Beckton Dickinson, Deutschland) unter anaeroben Bedingungen (10 %, CO_2, 10 % H_2, 80 % N_2) bei 37 °C in einem anaeroben Brut-Schrank der Firma Don Whitley Scientific (Meintrup DWS Laborgeräte GmbH, Deutschland) kultiviert. *Streptococcus sanguinis* (DSM 20567) wurde von der DSMZ (Deutschland) gekauft und auf BHI-Agarplatten (1,5 % Agar technical No 3, Oxoid, UK) unter aeroben Bedingungen (5 % CO_2) kultiviert.

Bakterielles Wachstum

Die Wirkung von P11-SSP-Monomeren und Hydrogelen auf das Bakterienwachstum wurde durch Trübheitsmessungen analysiert. *P. gingivalis* und *S. sanguinis* wurden auf eine Lebendkeimzahl (cfu, colonoy forming units) von $1*10^7$ CFU/ml im BHI-Medium eingestellt und mit P11-SSP-Monomeren oder Hydrogelen beimpft. Die optische Dichte (Trübung) bei 600 nm wurde mit einem SpectraMax® M2 Mikroplattenleser (Molecular Devices, USA) gemessen.

Bakterizider Effekt von P11-SSP Monomeren

Um die bakterizide Wirkung von P11-SSP-Monomeren zu untersuchen, wurden Bakteriensuspensionen seriell in PBS (± P11-SSP-Monomere) verdünnt und auf Blutagarplatten (*P. gingivalis*) bzw. BHI-Agarplatten (*S. sanguinis*) aufgebracht. Agarplatten wurden für mindestens 24 Stunden bei 37 °C unter anaeroben oder aeroben Bedingungen kultiviert. Schließlich wurden lebende Bakterien durch Zählen von Kolonie bildenden Einheiten auf Agarplatten quantifiziert.

Lebend/Tot Färbung

Die Vitalität der Bakterien auf P11-SSP-Hydrogelen wurde mit einem Lebend/Tot Färbeset bestimmt (LIVE/DEAD™ BacLight™ Bacterial Viability Kit, ThermoFisher Scientific, USA). SYTO9 (1:1000 in PBS) und PI (1:1000 in PBS) wurden 20 Minuten lang bei 37 °C unter anaeroben oder aeroben Bedingungen inkubiert. Die Bilder wurden mit einem konfokalen Laser-Scanning-Mikroskop (LSM 780, Zeiss, Deutschland) mit einem 60X-Objektiv aufgenommen.

3.5 Antibiotika Inkorporation und deren Freisetzung

Extrakte von P11-SSP-Hydrogelen mit eingebauten Antibiotika (Tetracyclin (TC), Ciprofloxacin (CX) und Doxycyclin Hyclat (DH)) wurden gesammelt. Die Quantifizierung der freigesetzten Antibiotika-Konzentration erfolgte mittels Hochleistungs-Flüssigkeitschromatographie-Massenspektrometrie (HPLC-MS, Agilent Technologies, Basel, Schweiz) unter Einsatz einer Zorbax Eclipse Plus C8-Säule (3,0 x 50 mm, 1,8 µm) (Agilent Technologies, Basel, Schweiz).

4 Resultate

4.1 Studie I

Mechanical characteristics of beta sheet-forming peptide hydrogels are dependent on peptide sequence, concentration and buffer composition.

Koch F, Müller M, König F, Meyer N, Gattlen J, Pieles U, Peters K, Kreikemeyer B, Mathes S, Saxer S. *Royal Society Open Science*. 2018; 5(3):171562

Zusammenfassung

In Studie I wurden die mechanischen Eigenschaften, die Netzwerk-Architektur sowie die Stabilität der vier ausgewählten SSP-Hydrogele evaluiert. Die untersuchten SSP-Hydrogele zeigten Steifigkeiten im Bereich von 0,6 bis 205 kPa. Dabei wurde die Hydrogelsteifigkeit hauptsächlich durch die Peptidsequenz, gefolgt von der Peptidkonzentration und der Pufferzusammensetzung, beeinflusst. Alle untersuchten SSP-Hydrogele bildeten eine nanofibrilläre Netzwerkstruktur aus. Die Inkubation der SSP-Hydrogele in verschiedenen Pufferlösungen nach 7 Tagen resultierte in einer Degradation von bis zu 20 %. Die Stabilität im Hinblick auf den enzymatischen und bakteriellen Abbau zeigte eine geringere Abbaurate im Vergleich zur Auflösungsrate der SSP-Hydrogele in Puffer. Zusammenfassend konnten die getesteten SSP-Hydrogele stabile fibrilläre Netzwerkstrukturen ausbilden und lieferten ein breites Spektrum mechanischer Steifigkeiten, die für eine regenerative Therapie im Bereich Weich-und Hartgewebe geeignet sein können.

ROYAL SOCIETY
OPEN SCIENCE

rsos.royalsocietypublishing.org

Research

Check for updates

Cite this article: Koch F, Müller M, König F, Meyer N, Gattlen J, Pieles U, Peters K, Kreikemeyer B, Mathes S, Saxer S. 2018 Mechanical characteristics of beta sheet-forming peptide hydrogels are dependent on peptide sequence, concentration and buffer composition. *R. Soc. open sci.* **5**: 171562. http://dx.doi.org/10.1098/rsos.171562

Received: 6 October 2017
Accepted: 9 February 2018

Subject Category:
Chemistry

Subject Areas:
biomaterials/bioengineering/supramolecular chemistry

Keywords:
self-assembling peptides (SAP), SAP hydrogel stiffness, nanofibrillar architecture, SAP hydrogel degradability

Author for correspondence:
Sina Saxer
e-mail: sina.saxer@fhnw.ch

This article has been edited by the Royal Society of Chemistry, including the commissioning, peer review process and editorial aspects up to the point of acceptance.

Electronic supplementary material is available online at https://dx.doi.org/10.6084/m9.figshare.c.4015708.

ROYAL SOCIETY OF CHEMISTRY

THE ROYAL SOCIETY
PUBLISHING

Mechanical characteristics of beta sheet-forming peptide hydrogels are dependent on peptide sequence, concentration and buffer composition

Franziska Koch[1], Michael Müller[2], Finja König[3], Nina Meyer[4], Jasmin Gattlen[4], Uwe Pieles[1], Kirsten Peters[5], Bernd Kreikemeyer[6], Stephanie Mathes[4] and Sina Saxer[1]

[1]School of Life Sciences, Institute for Chemistry and Bioanalytics, University of Applied Sciences and Arts Northwestern Switzerland, Muttenz, Switzerland
[2]Department for Health Science and Technology, Cartilage Engineering and Regeneration Laboratory, ETH Zurich, Zurich, Switzerland
[3]Master Program of Protein Science and Technology, Linköping University, Linköping, Sweden
[4]Department for Chemistry and Biotechnology, Tissue Engineering, Zurich University of Applied Sciences, Wädenswil, Switzerland
[5]Department of Cell Biology, University Medicine Rostock, Rostock, Germany
[6]Institute of Medical Microbiology, Virology and Hygiene, University Medicine Rostock, Rostock, Germany

FK, 0000-0002-0613-2018

Self-assembling peptide hydrogels can be modified regarding their biodegradability, their chemical and mechanical properties and their nanofibrillar structure. Thus, self-assembling peptide hydrogels might be suitable scaffolds for regenerative therapies and tissue engineering. Owing to the use of various peptide concentrations and buffer compositions, the self-assembling peptide hydrogels might be influenced regarding their mechanical characteristics. Therefore, the mechanical properties and stability of a set of self-assembling peptide hydrogels, consisting of 11 amino acids, made from four beta sheet self-assembling peptides in various peptide concentrations and buffer compositions were studied. The formed self-assembling peptide hydrogels exhibited stiffnesses ranging from 0.6 to 205 kPa. The hydrogel stiffness was mostly affected by peptide sequence followed by peptide concentration and buffer composition. All self-assembling peptide hydrogels examined provided a nanofibrillar network formation. A maximum self-assembling peptide hydrogel dissolution of 20% was observed for different buffer solutions after 7 days. The stability regarding enzymatic and bacterial digestion showed less degradation in comparison to the self-assembling peptide hydrogel dissolution rate in buffer. The tested set of self-assembling peptide hydrogels were able to form stable scaffolds and provided a broad spectrum of tissue-specific stiffnesses that are suitable for a regenerative therapy.

1. Introduction

Degradable polymeric hydrogels display several features to act as matrices for tissue engineering such as their nanofibrillar structure, high water content, elasticity and diffusion properties for small molecules [1]. Hydrogels are often polymers of natural (e.g. collagen and chitosan) or synthetic origin (e.g. poly(ethylene glycol) and poly(vinyl alcohol)) [2]. The strength and swelling properties of the three-dimensional hydrogel networks can be adjusted by the use of different covalent binding crosslinkers such as glutaraldehyde or formaldehyde or enzymatically by transglutaminase [3–6]. Alternatively, low molecular weight gelators such as peptides, saccharides or nucleotides can be used to build up the three-dimensional gel matrix based on different molecular recognition motifs [7,8]. These recognition motifs interact by hydrogen bonding, metal chelation, π–π bonding, van der Waals forces or hydrophobic bonding resulting in dynamic fibrillar hydrogels [9]. Variations in the composition of low molecular weight gelators allow us to tune the mechanical, chemical and biological properties of the resulting hydrogels and offer the advantage to generate hydrogel libraries. Furthermore, these hydrogels exhibit interesting features such as their low minimal gelation concentration and their reversible three-dimensional network formation, allowing them to sense and respond to their environment [8,9].

Among the low molecular weight gelators, self-assembling peptides (SAPs) have gained significant interest as injectable matrices [10]. To act as a potential scaffolds for tissue engineering or regenerative therapy, SAP hydrogels should closely match the nanofibrillar architecture of naturally occurring polymers (e.g. collagen) as it is known to affect cell polarity and cell migration [11–13]. Moreover, it was demonstrated that cell behaviour such as adhesion, proliferation and differentiation can be controlled by hydrogel stiffness [14–16]. Variable SAP hydrogel stiffnesses can be obtained, for example, by the increase of peptide concentration, as reported by Schneider *et al.* [17]. To ensure SAP hydrogel stability during tissue regeneration, the degradation rate of SAP hydrogels, which is determined by the environmental conditions, should occur in a similar time frame. For example, within the oral cavity, degradation rates of SAP hydrogels are influenced by the ionic strength (50 mM) [18] and pH (5.8–7.4) [19] or by enzymatic or bacterial digestion.

The first commercially available SAP was designed by Zhang *et al*., named RADA16, consisting of a repeated 16 amino acids long RADA motif [20]. This SAP hydrogel is able to induce chondrogenesis of bovine marrow stromal cells [21], osteoblast proliferation and differentiation *in vitro* [22]. Furthermore, RADA16 supports bone [23] and axon regeneration [24] in animal models. Besides RADA16, other SAPs such as the β-hairpin peptide MAX1, presented by Schneider and co-workers, have been shown to support the survival, adhesion and migration of fibroblasts [25–27]. Another class of SAP is called peptide amphiphile, which was designed by Stupp and co-workers and consists of an alkyl tail and a peptide head group that become increasingly hydrophilic [28]. These amphiphile gels were shown to sustain cells without the addition of cell adhesion motifs [29].

The rationally designed SAPs used in the present study were presented by Aggeli *et al*. [30–32], and consist of 11 amino acids. These SAPs assemble depending on peptide concentration, pH and ionic strength of the buffer into beta sheet and higher ordered structures such as fibrils and fibres [31]. The formed SAP hydrogels consist of fibrils and fibres with lengths in the range of several micrometres and typical fibril widths in the range of 12–19 nm [33]. The sequence of the first designed SAP called DN1 by the Aggeli group was repeatedly modified to create a SAP library with specific physico-chemical characteristics such as hierarchical self-assembly and morphology [30]. In the study of Carrick *et al*. [33], the secondary structure, made up of hierarchically stacked anti-parallel β-sheets, and fibril morphology of different Aggeli designed SAPs such as P11-4 and P11-8 were investigated at variable conditions such as pH and ionic strength.

However, a systemic evaluation of the mechanical properties (e.g. SAP hydrogel stiffness, gelation velocity or yield point) is pending. Yet, a tailored SAP hydrogel stiffness is of great interest to meet the mechanical requirements known for the different cell types and thus to induce tissue regeneration. Based on the rational design criteria defined by Bell *et al.*, Kyle *et al.* and Maude *et al.* regarding SAP net charges (+2/−2), sequences and their effect on cytotoxicity, P11-4, P11-8, P11-13/14 and P11-28/29 were selected out of the P11-library [34–36]. Therefore, the present study analyses the mechanical characteristics of four selected β-sheet SAP hydrogels using variable concentrations and buffer compositions, in order to determine their potential as three-dimensional scaffolds for cell culture and tissue engineering.

2. Material and methods

2.1. Materials

SAPs P11-4 (sequence: CH_3CO-QQRFEWEFEQQ-NH_2, peptide content 95%, ammonium salt), P11-8 (sequence: CH_3CO-QQRFOWOFEQQ-NH_2, peptide content 84.4%, TFA salt), P11-13 (sequence: CH_3CO-EQEFEWEFEQE-NH_2, peptide content 78.5%, ammonium salt), P11-14 (sequence: CH_3CO-QQOFOWOFOQQ-NH_2, peptide content 74.6%, TFA salt), P11-29 (sequence: CH_3CO-OQOFOWOFO QO-NH_2, peptide content 70.7%, TFA salt), and P11-28 (sequence: CH_3CO-QQEFEWEFEQQ-NH_2, peptide content 89.0%, ammonium salt) were purchased from CS Bio Co. and illustrated in electronic supplementary material, figure S1. Quality control was done by high-performance liquid chromatography and mass spectroscopy. Sodium chloride (NaCl), Trizma® base and magnesium sulfate ($MgSO_4$, anhydrous) were purchased from Sigma–Aldrich. Dulbecco's Modified Eagle Medium (Gibco™ DMEM) 1× medium was purchased from ThermoFisher Scientific. Artificial saliva was produced as described by Strafford *et al.* protocol using Tris (120 mM), $Ca(NO_3)$ (4 mM), KH_2PO_4 (2.4 mM). Calcium nitrate tetrahydrate ($Ca(NO_3 \cdot 4H_2O)$) and potassium dihydrogen phosphate (KH_2PO_4) were purchased from Sigma–Aldrich. Dulbecco's phosphate buffered saline (PBS) solution (Sigma–Aldrich) and glutaraldehyde solution (4% in borate buffer) were purchased from Sigma–Aldrich.

2.2. Methods

2.2.1. Peptide self-assembling

For each SAP system, buffer composition was adjusted due to the specific physico-chemical properties as demonstrated in table 1. The unary SAPs (P11-4 and P11-8) were prepared, by first dissolving the lyophilized peptide powder in 100 µl of buffer A to obtain a peptide monomer solution. To induce peptide self-assembly, 100 µl of buffer B was added to the peptide monomer solution. Complementary SAPs (P11-13/14 and P11-28/29) were dissolved separately with 100 µl of their peptide specific buffers. Afterwards, peptide pairs were mixed together 1 : 1, for example 100 µl P11-13 plus 100 µl P11-14 at equimolar concentrations to get a final volume of 200 µl P11-13/14. A final ionic strength of 140 mM and a pH of 7.2–7.4 were adjusted for P11-4, P11-13/14 and P11-28/29 using 0.1 M NaOH or 0.1 M HCl. For P11-8, a pH of 7.8–8.0 was adjusted using 0.1 M NaOH.

2.2.2. Determination of self-assembling peptide network architecture by scanning electron microscopy

Nanofibrillar structure of SAP hydrogels was formed for scanning electron microscopy (SEM) (Zeiss SUPRA® 40VP) at a concentration of 15 mg ml^{-1} in Tris–NaCl buffer to a final ionic strength of 140 mM and a final pH of 7.2–8.0, as described in table 1. SAP hydrogels were assembled overnight. Self-assembly was apparent due to the gelation and β-sheet formation of the fibrillar structure as described by Aggeli *et al.* and Carrick *et al.* (by circular dichroism, Fourier transform infrared spectroscopy and transmission electron microscopy) and was further confirmed in the present study for P11-4 and P11-8 (see electronic supplementary material, figures S4, S6 and S7) [31,33]. SAP hydrogels were fixed with a glutaraldehyde solution (4% in borate buffer, using 0.1 ml per 0.1 ml peptide hydrogel) for 24 h. Gels were then dehydrated by increasing ethanol concentration in steps (25%, 50%, 60%, 70%, 80%, 90%, 100% ethanol) at 15 min intervals. The last step (100% ethanol) was repeated three times. Afterwards, critical point drying (Balzers Union, CPD020) was applied to stabilize the natural three-dimensional network structure. Finally, the network structures were glued on an SEM stub with carbon tape and sputter coated with 2.5 nm gold–palladium (Thermo VG Scientific, Polaron, SC7620). SEM images were obtained at 10 kV with an in lens detector at a magnification of ×50 000 and a working distance of 6.0 mm. Fibre diameters were analysed with IMAGEJ software. Twenty-five fibre widths were measured for each picture.

Table 1. Self-assembling peptides preparation in four biological solutions.

	peptide sequence/net charge at pH 7	Tris–NaCl/$MgSO_4$	DMEM	artificial saliva
P11-4	CH_3CO-QQRFEWEFEQQ-NH_2 peptide net charge : −2	A: 0.055 M Tris, pH 8 B: 0.055 M Tris; 0.192 M NaCl/$MgSO_4$, pH 7.0	A: H_2O B: DMEM 2x, pH 7	A: H_2O B: 2x artificial saliva pH 7
P11-8	CH_3CO-QQRFOWOFEQQ-NH_2 peptide net charge : +2	A: H_2O, pH 6 B: 0.055 M Tris; 0.236 M NaCl/$MgSO_4$, pH 9	A: H_2O B: DMEM 2x, pH 8	A: H_2O B: 2x artificial saliva pH 8
P11-13	CH_3CO-EQEFEWEFEQE-NH_2 peptide net charge : −6	0.1 M Tris; 0.052 M NaCl/ $MgSO_4$, pH 8	A: DMEM 1x pH 8	A: artificial saliva 1x, pH 8
P11-29	CH_3CO-QQEFEWEFEQQ-NH_2 peptide net charge : −4			
P11-14	CH_3CO-QQOFOWOFOQQ-NH_2 peptide net charge : +4	0.055 M Tris; 0.096 M NaCl/$MgSO_4$, pH 7	B: DMEM 1x pH 7	B: artificial saliva 1x pH 7
P11-28	CH_3CO-OQOFOWOFOQO-NH_2 peptide net charge : +6			

2.2.3. Mechanical properties of self-assembling peptide hydrogels

Dynamic oscillatory amplitude sweeps up to 150% strain were performed at 37°C using an Anton Paar MCR301 rheometer equipped with a 10 mm diameter stainless steel parallel plate geometry at a 0.9 mm measuring gap. The amplitude sweep tests were performed to measure storage moduli (G') within the linear viscoelastic region. Calculations of the gel breaking points (yield points) were performed with MATLAB depending on the different peptide concentrations. Therefore, the yield strain was defined as the point where G' is less than 95% of its original value. Oscillatory time sweep experiments were performed to study the gelation speed and hydrogel stiffness. Time sweeps up to 150 min measuring time using a frequency of 1 rad s^{-1} and amplitude gamma of 0.05% were used. SAP hydrogel stiffness was determined after the equilibrium of the storage modulus (G') was reached ($t = 100$ min). To determine the gelation speed, the slope of increasing storage modulus over time was calculated in the interval from $t = 5$ to 10 min after placing peptide solutions onto the rheometer.

2.2.3.1. Effect of peptide concentration on mechanical properties of self-assembling peptide hydrogels

To study SAP hydrogel stiffness within the linear viscoelastic region and gel breaking points according to the peptide concentrations, unary SAP hydrogels (300 µl) were prepared in vials at concentrations of 15 mg ml^{-1}, 20 mg ml^{-1} and 30 mg ml^{-1} by dissolving first the lyophilized peptides in 150 µl of buffer A and then adding 150 µl of peptide-specific Tris–NaCl buffer B according to table 1. Complementary SAP hydrogels (P11-13/14 and P11-28/29) were obtained by dissolving 150 µl of P11-13 in 0.1 M Tris buffer + 0.052 M NaCl pH 8 and 150 µl P11-14 in 0.055 M Tris buffer + 0.096 M NaCl pH 7.2 (table 1). The P11-13 and P11-14 solutions were then mixed (1 : 1) to obtain 300 µl of complementary SAP hydrogel with a final ionic strength of 140 mM and a pH of 7.2. All SAP hydrogels were allowed to assemble overnight.

2.2.3.2. Effect of buffer composition on mechanical properties of self-assembling peptide hydrogels

To study the influence of divalent ions and different media on SAP hydrogel stiffness, gelation speed and gel breaking points (yield points), SAPs were prepared at a concentration of 15 mg ml^{-1} in the different media, Tris–NaCl, Tris–$MgSO_4$, DMEM or artificial saliva, according to table 1. All experiments were done at least in duplicate. Statistical evaluation was performed with GRAPHPAD PRISM version 6.0 based on a one-way ANOVA test followed by Tukey's multiple comparison test.

2.2.4. Biodegradability of self-assembling peptide hydrogels by enzymatic and bacterial exposure

SAP hydrogel dissolution and degradation properties of the peptides in the presence and absence of neutrophilic elastase and microorganisms were measured by determining the peptide content of the supernatant. Therefore, SAPs were assembled in PBS at concentrations of 20 mg ml^{-1} for P11-4 and 15 mg ml^{-1} for P11-8, P11-13/14 and P11-28/29. The assay was performed in a 96-well plate with gel volumes of 100 µl well^{-1}. 86 units ml^{-1} elastase (Innovative Research, USA) (100 µg ml^{-1}) were added to the assembled peptides in PBS solution. After 24 h incubation at 37°C and 5% CO_2, 10 µl of the supernatant was sterilely removed after 24 and 168 h and measured indirectly by monomeric peptide concentration in the supernatant using the Qubit® Protein Assay (Q33211; Thermo Fisher; fluorescence at 485/590 nm) and transferred back for the remainder of the experiment allowing peptide hydrogel degradation measurement without disturbing the hydrogel to buffer fluid balance. The measurements are based on the fact that degraded peptides cause disassembly of the fibrils [37], as assembly rules are no longer given, resulting in an increase in monomeric SAP in solution. SAP concentrations were calculated based on respective peptide standard curves. For data analysis, SAP concentrations measured in the supernatant were calculated as a percentage of the specific starting concentrations of each peptide system. Statistical analysis was done using a two-way ANOVA followed by Sidak's multiple comparison test.

The stability of the hydrogels versus bacterial degradation was tested by the exposure to the bacterial strains *Streptococcus mutans* (*S. mutans*), *Pseudomonas aeruginosa* (*P. aeruginosa*) and *Staphylococcus aureus* (*S. aureus*; all from Leibniz-Institut DSMZ GmbH). Therefore, the bacterial strains were applied (10^6 CFU ml^{-1}) on the top of each gel (20 mg ml^{-1} for P11-4 and 15 mg ml^{-1} for P11-8, P11-13/14 and P11-28/29) in their respective media (Neurobasal medium for *P. aeruginosa* (Thermo Fisher), Tryptic Soy Broth (TYSB) medium for *S. mutans* and *S. aureus*). After 1 and 7 days of incubation at 37°C, 10 µl of each supernatant was analysed subsequent to centrifugation of the samples using the Qubit® Protein Assay. Calculations were performed as described previously for the elastase degradation study. Statistical analysis was performed with Graphpad Prism version 6.0 using a two-way ANOVA followed by Dunnett's multiple comparison test.

3. Results and discussion

3.1. Nanofibrillar architecture

The topographical structure of SAP hydrogels is important for the three-dimensional arrangement of cells within scaffolds. Zhang *et al*. [38,39] state that the fibres of SAP hydrogels resemble the nanometre scale of natural polymer networks and thus allow three-dimensional cell growth. To prove the formation of nanofibrillar structure, SEM pictures were taken of dry SAP hydrogels from the four SAP sequences and compared to the literature [39] (figure 1). Quantitative analysis of fibre diameters, obtained from SEM images, revealed mean fibre widths in the following ascending order: 23 ± 4.2 nm (P11-28/29, figure 1*d*), 32 ± 6.6 nm (P11-4, figure 1*a*), 37 ± 6.6 nm (P11-8, figure 1*b*), 38 ± 10.6 nm (P11-13/14, figure 1*c*). Measured widths are at the upper level of other beta sheet peptide systems such as RADA16 with fibre diameters of approximately 10 nm [38,40].

Carrick *et al.* [33] demonstrated that P11-4 and P11-8 prepared in NaCl formed fibril widths of 14 nm. Moreover, they observed the formation fibre entanglements with diameters of 30 nm. The phenomenon of fibril clustering was also reported by Zhang *et al.* [41] for the peptides KFE8 and KLD12, characterized by a typical single fibre width of 7 nm and thicker diameters for the bundles of fibres. In alignment with the study of Leon [42] and Mishra *et al.* [43], we have also observed that the increase of SAP concentration resulted in a higher fibre density rather than in the formation of thicker fibres (see electronic supplementary material, figure S2). In addition, Branco *et al.* [44] demonstrated for MAX1 and MAX8 that the increased SAP concentration results in the formation of more fibrils that entangle and crosslink into the network. Furthermore, they draw the conclusion that higher weight per cent gels are more mechanically rigid and have smaller mesh sizes than gels of the same volume prepared with lower concentrations of peptide.

3.2. Mechanical properties

3.2.1. Adjusting mechanical strength by self-assembling peptide concentration

SAP hydrogel stiffness of P11-4, P11-8, P11-13/14 and P11-28/29 prepared in Tris–NaCl (table 1) buffer at 15, 20 and 30 mg ml^{-1} was assessed by oscillatory amplitude sweep tests (figure 2*a*). For all SAPs, higher storage moduli were obtained after increasing SAP concentration from 15 mg ml^{-1} to 30 mg ml^{-1}. SAP hydrogel stiffnesses ranged from low stiffness of P11-4 (2–4.6 kPa) and P11-28/29 (1.7–19 kPa),

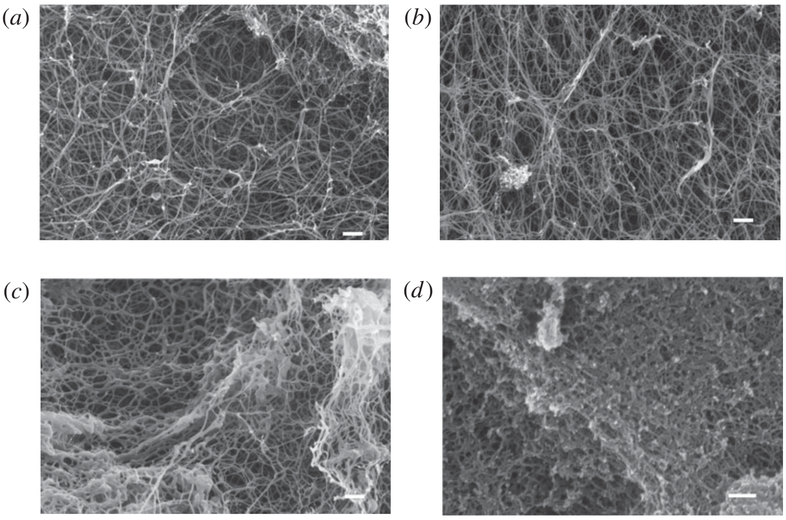

Figure 1. Scanning electron micrographs of self-assembling peptides in the dry state after critical point drying. (*a*) P11-4, (*b*) P11-8, (*c*) P11-13/14, (*d*) P11-28/29, magnified at ×50 000. Scale bar: 200 nm.

to high hydrogel stiffness obtained by P11-8 (31–120 kPa) and P11-13/14 (9.3–89 kPa). Furthermore, a concentration-dependent effect was found for P11-4, P11-8 and P11-28/29, whereas for P11-13/14 hydrogel stiffness did not increase further from 20 to 30 mg ml^{-1}. SAP hydrogel stiffness increased by a factor of 2 (for P11-4), 4 (for P11-8) and 10 (for P11-13/14 and P11-28/29) by doubling the SAP concentration from 15 to 30 mg ml^{-1}.

The beta hairpin folding peptide MAX1 developed by Schneider *et al.* [17] resulted in storage moduli in the range of 0.04 to 2.08 kPa (factor of 52) by increasing peptide concentration from 5 to 20 mg ml^{-1} (quadrupled peptide concentration) [44]. In comparison to MAX1 at 20 mg ml^{-1}, storage moduli of SAP hydrogels at 20 mg ml^{-1} used in the present study were found to be 2 to 28 times higher.

To evaluate the mechanical stability of P11-4, P11-8, P11-13/14 and P11-28/29 hydrogels, stress–strain tests were performed. Therefore, yield points, which are defined as crossover points where the hydrogel is starting to break and the material displaying fluid-like behaviour, were calculated and compared for every SAP and concentration. The earlier the yield point of a SAP hydrogel occurs, in the context of the resistance towards mechanical strain (%), the less it is tolerant towards mechanical strain. Higher hydrogel stiffness achieved by increasing SAP concentrations affects the resistance to mechanical strain as yield points decline with increasing SAP concentration (figure 2*b*). SAP concentrations of 30 mg ml^{-1} were found to have the lowest yield point, independent of the SAP sequence. The highest yield point (6.6% strain) was determined for P11-28/29 at 15 mg ml^{-1}. Lowest yield points were determined for P11-8 in the range of 0.3–1.2% strain. For P11-4, yield points in the range of 1.2–2.2% strain were assessed.

As reported previously, SAP hydrogels showed low resistance to mechanical strain, approximately ≤10% [45]. For example, Goktas *et al.* [46] measured yield points below 0.5% strain for an amphiphilic peptide system and Ramachandran *et al.* [47] found that the self-assembling decapeptide system (KVW10/EVW10) did not resist strain ≥2%. Furthermore, Kirchmajer *et al.* [48] showed that the increase in genipin cross-linking of gelatin hydrogels resulted in a greater amount of elastic stiffness but reduced the extent of deformation before the hydrogel fails, which is in line with the lower yield points observed in this study.

Taken together, the increase in peptide concentration in the present study resulted in higher storage moduli (SAP hydrogel stiffness) due to the formation of more fibres at higher concentrations. The fibres exhibited additional entanglement and cross-linking into a firmer network, which led to a decrease in strain tolerance.

3.2.2. Effect of ion type on mechanical properties of self-assembling peptide hydrogels

Caplan *et al.* [49] demonstrated that hydrogel stiffness and the critical concentration of peptide self-assembling depend on the valence of counterions. Therefore, the influence of mono- and divalent ions on SAP hydrogel stiffness, gelation speed and yield point was analysed (figure 3). To study the effect of

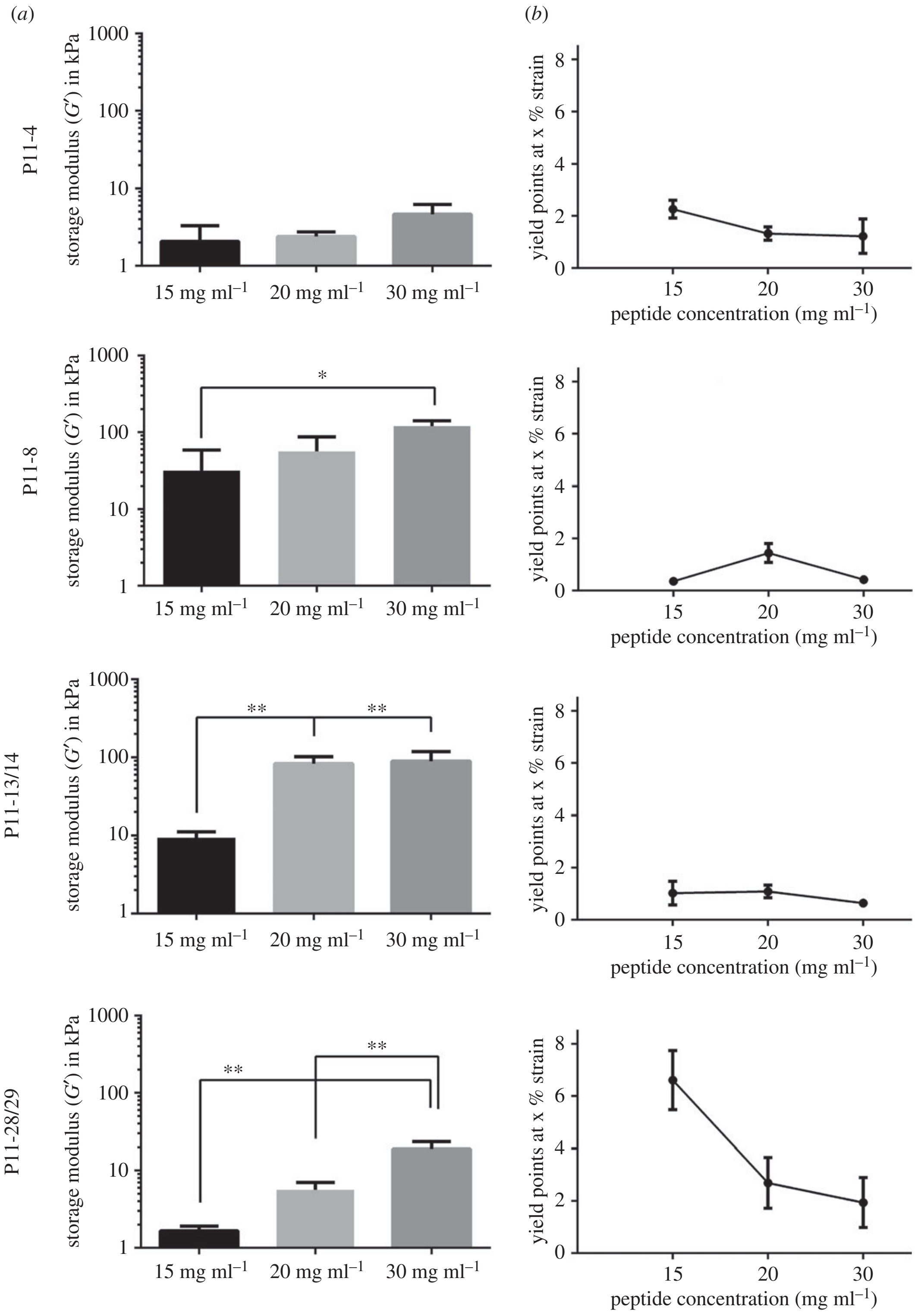

Figure 2. SAP hydrogel stiffnesses (*a*) in relation to the peptide concentration at 15, 20 and 30 mg ml^{-1} prepared in Tris–NaCl buffer and the influence of peptide concentration on yield points (*b*). Measurements were performed with an oscillatory amplitude sweep test on a plate to plate rheometer. *p-value ≤ 0.05, **p-value ≤ 0.01, $n = 3$.

ion valency on the mechanical properties, SAP hydrogels were prepared with either Tris–NaCl or $MgSO_4$ (table 1).

For the unary system P11-8, storage moduli increased significantly by a factor of 1.8, if SAP buffer was prepared with divalent ions such as Mg^{2+} and $SO_4{}^{2-}$ in comparison with monovalent ions such as

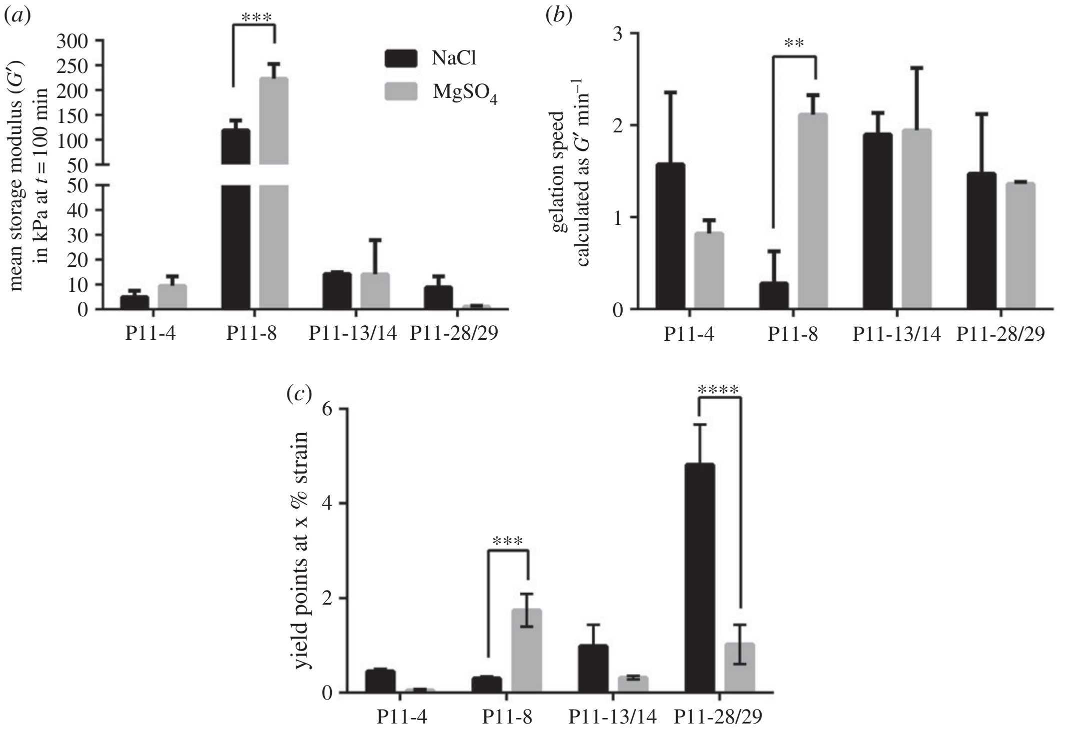

Figure 3. Influence of monovalent and divalent ions on SAP hydrogel stiffness (*a*), gelation speed (*b*) and yield point (*c*). SAPs were prepared either with Tris–NaCl as indicated by black bars or with Tris–$MgSO_4$ indicated by grey bars. *p*-values ≤ 0.05 were defined as significant. ***p*-value ≤ 0.01, ****p*-value ≤ 0.001, *****p*-value ≤ 0.0001, $n = 3$.

Na^+ and Cl^-. Additionally, the gelation speed of, for example, P11-8 prepared with $MgSO_4$ resulted in four times faster assembling time (figure 3*b*).

The increase in hydrogel stiffness and gelation speed of P11-8 prepared with $MgSO_4$ was in line with an increase in resistance to mechanical strain, as the yield point increased from 0.8 to 1.6% strain (figure 3*c*). On the other hand, the preparation of P11-28/29 with $MgSO_4$ resulted in a higher sensitivity to mechanical strain as the yield point declined significantly from 4.8 to 1% strain. The use of divalent ions (Mg^{2+} and $SO_4{}^{2-}$) increased storage moduli of P11-8 significantly and non-significantly for P11-4, whereas for P11-28/29 there was a decrease in hydrogel stiffness. The influence of ion valency was also observed for the SAP EAK16(II)GGH, investigated by Yang *et al.* [50], where pure beta sheet formation and extended fibre length were observed upon addition of divalent sulfate anions. These observations were explained by the salt bridge effect of $SO_4{}^{2-}$ linking two peptide molecules together.

Moreover, the type of mono- or divalent ions can further affect binding geometry and strength to the corresponding amino acid differently, as shown for glutamic acid and tryptophan by Zou *et al.* [51]. Thus for P11-15, a member of the presently investigated self-assembling peptide family, it was shown that Ca^{2+} binding site is made up of four central glutamic acid residues (two from each strand). Owing to the favourable binding energies, binding of the divalent Ca^{2+} causes a more stable fibre structure [52]. As the glutamic acid residues are also present in P11-4, and Ca^{2+} is similar to Mg^{2+}, a similar behaviour can be expected for binding of Mg^{2+}. The binding site is different in the complementary systems (P11-13/14 and P11-28/29) where two of the glutamates are exchanged to by ornithine leading to a less favourable binding energy and resulting in a reduced SAP hydrogel stiffness.

3.2.3. Effect of ion composition on mechanical properties of self-assembling peptide hydrogels

As SAP hydrogels are dynamic systems, which respond to their environmental conditions such as ionic strength and pH by de-assembling and re-assembling, it is important to test how the mechanical properties of the four selected SAPs will be affected under biologically relevant conditions as found within the human body. Therefore, the SAP hydrogel stiffness and gelation kinetics of P11-4, P11-8, P11-13/14 and P11-28/29 were studied in serum-free DMEM and artificial saliva (table 1). Based on the observation that different ion types have an effect on hydrogel stiffness and gelation time, it was

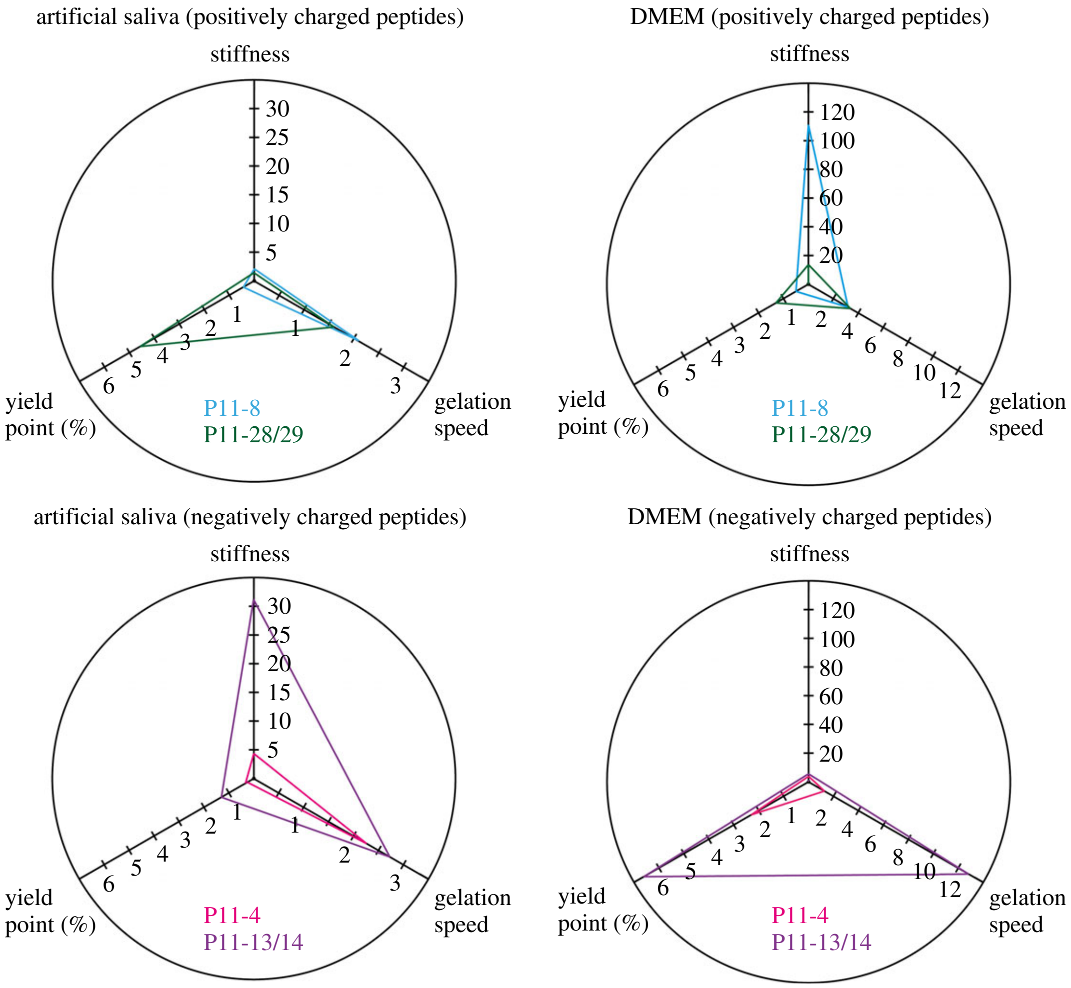

Figure 4. SAP hydrogel stiffness, gelation speed and yield point of P11-4, P11-8, P11-13/14, P11-28/29 as adjustable mechanical properties based on the different buffer compositions of artificial saliva and DMEM. SAP hydrogel stiffness (storage modulus G' at $t = 100$ min) and gelation speed (dG'/dt 5–10 min) were determined by an oscillatory time sweep test at 0.3% strain. Oscillatory amplitude sweep experiments up to 100% strain were performed to calculate yield points, $n = 3$.

assumed that different biological media will affect also SAP hydrogel properties. Therefore, the effects of DMEM and artificial saliva, consisting of different compounds and different ion concentrations, on self-assembling kinetics, hydrogel stiffness and yield point were studied.

The preparation with DMEM or artificial saliva showed a significant difference in SAP hydrogel stiffness for negatively and positively charged SAP hydrogels (figure 4). In addition, there was an increase in hydrogel stiffness for SAPs with a positive overall net charge such as P11-8 (by a factor of 50) and P11-28/29 (by a factor of 9) if they were prepared with DMEM. On the other hand, hydrogel stiffness for P11-4 and P11-13/14 increased by a factor of 12 and a factor of 34, if they were prepared with artificial saliva. The gelation of both complementary SAPs P11-13/14 and P11-28/29 increased by a factor of 5 and a factor of 2 respectively, if diluted in artificial saliva.

Gelation speed increased by a factor of 1.5 for P11-8 prepared in DMEM and 1.8-fold for P11-4 in artificial saliva. For the positive complementary SAP (P11-28/29), increased gelation speed was also detected for P11-13/14 prepared in DMEM by a factor of 4.

As described in figure 3, higher storage moduli correspond to an increase in hydrogel brittleness and result in earlier yield points. This has also been observed for the different peptide preparations in biological media. For example, for P11-28/29 yield point decreases from 4.6% strain to 1.3% strain if hydrogel stiffness increased by a factor of 9, if the system was prepared with DMEM. Yield points of P11-13/14 increased from 1.3% (prepared with artificial saliva) to 6.6% (prepared with DMEM) when decreasing hydrogel stiffness by a factor of 34.

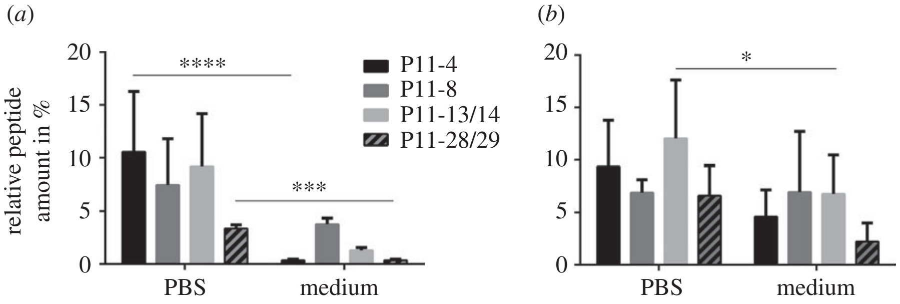

Figure 5. SAP hydrogel stability of P11-4, P11-8, P11-13/14 and P11-28/29 was measured by the determination of peptide concentration in the supernatant after 1 day (*a*) and 7 days (*b*) of incubation with PBS or TYSB medium. Peptide concentrations were calculated as a percentage of the peptide starting concentration, termed as % to control ($n = 3$). *p-value ≤ 0.05, ***p-value ≤ 0.001, ****p-value ≤ 0.0001.

In general, both complementary SAPs (P11-13/14 and P11-28/29) were found to demonstrate a higher stability to mechanical strain (yield points in the range of 1.3–6.6%) in comparison with the unary SAPs (P11-4 and P11-8) that show yield points in the range of 0.3–2.3% strain. Moreover, an increasing hydrogel stiffness for negatively charged peptides such as P11-4 and P11-13/14 prepared with artificial saliva was observed. Ca^{2+} ions are present in artificial saliva and have a high affinity to glutamic acid [53], and we assume a similar binding site as previously described for P11-15 [52]. This is in agreement with the observations of Kirkham *et al*. [54] and Kind *et al.* [55], who demonstrated an attraction of Ca^{2+} causing crystallization of calcium phosphate from artificial saliva on P11-4 fibrillar networks.

3.2.4. Testing of self-assembling peptide hydrogel stability

Stability and degradation properties of SAP hydrogels should ideally be similar to the formation rate of new tissue-specific extracellular matrix (ECM) in order to allow tissue regeneration and are thus critical parameters to be assessed [56–59]. Implanted hydrogels are exposed to inflamed tissue regions and thus to a specific mixture of cells, wound fluid, secreted enzymes and in case of an infected region also to bacteria. Thus, a preliminary test of the degradation characteristics of the four SAPs was performed after incubation with different buffers, an enzyme and bacterial strains under physiological conditions.

3.2.4.1. Self-assembling peptide hydrogel dissolution in different buffer systems

SAP hydrogel stability was first determined by measuring SAP concentration within the supernatant after 1 and 7 days of incubation at 37°C in PBS and TYSB medium, which are characterized by different buffer capacity and buffer composition (figure 5). After 1 day incubation, SAP hydrogel dissolution of P11-4, P11-8, P11-13/14 and P11-28/29 was higher in PBS than in TYSB medium (figure 5*a*). Especially, this observation was true for P11-4 and P11-28/29 hydrogels, showing highly significant differences in PBS and TYSB SAP hydrogel stability. This effect can be explained by the different buffer composition and strength regulating the pH of the hydrogel surroundings. TYSB medium has a higher amount of K_2HPO_4 compared with PBS resulting in a higher buffer strength of TYSB. As the self-assembling process of the tested SAPs is known to be influenced by pH, TYSB medium keeps the pH condition stable during *in vitro* culturing when compared with PBS. Therefore, less peptide dissolution occurred in TYSB medium. Of all SAP hydrogels, P11-28/29 showed least SAP dissolution and had thus the highest SAP hydrogel stability.

3.2.4.2. Self-assembling peptide hydrogel degradation by human neutrophil elastase

Human neutrophil elastase represents the most abundant enzyme in inflammation-associated diseases such as diabetes [60], rheumatoid arthritis [61], cancer [62] and gingivitis [63]. It is known to cleave polyalanine (AAA) sequences [64]. SAP hydrogels were incubated with human neutrophil elastase and tested after 1 day and 7 days by measuring SAP content in the supernatant. P11-28/29 degrades two times less than the other SAP hydrogels (figure 6*a*). There was no significant difference in SAP hydrogels treated with elastase or solely PBS. The SAP hydrogels were not susceptible to elastase-mediated degradation due to the missing polyalanine sequences (AAA) of the tested SAPs. The increased standard

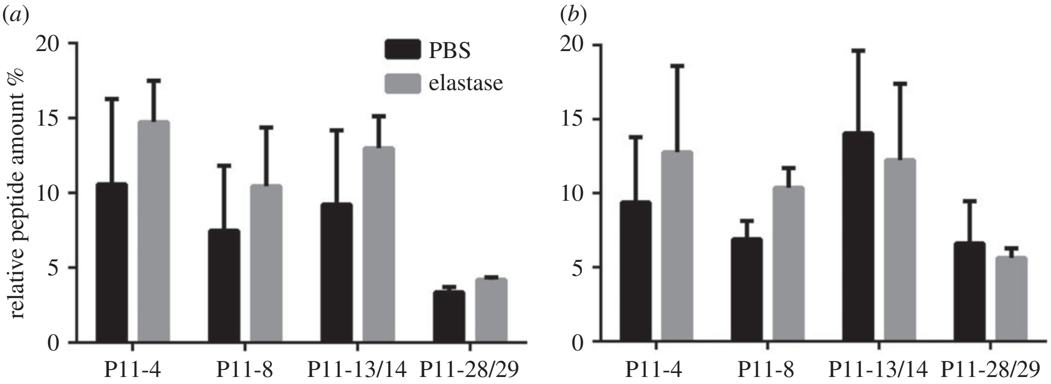

Figure 6. Enzymatic degradation of the unary SAP systems (P11-4, P11-8) and complementary SAP systems (P11-13/14 and P11-28/29) after 1 day (*a*) and 7 days (*b*) of incubation in PBS or in human neutrophil elastase supplemented PBS solution (100 µg ml^{-1}). Peptide concentrations measured in the supernatant were calculated as a percentage of the peptide starting concentration, termed as % to control ($n = 3$).

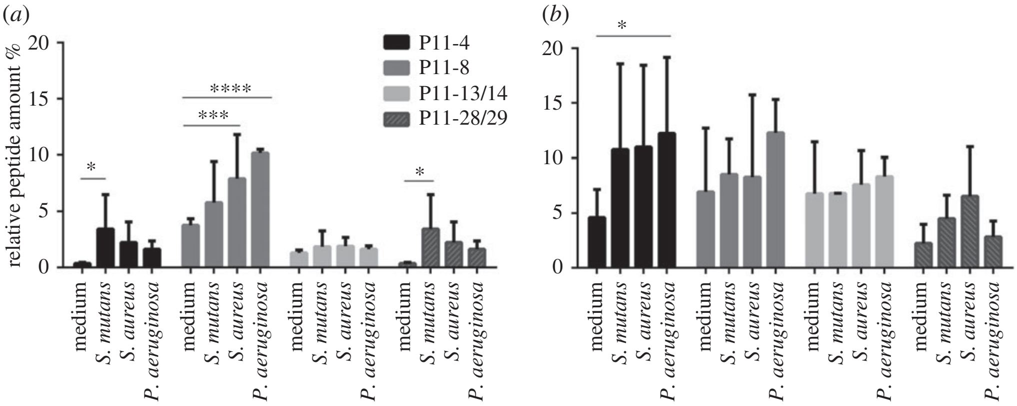

Figure 7. SAP hydrogel degradation after the incubation in medium and with *P. aeruginosa*, *S. aureus*, *S. mutans* was measured after 1 day (*a*) and 7 days (*b*) using 10^6 CFU ml^{-1}. The represented data were calculated in % to the peptide starting concentration (termed as % to control) of every peptide system, $n = 3$. p-values ≤ 0.05 were defined as significant. **p-value ≤ 0.01, ***p-value ≤ 0.001, ****p-value ≤ 0.0001.

deviation after 7 days of incubation is due to static conditions and evaporation. By comparing all four SAPs incubated solely with PBS, we conclude that the medium is the main driver which determines peptide-specific degradation rates. None of the SAP sequences have an endopeptidase cleavage site; the main degradation would, thus, be by exoproteases. Based on the insignificant SAP hydrogel degradation observed with human neutrophil elastase, it can be concluded that the gel integrity is not affected by it. In the case of a biomedical application, we assume that a specific cocktail of enzymes can digest the SAP hydrogel in short peptide fragments and single amino acids.

3.2.4.3. Self-assembling peptide hydrogel degradation by bacterial strains

Bacterial degradation is plausible for applications in tissue with high bacterial density such as in the oral cavity. Thus, SAP hydrogel degradation was tested after 1 day and 7 days of exposure to the three following strains: *Pseudomonas aeruginosa*, *Staphylococcus aureus* and *Streptococcus mutans*, which are common in oral cavities (figure 7). The four tested SAP hydrogels behave differently to bacterial exposure (figure 7). In the case of P11-4, P11-8 and P11-28/29, bacterial exposure affects hydrogel degradation in comparison to the medium control. Furthermore, SAP hydrogel degradation rates differ depending on the bacterial strain tested. On the other hand, no significant increase in peptide content was found for P11-13/14 after bacterial exposure. As with the enzyme degradation experiments, P11-28/29 hydrogels were degraded to a lesser extent than the other three peptide systems which were prone to be influenced by media effects. Moreover, after 7 days of exposure to bacterial strains, high standard deviations were observed due to different bacterial growth rates which led to the production of acidic metabolites and thus to a shift in pH [65]. Furthermore, the increase of data variability was caused by evaporation effects over time leading to an increase in ionic strength in the media.

In summary, the characterization of the four selected SAP hydrogels (P11-4, P11-8, P11-13/14 and P11-28/29) suggests that they are attractive candidates for a variety of tissue engineering applications due to their nanofibrillar network, adaptable stiffness by varying peptide concentration/buffer composition and degradation behaviour after enzymatic and bacterial digestion. However, it is essential, prior to clinical use, that favourable peptide candidates undergo an extensive *in vitro* evaluation with cell types specific for the selected biomedical application. Such evaluation should contain studies about cytocompatibility, inflammatory response, cell survival and adhesion as well as cell growth and differentiation capacities.

4. Conclusion

We have demonstrated that the SAPs (P11-4, P11-8, P11-13/14 and P11-28/29) evaluated in the present study form fibrillar networks with fibril diameters in the range of 23–38 nm. The network architecture of the peptide hydrogels closely matched fibril diameters of the reported literature and naturally occurring ECM proteins, e.g. for collagen type fibrils (20–200 nm). A broad range of SAP hydrogel stiffnesses were in agreement with the stiffnesses of the different body tissue, ranging from soft (0.6 kPa) to hard (205 kPa) tissue. This stiffness variability was achieved by different assembling conditions such as peptide concentration, ionic charge and buffer composition. The self-assembling conditions were also found to affect the gelation speed and the yield point. SAP hydrogel degradation rates were mostly affected by bacterial digestion and not by enzymatic cleavage of human neutrophil elastase. Therefore, the characteristics of the SAP hydrogel environment have to be taken into account for the evaluation in future applications. Thus, we have demonstrated that the four SAPs can be modified into 48 different SAP hydrogels by varying peptide sequences, concentrations and buffer compositions. These SAP hydrogels matched the mechanical properties of soft and hard tissue stiffness and thus are potential scaffolds for regenerative therapies.

Data accessibility. All relevant data are within the paper and its electronic supplementary material files.

Authors' contributions. F.K. designed the study. F.K., M.M., F.Kö. conducted the rheological and SEM studies. N.M. and J.G. carried out peptide degradability studies. F.K. and S.S. wrote the manuscript. U.P., S.M., B.K., K.P. reviewed and approved the manuscript and contributed with scientific expertise. All authors gave final approval for publication.

Competing interests. All authors have no competing interests.

Funding. This work was funded and supported by credentis AG (Windisch, Switzerland) and the Commission for Technology and Innovation (CTI, project number 17310.1 PFLS-LS, Forschungsfond Aargau project number 20150831_11, Switzerland)

Acknowledgements. We thank Prof. Dr Marcy Zenobi-Wong and co-workers (Department for Health Sciences and Technology, ETH, Zurich) for their assistance with instrumentation and technical support.

References

1. Kharkar PM, Kiick KL, Kloxin AM. 2013 Designing degradable hydrogels for orthogonal control of cell microenvironments. *Chem. Soc. Rev.* **42**, 7335–7372. (doi:10.1039/C3CS60040H)
2. Zhu J. 2010 Bioactive modification of poly(ethylene glycol) hydrogels for tissue engineering. *Biomaterials* **31**, 4639–4656. (doi:10.1016/j.biomaterials.2010.02.044)
3. Gulati N, Nagaich U, Sharma V, Khosa R. 2011 Effect of polymer and cross linking agent on *in vitro* release of quercetin from microbeads. *Asian J. Pharm. Life Sci.* **1**, 401–405.
4. Ramamurthi A, Vesely I. 2003 Ultraviolet light-induced modification of crosslinked hyaluronan gels. *J. Biomed. Mater. Res. A* **66**, 317–329. (doi:10.1002/jbm.a.10588)
5. Denizli BK, Can HK, Rzaev ZM, Guner A. 2004 Preparation conditions and swelling equilibria of dextran hydrogels prepared by some crosslinking agents. *Polymer* **45**, 6431–6435. (doi:10.1016/j.polymer.2004.07.067)
6. Kuo CK, Ma PX. 2001 Ionically crosslinked alginate hydrogels as scaffolds for tissue engineering: part 1. Structure, gelation rate and mechanical properties. *Biomaterials* **22**, 511–521. (doi:10.1016/S0142-9612(00)00201-5)
7. Estroff LA, Hamilton AD. 2004 Water gelation by small organic molecules. *Chem. Rev.* **104**, 1201–1218. (doi:10.1021/cr0302049)
8. de Loos M, Feringa BL, van Esch JH. 2005 Design and application of self-assembled low molecular weight hydrogels. *Eur. J. Org. Chem.* **2005**, 3615–3631. (doi:10.1002/ejoc.200400723)
9. Webber MJ, Appel EA, Meijer E, Langer R. 2016 Supramolecular biomaterials. *Nat. Mater.* **15**, 13–26. (doi:10.1038/nmat4474)
10. Pashuck ET, Cui H, Stupp SI. 2010 Tuning supramolecular rigidity of peptide fibers through molecular structure. *J. Am. Chem. Soc.* **132**, 6041–6046. (doi:10.1021/ja908560n)
11. Dickinson RB, Guido S, Tranquillo RT. 1994 Biased cell migration of fibroblasts exhibiting contact guidance in oriented collagen gels. *Ann. Biomed. Eng.* **22**, 342–356. (doi:10.1007/BF02368241)
12. Perentes JY, McKee TD, Ley CD, Mathiew H, Dawson M, Padera TP, Munn LL, Jain RK, Boucher Y. 2009 *In vivo* imaging of extracellular matrix remodeling by tumor-associated fibroblasts. *Nat. Meth.* **6**, 143–145. (doi:10.1038/nmeth.1295)
13. Jana S, Leung M, Chang J, Zhang M. 2014 Effect of nano- and micro-scale topological features on alignment of muscle cells and commitment of myogenic differentiation. *Biofabrication* **6**, 035012. (doi:10.1088/1758-5082/6/3/035012)

14. Kraehenbuehl TP, Zammaretti P, Van der Vlies AJ, Schoenmakers RG, Lutolf MP, Jaconi ME, Hubbell JA. 2008 Three-dimensional extracellular matrix-directed cardioprogenitor differentiation: systematic modulation of a synthetic cell-responsive PEG-hydrogel. *Biomaterials* **29**, 2757–2766. (doi:10.1016/j.biomaterials.2008.03.016)
15. Ventre M, Causa F, Netti PA. 2012 Determinants of cell–material crosstalk at the interface: towards engineering of cell instructive materials. *J. R. Soc. Interface* **9**, 2017–2032. (doi:10.1098/rsif.2012.0308)
16. Ventre M, Netti PA. 2016 Engineering cell instructive materials to control cell fate and functions through material cues and surface patterning. *ACS Appl. Mater. Interfaces* **8**, 14 896–14 908. (doi:10.1021/acsami.5b08658)
17. Schneider JP, Pochan DJ, Ozbas B, Rajagopal K, Pakstis L, Kretsinger J. 2002 Responsive hydrogels from the intramolecular folding and self-assembly of a designed peptide. *J. Am. Chem. Soc.* **124**, 15 030–15 037. (doi:10.1021/ja027993g)
18. Bolscher JG, Adao R, Nazmi K, van den Keybus PA, van't Hof W, Amerongen AVN, Bastos M, Veerman E. 2009 Bactericidal activity of LFchimera is stronger and less sensitive to ionic strength than its constituent lactoferricin and lactoferrampin peptides. *Biochimie* **91**, 123–132. (doi:10.1016/j.biochi.2008.05.019)
19. Randale SA, Dabhi CS, Tekade AR, Belgamwar VS, Gattani SG, Surana SJ. 2010 Rapidly disintegrating tablets containing taste masked metoclopramide hydrochloride prepared by extrusion–precipitation method. *Chem. Pharm. Bull.* **58**, 443–448. (doi:10.1248/cpb.58.443)
20. Sun L, Zhao X. 2012 A self-assembling peptide RADA16-I integrated with spider fibroin uncrystalline motifs. *Int. J. Nanomed.* **7**, 571–580.
21. Kopesky PW, Vanderploeg EJ, Sandy JS, Kurz B, Grodzinsky AJ. 2009 Self-assembling peptide hydrogels modulate *in vitro* chondrogenesis of bovine bone marrow stromal cells. *Tissue Eng. Part A* **16**, 465–477. (doi:10.1089/ten.tea.2009.0158)
22. Horii A, Wang X, Gelain F, Zhang S. 2007 Biological designer self-assembling peptide nanofiber scaffolds significantly enhance osteoblast proliferation, differentiation and 3-D migration. *PLoS ONE* **2**, e190. (doi:10.1371/journal.pone.0000190)
23. Misawa H *et al.* 2006 PuraMatrixTM facilitates bone regeneration in bone defects of calvaria in mice. *Cell Transplant.* **15**, 903–910. (doi:10.3727/000000006783981369)
24. Ellis-Behnke RG, Liang YX, You SW, Tay DK, Zhang S, So KF, Schneider GE. 2006 Nano neuro knitting: peptide nanofiber scaffold for brain repair and axon regeneration with functional return of vision. *Proc. Natl Acad. Sci. USA* **103**, 5054–5059. (doi:10.1073/pnas.0600559103)
25. Haines LA, Rajagopal K, Ozbas B, Salick DA, Pochan DJ, Schneider JP. 2005 Light-activated hydrogel formation via the triggered folding and self-assembly of a designed peptide. *J. Am. Chem. Soc.* **127**, 17 025–17 029. (doi:10.1021/ja054719o)
26. Haines-Butterick L, Rajagopal K, Branco M, Salick D, Rughani R, Pilarz M, Lamm MS, Pochan DJ, Schneider JP. 2007 Controlling hydrogelation kinetics by peptide design for three-dimensional encapsulation and injectable delivery of cells. *Proc. Natl Acad. Sci. USA* **104**, 7791–7796. (doi:10.1073/pnas.0701980104)
27. Kretsinger JK, Haines LA, Ozbas B, Pochan DJ, Schneider JP. 2005 Cytocompatibility of self-assembled β-hairpin peptide hydrogel surfaces. *Biomaterials* **26**, 5177–5186. (doi:10.1016/j.biomaterials.2005.01.029)
28. Maude S, Ingham E, Aggeli A. 2013 Biomimetic self-assembling peptides as scaffolds for soft tissue engineering. *Nanomedicine* **8**, 823–847.
29. Beniash E, Hartgerink JD, Storrie H, Stendahl JC, Stupp SI. 2005 Self-assembling peptide amphiphile nanofiber matrices for cell entrapment. *Acta Biomater.* **1**, 387–397. (doi:10.1016/j.actbio.2005.04.002)
30. Aggeli A, Bell M, Boden N, Keen JN, Knowles PF, McLeish TCB, Pitkeathly M, Radford SE. 1997 Responsive gels formed by the spontaneous self-assembly of peptides into polymeric β-sheet tapes. *Nature* **386**, 259–262. (doi:10.1038/386259a0)
31. Aggeli A, Nyrkova IA, Bell M, Harding R, Carrick L, McLeish TC, Semenov AN, Boden N. 2001 Hierarchical self-assembly of chiral rod-like molecules as a model for peptide beta -sheet tapes, ribbons, fibrils, and fibers. *Proc. Natl Acad. Sci. USA* **98**, 11 857–11 862. (doi:10.1073/pnas.191250198)
32. Aggeli A, Bell M, Boden N, Carrick LM, Strong AE. 2003 Self-assembling peptide polyelectrolyte beta-sheet complexes form nematic hydrogels. *Angew. Chem. Int. Ed. Engl.* **42**, 5603–5606. (doi:10.1002/anie.200352207)
33. Carrick LM, Aggeli A, Boden N, Fisher J, Ingham E, Waigh TA. 2007 Effect of ionic strength on the self-assembly, morphology and gelation of pH responsive β-sheet tape-forming peptides. *Tetrahedron* **63**, 7457–7467. (doi:10.1016/j.tet.2007.05.036)
34. Bell CJ, Carrick LM, Katta J, Jin Z, Ingham E, Aggeli A, Boden N, Waigh TA, Fisher J. 2006 Self-assembling peptides as injectable lubricants for osteoarthritis. *J. Biomed. Mater. Res. A* **78**, 236–246. (doi:10.1002/jbm.a.30672)
35. Kyle S, Aggeli A, Ingham E, McPherson MJ. 2010 Recombinant self-assembling peptides as biomaterials for tissue engineering. *Biomaterials* **31**, 9395–9405. (doi:10.1016/j.biomaterials.2010.08.051)
36. Maude S, Miles DE, Felton SH, Ingram J, Carrick LM, Wilcox RK, Ingham E, Aggeli A. 2011 De novo designed positively charged tape-forming peptides: self-assembly and gelation in physiological solutions and their evaluation as 3D matrices for cell growth. *Soft Matter* **7**, 8085–8099. (doi:10.1039/c0sm00974a)
37. Jun HW, Yuwono V, Paramonov SE, Hartgerink JD. 2005 Enzyme-mediated degradation of peptide-amphiphile nanofiber networks. *Adv. Mater.* **17**, 2612–2617. (doi:10.1002/adma.200500855)
38. Zhang S, Holmes T, Lockshin C, Rich A. 1993 Spontaneous assembly of a self-complementary oligopeptide to form a stable macroscopic membrane. *Proc. Natl Acad. Sci. USA* **90**, 3334–3338. (doi:10.1073/pnas.90.8.3334)
39. Zhang S, Holmes TC, DiPersio CM, Hynes RO, Su X, Rich A. 1995 Self-complementary oligopeptide matrices support mammalian cell attachment. *Biomaterials* **16**, 1385–1393. (doi:10.1016/0142-9612(95)96874-Y)
40. Holmes TC, de Lacalle S, Su X, Liu G, Rich A, Zhang S. 2000 Extensive neurite outgrowth and active synapse formation on self-assembling peptide scaffolds. *Proc. Natl Acad. Sci. USA* **97**, 6728–6733. (doi:10.1073/pnas.97.12.6728)
41. Zhang S, Gelain F, Zhao X. 2005 Designer self-assembling peptide nanofiber scaffolds for 3D tissue cell cultures. *Semin. Cancer Biol.* **15**, 413–420. (doi:10.1016/j.semcancer.2005.05.007)
42. Leon EJ, Verma N, Zhang S, Lauffenburger DA, Kamm RD. 1998 Mechanical properties of a self-assembling oligopeptide matrix. *J. Biomater. Sci. Polym. Ed.* **9**, 297–312. (doi:10.1163/156856298X00668)
43. Mishra A, Loo Y, Deng R, Chuah YJ, Hee HT, Ying JY, Hauser CAE. 2011 Ultrasmall natural peptides self-assemble to strong temperature-resistant helical fibers in scaffolds suitable for tissue engineering. *Nano Today* **6**, 232–239. (doi:10.1016/j.nantod.2011.05.001)
44. Branco MC, Pochan DJ, Wagner NJ, Schneider JP. 2009 Macromolecular diffusion and release from self-assembled beta-hairpin peptide hydrogels. *Biomaterials* **30**, 1339–1347. (doi:10.1016/j.biomaterials.2008.11.019)
45. Raeburn J, Zamith Cardoso A, Adams DJ. 2013 The importance of the self-assembly process to control mechanical properties of low molecular weight hydrogels. *Chem. Soc. Rev.* **42**, 5143–5156. (doi:10.1039/c3cs60030k)
46. Goktas M, Cinar G, Orujalipoor I, Ide S, Tekinay AB, Guler MO. 2015 Self-assembled peptide amphiphile nanofibers and PEG composite hydrogels as tunable ECM mimetic microenvironment. *Biomacromolecules* **16**, 1247–1258. (doi:10.1021/acs.biomac.5b00041)
47. Ramachandran S, Tseng Y, Yu YB. 2005 Repeated rapid shear-responsiveness of peptide hydrogels with tunable shear modulus. *Biomacromolecules* **6**, 1316–1321. (doi:10.1021/bm049284w)
48. Kirchmajer DM, Watson CA, Ranson M. 2013 Gelapin, a degradable genipin cross-linked gelatin hydrogel. *RSC Adv.* **3**, 1073–1081. (doi:10.1039/C2RA22859A)
49. Caplan MR, Moore PN, Zhang S, Kamm RD, Lauffenburger DA. 2000 Self-assembly of a β-sheet protein governed by relief of electrostatic repulsion relative to van der Waals attraction. *Biomacromolecules* **1**, 627–631. (doi:10.1021/bm005586w)
50. Yang H, Pritzker M, Fung SY, Sheng Y, Wang W, Chen P. 2006 Anion effect on the nanostructure of a metal ion binding self-assembling peptide. *Langmuir* **22**, 8553–8562. (doi:10.1021/la061238p)
51. Zou R, Wang Q, Wu J, Wu J, Schmuck C, Tian H. 2015 Peptide self-assembly triggered by metal ions. *Chem. Soc. Rev.* **44**, 5200–5219. (doi:10.1039/C5CS00234F)
52. Thomson BM, Hardaker L, Davies RPW, Dennis C, Bronowska A, Aggeli A, Kirkham J, Lysek DA. 2014 P11-15 (NNRFEWEFENN): a biocompatible, self-assembling peptide with potential to promote enamel remineralisation. Abstract 47. *Caries Res.* **48**, 411.
53. Kohn WD, Kay CM, Sykes BD, Hodges RS. 1998 Metal ion induced folding of a de novo designed coiled-coil peptide. *J. Am. Chem. Soc.* **120**, 1124–1132. (doi:10.1021/ja973673z)
54. Kirkham J, Firth A, Vernals D, Boden N, Robinson C, Shore RC, Brookes SJ, Aggeli A. 2007

Self-assembling peptide scaffolds promote enamel remineralization. *J. Dent. Res.* **86**, 426–430. (doi:10.1177/154405910708600507)

55. Kind L, Stevanovic S, Wuttig S, Wimberger S, Hofer J, Müller B, Pieles U. 2017 Biomimetic remineralization of carious lesions by self-assembling peptide. *J. Dent. Res.* **96**, 790–797. (doi:10.1177/0022034517698419)
56. Liu Y, Shu XZ, Prestwich GD. 2006 Osteochondral defect repair with autologous bone marrow-derived mesenchymal stem cells in an injectable, in situ, cross-linked synthetic extracellular matrix. *Tissue Eng.* **12**, 3405–3416. (doi:10.1089/ten.2006.12.3405)
57. Tan H, Marra KG. 2010 Injectable, biodegradable hydrogels for tissue engineering applications. *Materials* **3**, 1746–1767. (doi:10.3390/ma3031746)
58. Lutolf MP, Hubbell JA. 2005 Synthetic biomaterials as instructive extracellular microenvironments for morphogenesis in tissue engineering. *Nat. Biotechnol.* **23**, 47–55. (doi:10.1038/nbt1055)
59. Tian YF, Hudalla GA, Han H, Collier JH. 2013 Controllably degradable beta-sheet nanofibers and gels from self-assembling depsipeptides. *Biomater. Sci.* **1**, 1037–1045. (doi:10.1039/C3BM60161G)
60. Koulmanda M *et al.* 2008 Curative and β cell regenerative effects of α1-antitrypsin treatment in autoimmune diabetic NOD mice. *Proc. Natl Acad. Sci. USA* **105**, 16 242–16 247. (doi:10.1073/pnas.0808031105)
61. Choy EH, Panayi GS. 2001 Cytokine pathways and joint inflammation in rheumatoid arthritis. *N. Eng. J. Med.* **344**, 907–916. (doi:10.1056/NEJM200103223441207)
62. Schäfer M, Werner S. 2008 Cancer as an overhealing wound: an old hypothesis revisited. *Nat. Rev. Mol. Cell Biol.* **9**, 628–638. (doi:10.1038/nrm2455)
63. Ohlsson K, Olsson I, Tynelius-Bratthall G. 1974 Neutrophil leukocyte collagenase, elastase and serum protease inhibitors in human gingival crevices. *Acta Odontol. Scand.* **32**, 51–59. (doi:10.3109/00016357409002532)
64. Castelletto V, Gouveia RJ, Connon CJ, Hamley IW, Seitsonen J, Ruokolainen J, Longo E, Siligardi G. 2014 Influence of elastase on alanine-rich peptide hydrogels. *Biomater. Sci.* **2**, 867–874. (doi:10.1039/C4BM00001C)
65. Myhre B, Demianew S, Yoshimori R, Nelson E, Carmen R. 1985 pH changes caused by bacterial growth in contaminated platelet concentrates. *Ann. Clin. Lab. Sci.* **15**, 509–514.

4.2 Studie II

Amino acid composition of nanofibrillar self-assembling peptide hydrogels affects responses of periodontal tissue cells *in vitro.*

Koch F, Wolff A, Mathes S, Pieles U, Saxer S, Kreikemeyer B, Peters K. *Journal of International Nanomedicine*. 2018;13: 6717-6733

Zusammenfassung

In Studie II wurden die vier ausgewählten SSP-Hydrogele (davon zwei Einkomponenten-Systeme und zwei Komplementär-Systeme) auf ihre Materialeigenschaften, wie z. B. Porosität, Schwelleigenschaften, Oberflächenladung und Proteinadsorption, untersucht. Des Weiteren wurde der Einfluss von P11-SSP-Hydrogelen auf die zelluläre Reaktion, wie z. B. die Zelladhäsion, Morphologie, Wachstum, und Differenzierung, analysiert. Die variierende Aminosäurezusammensetzung der SSP führt zu deutlichen Veränderungen in der Porosität der Hydrogele und der Proteinadsorption. Diese Unterschiede in den physikochemischen Eigenschaften der Hydrogele scheinen im Zusammenhang mit den zellulären Reaktionen zu stehen. So induzierten die Einkomponenten-SSP-Hydrogele eine fast verdoppelte Zelladhäsion und ein gesteigertes Zellwachstum im Vergleich zu den komplementären SSP-Hydrogelen. Darüber hinaus wurde für die Einkomponenten-Hydrogele im Vergleich zu Standardzellkulturen eine signifikant verbesserte osteogene Differenzierung humaner Osteoblasten festgestellt. Einkomponenten-SSP-Hydrogele besitzen daher ein hohes Potential zur Eignung als Biomaterial für die Parodontaltherapie.

International Journal of Nanomedicine

Dovepress
open access to scientific and medical research

Open Access Full Text Article

ORIGINAL RESEARCH

Amino acid composition of nanofibrillar self-assembling peptide hydrogels affects responses of periodontal tissue cells in vitro

This article was published in the following Dove Press journal:
International Journal of Nanomedicine

Franziska Koch,[1–3] Anne Wolff,[2] Stephanie Mathes,[4] Uwe Pieles,[1] Sina S Saxer,[1] Bernd Kreikemeyer,[3] Kirsten Peters[2]

[1]Institute for Chemistry and Bioanalytics, School of Life Sciences, University of Applied Sciences and Arts Northwestern Switzerland, Muttenz, Switzerland; [2]Department of Cell Biology, University Medicine Rostock, Rostock, Germany; [3]Institute of Medical Microbiology, Virology and Hygiene, University Medicine Rostock, Rostock, Germany; [4]Department for Chemistry and Biotechnology, Tissue Engineering, Zurich University of Applied Sciences, Wädenswil, Switzerland

Video abstract

Point your SmartPhone at the code above. If you have a QR code reader the video abstract will appear. Or use:
http://youtu.be/5SQp6GLigG4

Correspondence: Kirsten Peters
University Medicine Rostock, Department of Cell Biology, Schillingallee 69, 18057 Rostock (DE), Germany
Tel +49 381 494 7757
Email kirsten.peters@med.uni.rostock.de

Background: The regeneration of tissue defects at the interface between soft and hard tissue, eg, in the periodontium, poses a challenge due to the divergent tissue requirements. A class of biomaterials that may support the regeneration at the soft-to-hard tissue interface are self-assembling peptides (SAPs), as their physicochemical and mechanical properties can be rationally designed to meet tissue requirements.

Materials and methods: In this work, we investigated the effect of two single-component and two complementary β-sheet forming SAP systems on their hydrogel properties such as nanofibrillar architecture, surface charge, and protein adsorption as well as their influence on cell adhesion, morphology, growth, and differentiation.

Results: We showed that these four 11-amino acid SAP (P11-SAP) hydrogels possessed physicochemical characteristics dependent on their amino acid composition that allowed variabilities in nanofibrillar network architecture, surface charge, and protein adsorption (eg, the single-component systems demonstrated an ~30% higher porosity and an almost 2-fold higher protein adsorption compared with the complementary systems). Cytocompatibility studies revealed similar results for cells cultured on the four P11-SAP hydrogels compared with cells on standard cell culture surfaces. The single-component P11-SAP systems showed a 1.7-fold increase in cell adhesion and cellular growth compared with the complementary P11-SAP systems. Moreover, significantly enhanced osteogenic differentiation of human calvarial osteoblasts was detected for the single-component P11-SAP system hydrogels compared with standard cell cultures.

Conclusion: Thus, single-component system P11-SAP hydrogels can be assessed as suitable scaffolds for periodontal regeneration therapy, as they provide adjustable, extracellular matrix-mimetic nanofibrillar architecture and favorable cellular interaction with periodontal cells.

Keywords: self-assembling peptides, SAPs, P11-SAP hydrogels, surface charge, protein adsorption, cell proliferation, osteogenic differentiation, periodontal tissue regeneration

Introduction

The development of therapies for the regeneration of tissue defects at the interface between soft and hard tissue (eg, ligament-to-bone within the periodontium) poses a challenge due to the diverging tissue requirements. The periodontium consists of the gingiva, periodontal ligament, cementum, and alveolar bone.[1] Periodontal diseases lead to the breakdown of the periodontium by bacterial infection, if untreated ultimately resulting in tooth loss.[2] Several techniques have been developed, which aim to support natural periodontal regeneration such as guided tissue regeneration and bone grafting, either with or without the use of enamel matrix derivative or growth factors.[3] Yet, these different therapeutic options frequently lead to unsatisfactory clinical results

http://dx.doi.org/10.2147/IJN.S173702

(ie, tooth loss), and thus, a medical need remains for the development of biomaterials specifically designed for the conditions at the soft-to-hard tissue interface. It is known that the physicochemical characteristics of biomaterials, such as surface charge and scaffold architecture, can control cellular responses and thus influence tissue regeneration.[4–7] For example, cell growth, cell migration, and cell differentiation are influenced by the aforementioned parameters.[5,8,9] Thus, the knowledge about possible coherences between the physicochemical characteristics and the resulting cellular reactions can be decisive for the development of suitable biomaterials. Soft-to-hard tissue interfaces therefore require an ambilateral adaptation to physicochemical and mechanical characteristics of both interfaces.

A class of material that could meet the requirements at the soft-to-hard tissue interface are self-assembling peptides (SAPs), as their physicochemical and mechanical properties can be tuned by rational design.[10] SAPs are shown to exhibit an adjustable biodegradability, a lack of immunogenicity, and a possibility to be applied with minimal invasive procedures (eg, injection into the periodontal pocket).[11] Previous reports have provided a first indication of the suitability of SAPs for periodontal therapy. For example, RADA16, a 16-amino acid β-sheet-forming SAP, is reported to facilitate attachment, proliferation, and migration of human periodontal ligament fibroblasts (HPDLFs) and induce the deposition of collagen type I and III, the main components of the periodontal ligament.[12] An animal study investigating the efficacy of RADA16 in periodontal regeneration demonstrated new bone and periodontal ligament-like collagen bundle formation, indicating periodontal regeneration.[13] Yet, despite the promising results, no SAP is available for treatment in the clinic.

Recently, the 11-amino acid SAPs (P11-SAPs) gained attention for the regeneration of dental hard tissue, as they have been shown to deposit calcium phosphate.[14–16] Moreover, it was demonstrated that these P11-SAPs form antiparallel β-sheet structures as well as higher-order structures such as fibrils and fibers under physiological conditions.[17–19] Thus, fibrillar P11-SAP hydrogels are suitable as scaffolds for tissue regeneration as they can self-assemble under physiological conditions and have adaptable SAP hydrogel stiffnesses brought on by modulating the peptide concentration and buffer composition.[17,19,20] In animal studies, P11-SAP scaffolds have been shown to lack immunogenicity[21] and to possess a high biocompatibility.[11,22] Hence, these P11-SAPs are promising candidates for a detailed in vitro evaluation of their suitability as scaffolds in soft and hard tissue regeneration. For this purpose, we tested four different P11-SAP systems. Two complementary systems (P11-13/14 and P11-28/29) were selected for their dual-syringe application mode, their favorable assembly kinetics, and their capacity as drug delivery carriers. Two single-component systems (P11-4, P11-8) were selected because they had previously been demonstrated as suitable matrices for mineralization.[23–25]

To this end, we investigated several physicochemical properties of P11-SAPs scaffolds that are known to govern their interactions with cells, ie, nanofibrillar architecture, surface charge, and swelling ratio in the context of their composition. As a consecutive step, the impact of the four P11-SAP scaffolds was tested with respect to their biocompatibility, cell morphology, adhesion, proliferation, and osteogenic differentiation by using cells involved in the periodontal regeneration (ie, HPDLFs, human calvarial osteoblasts [HCO]).

Materials and methods

Peptide hydrogel preparation

P11-SAPs, P11-4 (sequence: Table 1, peptide content 95%, ammonium salt), P11-8 [sequence: Table 1, peptide content 84.4%, trifluoroacetic acid (TFA) salt], P11-13 (sequence: Table 1, peptide content 78.5%, ammonium salt), P11-14 (sequence: Table 1, peptide content 74.6%, TFA salt), P11-28 (sequence: Table 1, peptide content 70.7%, TFA salt), and P11-29 (sequence: Table 1, peptide content 89.0%, ammonium salt) were purchased from CS Bio Company, Menlo Park, CA, USA. Release analytics were performed by HPLC and mass spectroscopy. Sodium chloride (NaCl) and Trizma® bases used for peptide buffer preparation were purchased

Table 1 P11-SAP composition and preparations in four different solutions

Peptide	Peptide composition	Peptide net charge	Solution A	Solution B
P11-4	QQRFEWEFEQQ	–2	55 mM Tris, pH 8	55 mM Tris, 192 mM NaCl, pH 6.8
P11-8	QQRFOWOFEQQ	+2	H_2O, pH 6	55 mM Tris, 236 mM NaCl, pH 8.5
P11-13	EQEFEWEFEQE	–2	100 mM Tris, 52 mM NaCl, pH 8	
P11-29	QQEFEWEFEQQ			
P11-14	QQOFOWOFOQQ	+2	55 mM Tris, 96 mM NaCl, pH 7	
P11-28	OQOFOWOFOQO			

from Sigma-Aldrich, Buchs, Switzerland. For each peptide system, buffer composition was adjusted to their specific physicochemical properties (Table 1).

Single-component P11-SAP hydrogels (P11-4 and P11-8) were prepared by dissolving the lyophilized peptide powder in 100 µL of solution A, thus obtaining a monomeric peptide solution. To induce self-assembly, 100 µL of solution B was added to the peptide monomer solution, adjusting the pH and thereby triggering self-assembly. Complementary P11-SAPs (P11-13/14 and P11-28/29) were dissolved separately in 100 µL of their peptide-specific solutions. Peptide pairs were mixed 1:1; eg, 100 µL P11-13 plus 100 µL P11-14 at equimolar concentrations to obtain a final volume of 200 µL P11-13/14 and a concentration of 10 mg/mL. A final concentration of 140 mM and a pH of 7.2–7.4 were adjusted for P11-4, P11-13/14, and P11-28/29 using 0.1 M NaOH or 0.1 M HCl (Sigma-Aldrich). For P11-8, a pH of 7.8–8.0 was adjusted using 0.1 M NaOH. For cell culture experiments, P11-SAP hydrogels were assembled overnight at 37°C, followed by 15 minutes of UV light exposure for hydrogel sterilization.

Analysis of nanofibrillar P11-SAP hydrogels

Scanning electron microscopy (SEM) studies

To analyze the nanofibrillar network architecture of the P11-SAP hydrogels in detail, SEM images, which had been previously prepared and recorded by us in the study of Koch et al,[17] were further processed by ImageJ version 2.0 using the DiameterJ plugin.[26] Therefore, the images were converted to black (background) and white (fibers) by the segmentation process and subsequently the M5 algorithm was applied. Parameters such as porosity, intersection density, and fiber diameter were calculated as a function of the DiameterJ software based on the segmented SEM images. Five SEM images were analyzed for each peptide system.

Zeta potential measurements for surface charge

Zeta potential measurements were performed with the Zetasizer Nanoseries (Malvern Instruments, Malvern, UK) to compare theoretical calculated SAP net charges with the monomer and fibril charges present at a pH of 3, 7, and 12 in 0.001 M NaCl. The pH of the different SAP solutions was adjusted by using 0.1 M NaOH and 0.1 M HCl. P11-SAP concentrations of 3 mg/mL together with a Zetasizer Clear Disposable Cell (Malvern) were used. Measurements were performed at room temperature (RT) directly after adjusting the pH. All experiments were done in triplicate.

Swelling ratio

To determine the P11-SAP hydrogel swelling behavior, samples were prepared at a peptide concentration of 15 mg/mL in 55 mM Tris buffer with additional NaCl (final salt concentration 140 mM) and were allowed to assemble overnight. PBS (Sigma-Aldrich) was added, and the hydrogels were incubated for 24 hours at RT. Samples were weighed before and after the swelling process to evaluate water uptake into the P11-SAP hydrogels. Finally, peptide hydrogels were lyophilized overnight with a Christ Lyophilizer (Christ® freeze dryer alpha 1-4 LSC, Germany) at –50°C and 1.0×10^{-3} Pa and weighed again to calculate the swelling ratios according to:

$$\mathrm{SW} = \frac{\mathrm{Ws} - \mathrm{Wd}}{\mathrm{Wd}}$$

where Ws and Wd are the weights of the hydrogels in the equilibrium swelling and in the freeze-dried state, respectively.[27]

Cell culture experiments

HPDLF and HCO were cultured up to 80%–90% confluency and in fibroblast or osteoblast medium (cells and media from ScienCell, Carlsbad, CA, USA), respectively, before they were passaged using 0.5% Trypsin-EDTA solution (Gibco™ by Life Technologies, Darmstadt, Germany). One passage took 5 days. Both cell types were used at passage 4 for every experiment. Cell culture medium was changed at passage 3 to the expansion medium DMEM (Gibco™ by Life Technologies) containing 10% FBS (PAN-Biotech, Germany) and 1% Penicillin (P)/Streptomycin (S) (Gibco® by Life Technologies) 2 days before they were seeded onto P11-SAP hydrogels.

Cytocompatibility testing of P11-SAP monomers and P11-SAP hydrogel extracts

To assess cell viability, P11-SAP monomer solutions were prepared at 1 mg/mL and 5 mg/mL in the respective cell culture media. HPDLF and HCO cells (6,800 cells per well) were incubated in a 96-well plate with peptide-containing medium for 24 hours at 37°C and analyzed afterward by using PrestoBlue® Viability Reagent (Invitrogen-Life Technologies). For this purpose, the cell culture supernatants were removed, and the PrestoBlue Viability Reagent was added to the cells, diluted 1:10 with cell culture medium, and incubated for 3 hours at 37°C. Finally, 100 µL of supernatant was placed into a new, 96-well plate and fluorescence was measured at

560 nm excitation and 590 nm emission with a fluorescence microplate reader (TECAN, Crailsheim, Germany).

The indirect cytotoxicity of P11-SAP hydrogel extracts was assessed according to the ISO 10993-5 standard test protocol. P11-SAP hydrogels were prepared at 20 mg/mL, as described above. P11-SAP hydrogels were incubated with 230 µL of the respective cell culture media for 24 hours at 37°C. Afterward, cell culture medium extracts were removed and further diluted in steps with fresh medium to achieve a final extract concentration of 10, 5, and 1 mg/mL. One hundred microliters per well of the original extract (20 mg/mL) and the diluted extracts were added to 6,800 cells (either HPDLF or HCO) per well of a 96-well plate (F-bottom, crystal clear, Greiner Bio-One, Frickenhausen, Germany). The standard cell cultures were grown on tissue culture polystyrene (TCPS) as a control. Sample extracts and controls were exposed to the cells for 24 hours at 37°C. Finally, lactate dehydrogenase (LDH) leakage from damaged cells and therefore cell vitality was determined by an LDH cytotoxicity test kit (Roche, Mannheim, Germany) according to the manufacturer's protocol. LDH activity was normalized by the quantification of the cell amount using crystal violet (Merck, Darmstadt, Germany) staining.

Cellular phenotype and cell adhesion in contact with P11-SAP hydrogels

To investigate the cellular phenotype, 200 µL of P11-SAP hydrogels was prepared at 15 mg/mL for P11-4/P11-8 and 10 mg/mL for P11-13/14/P11-28/29 in chamber slides (SPL Life Sciences, Gyeonggi-do, Korea) and were incubated overnight. Cells cultured on the uncoated chamber slide surfaces were taken as a control.

P11-SAP hydrogels were equilibrated with DMEM+10% FBS for 1 hour at 37°C. Afterward, 10,000 cells per well (HPDLF and HCO) were seeded in DMEM medium. After 24 hours, cells were washed twice with Dulbecco's PBS (DPBS) and fixed with 4% paraformaldehyde (Sigma-Aldrich, Taufkirchen, Germany) solution in DPBS for 20 minutes. To permeabilize the cell membranes, 0.1% Triton-X100-PBS (Fluka) was added for 5 minutes. After washing the cells twice with DPBS, cells were incubated with 1% BSA (Cell Signaling Technology, Frankfurt am Main, Germany) solution in DPBS for 30 minutes to reduce unspecific binding. Finally, Rhodamine-conjugated phalloidin (Thermo Fisher Scientific, Reinach, Switzerland) was added 1:40 (stock 1:1,000 in methanol) in PBS and incubated for 30 minutes in the dark. Cells were then washed three times prior to visualization with a confocal laser scanning microscope (LSM 780, Zeiss, Jena, Germany).

Furthermore, the adhesion of HPDLF and HCO cells on P11-SAP hydrogels was evaluated. Cells were seeded onto the 70 µL of P11-SAP hydrogel surfaces at 6,800 cells/cm^2 in DMEM. For the indirect quantification of the number of adhered cells, the supernatant including the nonadhered cells was carefully removed and the metabolic activity of the surface/hydrogel adhered cells was quantified using the PrestoBlue Viability Reagent as described by the manufacturer.

Metabolic activity of HPDLF and HCO

P11-SAP hydrogels (prepared at 15 mg/mL for P11-4/P11-8 and 10 mg/mL for P11-13/14/P11-28/29) were prepared in 96-well plates according to Table 1 and seeded with 6,800 cells/cm^2 (HPDLF and HCO) in DMEM supplemented with 10% FBS and 1% P/S. Cellularized P11-SAP hydrogels were cultured up to 14 days, whereby every third day the medium was replaced. Metabolic activity was assessed after 1, 3, 7, and 14 days of culturing using a resazurin-based, redox-sensitive assay PrestoBlue Viability Reagent.

Protein adsorption on P11-SAP hydrogels and its influence on cell phenotype

To investigate the cell phenotype as a function of the electrostatic interaction and the protein adsorption, 200 µL of P11-SAP hydrogels were prepared in chamber slides (SPL Life Sciences) at 15 mg/mL for the single-component SAPs (P11-4 and P11-8) and at 10 mg/mL for the complementary SAPs (P11-13/14 and P11-28/29). P11-SAP hydrogels were equilibrated with either serum-free DMEM or fibronectin- (from bovine plasma, Sigma-Aldrich) supplemented DPBS (PAN-Biotech) (300 µg/mL) for 1 hour at 37°C. Cells were seeded at a density of 10,000 per well and stained for actin cytoskeleton as described in "Cellular phenotype and cell adhesion in contact to P11-SAP hydrogels", cellular phenotype and adhesion. For the quantification of fibronectin adsorption on the P11-SAP hydrogels tested, hydrogels were prepared in SPL slides as described above. Fibronectin (300 µg/mL, DPBS) solution was incubated on peptide hydrogels for 1 hour at 37°C. P11-SAP hydrogels were then washed twice with ultrapure water to remove unbound fibronectin before being first mechanically disintegrated by pipetting up and down with a high viscosity pipet (Gilson, Mettmenstetten, Switzerland) and finally chemically disintegrated using 1 M NaOH or 1 M HCL. De-assembled P11-SAP hydrogels were homogenized three times for 10 seconds on ice using a Branson Sonifier 250 (Heinemann, Schwäbisch Gmünd, Germany). Afterward, samples were centrifuged at 12,000 rpm for 10 minutes at 4°C. To determine the amount of fibronectin, 10 μL of each sample was measured with the Qubit® Protein Assay (Thermo Fisher Scientific). As a 100% control, 10 μL of the initial fibronectin solution was measured. All experiments were done at least in triplicate. As a subsequent experiment, bound fibronectin on the complementary SAPs P11-13/14 and P11-28/29 (prepared at 100 μg/mL) was visualized by a primary rabbit polyclonal antifibronectin antibody (1:100, DPBS, Abcam, Cambridge, UK) incubated overnight at 4°C, followed by the incubation with a goat antirabbit-Alexa Fluor 594-conjugated antibody (1:100, DPBS, Abcam). Samples were washed with DPBS prior to, in between, and after antibody incubation. Samples were assessed with a confocal laser scanning microscope (LSM 780, Zeiss) using a 20× objective.

Cellular phenotype on hydrogels with different stiffnesses

To investigate cell phenotype as a function of reduced P11-SAP hydrogel stiffness, P11-13/14 and P11-28/29 were prepared at 5 and 10 mg/mL and first measured with an oscillatory amplitude sweep test using an Anton Paar MCR301 (Anton Paar, Buchs, Switzerland) rheometer equipped with a 10 mm diameter stainless steel parallel plate geometry at a 0.9 mm measuring gap. To determine the HPDLF and HCO phenotype, 10,000 cells of each cell type were incubated in chamber slides (SPL Life Sciences) for 24 hours on 200 μL of P11-13/14 and P11-28/29 P11-SAP hydrogels (5 mg/mL and 10 mg/mL). Staining for actin cytoskeleton was performed according to section "Cellular phenotype and cell adhesion in contact to P11-SAP hydrogels."

Analysis of osteogenic differentiation

Quantification of ALP activity

The ALP activity was analyzed by the colorimetric ALP assay kit (Abcam). Cell lysate samples at 1, 7, and 14 days of incubation on P11-4 and P11-8 peptide hydrogels (15 mg/mL) were investigated (lysate harvesting as described for the Milliplex assay above). Staining was performed according to the manufacturer's instructions. The absorbance was read at 450 nm with a fluorescence microplate reader (TECAN).

Quantification of osteoprotegerin (OPG)

For the quantification of the osteogenic marker OPG, 200 μL P11-4 and P11-8, P11-SAP hydrogels were prepared at 15 mg/mL in chamber slides. Complementary P11-SAP hydrogels (P11-13/14; P11-28/29) were not considered as appropriate for further studies due to the lower metabolic activity after 14 days of HCO culture. HCO were seeded on top of the P11-SAP hydrogels at a density of 10,000 cells/cm^2. Osteogenic differentiation of HCO was induced by exposure to osteogenic differentiation medium containing DMEM 10% FBS, 1% P/S, 1 μM dexamethasone (Sigma-Aldrich), 250 μg/mL ascorbate (Sigma-Aldrich), and 10 mM β-glycerophosphate (Sigma-Aldrich).

The medium was changed every 2 to 3 days. Undifferentiated HCO grown in expansion medium was used as control. After 1, 7, and 14 days, cell culture supernatants were collected and stored at –20°C for further analysis. To analyze the total secretion of osteogenic markers, 130 μL of P11-SAP hydrogel matrices containing differentiated and undifferentiated HCOs were dissolved by transferring the gels in 1.5 mL low protein-binding tubes (Eppendorf, Hamburg, Germany) with a cell scraper, followed by the addition of 130 μL of cell lysis buffer and either 1 μL of 1 M NaOH to de-assemble P11-4 hydrogels or 1 M HCl to de-assemble P11-8 hydrogels. To ensure complete cell lysis, the tubes were agitated for 30 minutes at 4°C. Afterward, cell lysates containing de-assembled P11-SAP hydrogels were homogenized (Branson Sonifier 250, Heinemann) three times for 10 seconds on ice. Cell debris was eliminated by centrifugation at 12,000 rpm for 10 minutes at 4°C. Finally, cell culture supernatants and supernatants extracted from cell lysates were thawed and analyzed by the Milliplex MAP Human Bone Magnetic Bead Kit (Merck Millipore, Germany) according the manufacturer's protocol. Samples were measured with a Bio-Plex 200 system (Bio-Rad, Germany).

Quantification of mineralization

For the quantification of the calcium deposition of HCOs on P11-4 and P11-8, P11-SAP hydrogels, cells were cultured up to 30 days in osteogenic differentiation medium or expansion medium as a negative control. P11-SAP hydrogels were prepared in a 96-well plate as described in "Metabolic activity of HPDLF and HCO" (metabolic activity). Medium was replaced every third day during cultivation. After 1 and 30 days, the medium was removed, and the cell-seeded P11-SAP hydrogels were rinsed twice with PBS. Subsequently, the hydrogels were fixed with 4% PFA in PBS for 10 minutes, followed by rinsing them twice with ultrapure water. One hundred microliters per well o-cresolphthalein complexone (Sigma-Aldrich) solution at 0.1 mg/mL was added and incubated for 5 minutes at RT. Afterward, 100 μL 2-amino-2-methyl-3-propanolbuffer (1.5 M, pH 10.8, Sigma-Aldrich) with o-cresolphthalein complexone (Sigma-Aldrich) were added per well and incubated for 15 minutes. Finally, 100 µL of supernatant was transferred to a new 96-well plate and analyzed at 580 nm using a fluorescence microplate reader (TECAN).

Statistics

All experiments were done with cells from three independent donors and with three technical replicates per run. Data are presented by mean±SD. To test for significant differences between groups, a one-way or two-way ANOVA followed by Dunnett's or Tukey's multiple comparison post hoc test was performed using GraphPad Prism version 6.00 for Windows. A *P*-value of ≤ 0.01 was considered significant.

Results

Nanofibrillar network architecture and physicochemical characterization of P11-SAP hydrogels

SEM images of nanofibrillar P11-SAP hydrogels, which were prepared and examined in the study of Koch et al,[17] were further processed and analyzed with software-supported image analysis to gain more insight into the fibrillar network properties. Prior to the calculation of the different parameters, the images were converted and segmented to black and white pictures as presented in Figure 1. The single-component P11-SAPs P11-4 (Figure 1A) and P11-8 (Figure 1B) formed a relatively homogeneous nanofibrillar network structure with a majority of uniform mesh widths. The complementary P11-SAPs P11-13/14 (Figure 1C) and P11-28/29 (Figure 1D) developed more heterogeneous fibrillar networks with an irregular mesh width distribution.

Analysis of the SEM images with the ImageJ plugin DiameterJ was performed to evaluate the following parameters: fiber network porosity (%), intersection density (number of intersections/µm^2), and mean fiber diameter (in nm) (Table 2). The network porosity of P11-4 and P11-8 was found to be 46%, which is about 14% higher in relation to the complementary P11-SAPs P11-13/14 and P11-28/29. The network density (ie, the intersection density in number/µm^2) was almost identical for single-component P11-SAPs, ie, 62.1/µm^2 for P11-4 and 60.6/µm^2 for P11-8. For the complementary P11-SAPs P11-28/29, a two-fold higher intersection density was observed with 106.9±24.5 number/µm^2.

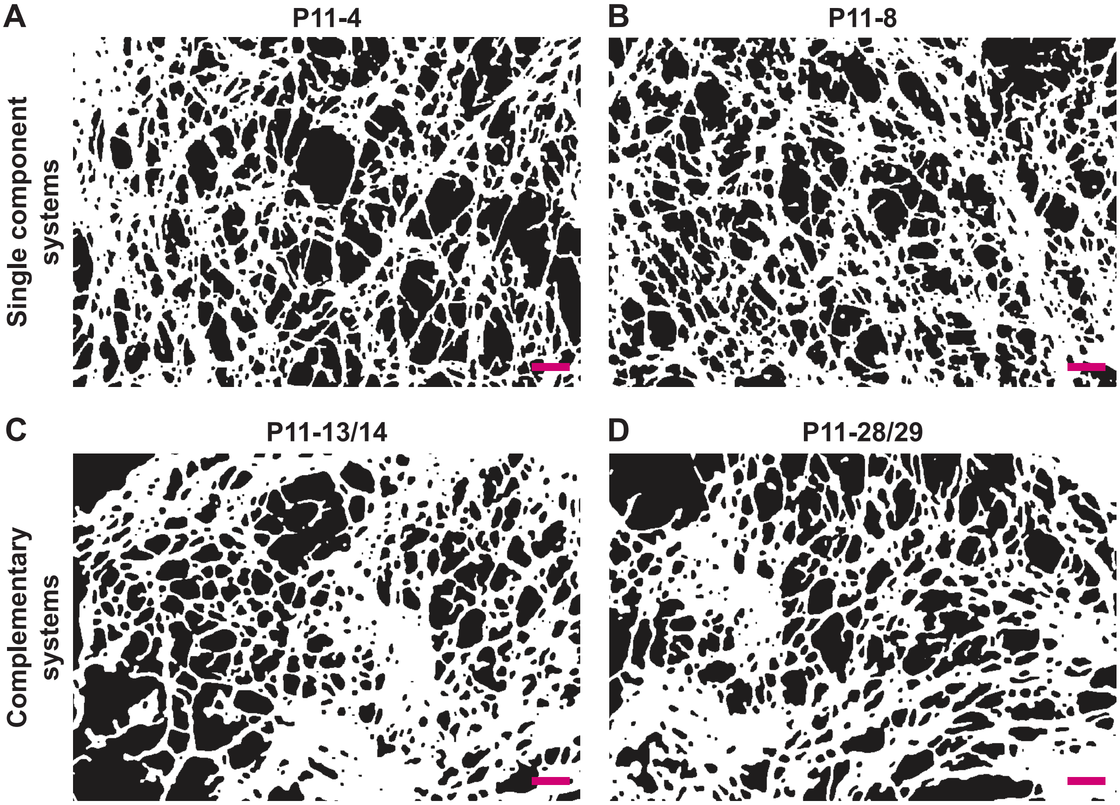

Figure 1 Processed SEM images of fibrillar P11-SAP hydrogels.

Note: (**A**) P11-4, (**B**) P11-8, (**C**) P11-13/14, and (**D**) P11-28/29 (peptide hydrogels were prepared at 15 mg/mL, scale bar 200 nm, images were converted to black and white pictures).

Abbreviation: SEM, scanning electron microscope.

Table 2 Analysis of nanofibrillar P11-SAP hydrogel SEM images

	Fiber network porosity (%)	Intersection density (number/μm²)	Mean fiber diameter (nm)
P11-4	46±1.0	62.1±6.9	41.0±1.2
P11-8	46±1.0	60.6±1.6	40.8±0.5
P11-13/14	31±7.0	79.7±8.6	44.5±5.2
P11-28/29	34±5.0	106.9±24.5	36.8±2.7

Note: The parameters "porosity," "intersection density," and "fiber diameter" were assessed by the conversion of SEM images into black and white pictures and further processed and analyzed using Diameter J.
Abbreviation: SEM, scanning electron microscope.

Furthermore, the image analysis identified a relative homogeneous fiber diameter for the single-component P11-SAPs with 41±1.2 nm for P11-4 and 40.8±0.5 nm for P11-8. The complementary P11-SAPs' fiber diameters showed a higher variability with 44.5 nm (±5.2 nm) for P11-13/14 and 36.8 nm (±2.7 nm) for P11-28/29.

The P11-SAP hydrogels were further analyzed regarding the physicochemical characteristics of surface charge and swelling ratio (Figure 2). To determine the surface charge, zeta potential measurements were performed as a function of pH (Figure 2A). At pH 3, all P11-SAPs revealed a positive zeta potential, whereas at pH 12 all P11-SAPs displayed a negative zeta potential. At pH 7, P11-SAPs with a negative surface "–2"-net charge (P11-4; P11-13/14) showed a negative zeta potential, whereas a positive zeta potential for P11-SAPs with a "+2"-net charge (P11-8; P11-28/29) was determined.

The theoretically calculated surface net charges (at pH 7) of the P11-SAPs were "–2" for P11-4 and P11-13/14 and "+2" for P11-8 and P11-28/29 (Table 1). Thus, the measured zeta potentials were clearly different from the calculated values. For example, P11-4 and P11-13/14 both have a calculated surface "–2"-net charge at pH 7 but a zeta potential difference by a factor of 1.5. Similarly, P11-8 and P11-28/29, with a "+2"-surface net charge, revealed a positive zeta potential, although it varied by a factor of 3.

Based on the hydrophilic nature of the tested P11-SAPs hydrogels, they are supposed to retain large amounts of water in their three-dimensional structure. Therefore, swelling ratios were measured at the equilibrium state after 24 hours in PBS (Figure 2B). Swelling ratios for the single-component P11-SAP hydrogels were found to be higher compared with the complementary P11-SAP hydrogels, ie, for P11-4 and P11-8, a swelling ratio of 37.8%±1.3% and 43.8%±4.7% was measured, respectively. In contrast, the complementary P11-SAP hydrogels P11-13/14 and P11-28/29 resulted in swelling ratios of 30.0%±0.6% and 26.4%±3.4%, respectively.

Impact on cellular reactions

Cytocompatibility

Initially, the cytocompatibility of the disassembled, monomeric P11-SAPs dissolved in cell culture medium was analyzed in different concentrations on HPDLF (Figure 3A) and HCO by measuring the metabolic activity after 24-hour incubation by a resazurin-based, redox-sensitive assay. The incubation of P11-SAP monomers, prepared at 1 mg/mL and 5 mg/mL in cell culture medium, showed only minor effects on the metabolic activity of HPDLF. At higher concentrations (5 mg/mL), P11-13 and P11-28 induced a slight but statistically significant decrease of the metabolic activity of about 15%. The metabolic activity of the osteoblasts showed a similar trend without statistically significant differences (Figure S1A). Furthermore, the cytocompatibility of the different P11-SAPs

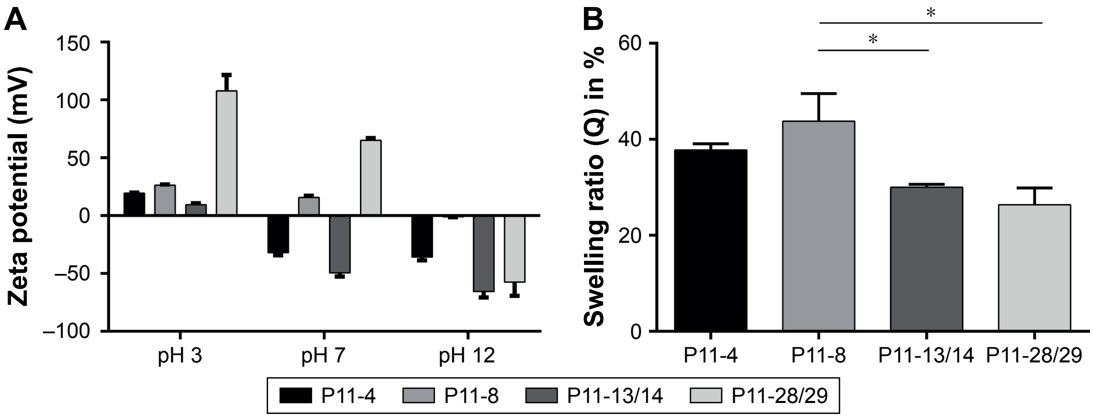

Figure 2 Analysis of surface charge and swelling ratio of the P11-SAPs.
Notes: (**A**) Surface charge, measured by zeta potential, was determined as a function of pH for P11-SAPs in monomeric and fibrillar state (P11-SAP concentration of 3.0 mg/mL, n=3, measured at pH 3, 7, and 12). (**B**) Swelling ratios measured after 24-hour incubation in PBS (P11-SAP concentration of 15 mg/mL, n=3, *$P \leq 0.01$).
Abbreviation: P11-SAP, 11-amino acid self-assembling peptides.

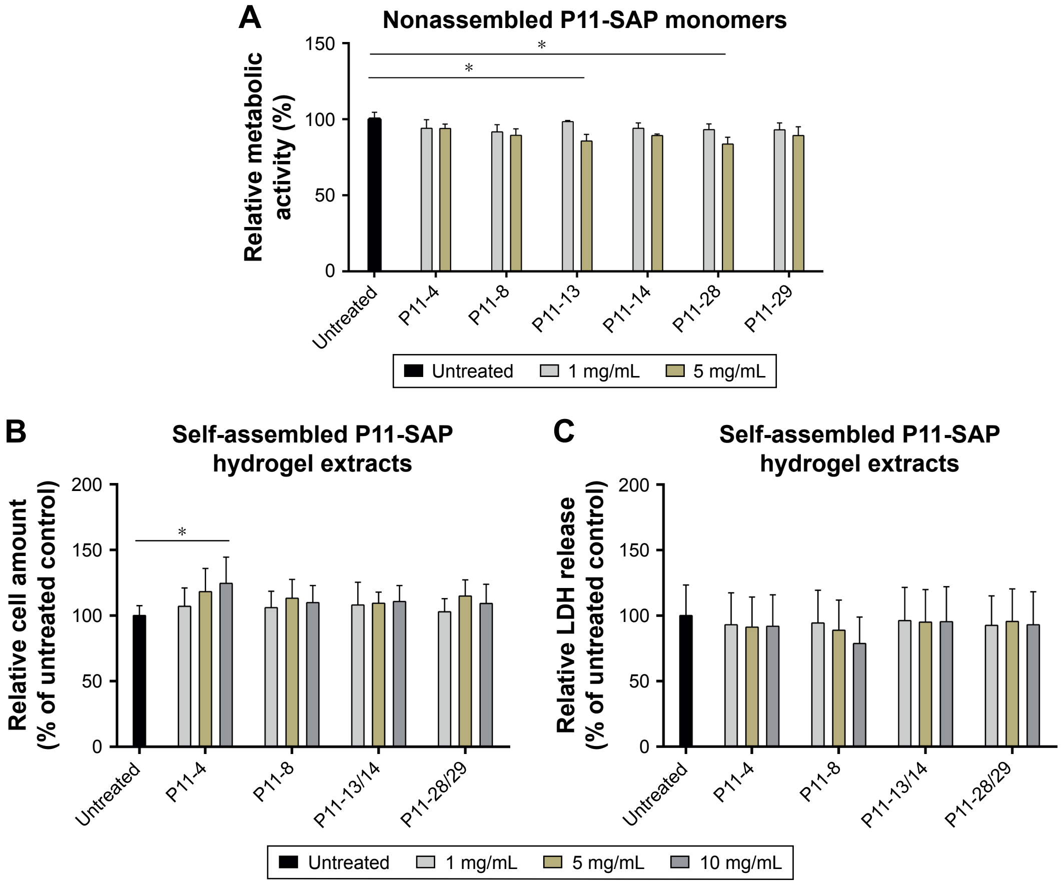

Figure 3 Testing cytocompatibility of monomeric P11-SAP solution and extracts of P11-SAP hydrogels in HPDLF.

Notes: (**A**) Metabolic activity of HPDLF exposed for 24 hours with the P11-SAP monomers (concentrations: 1 and 5 mg/mL, PrestoBlue® Cell Viability Reagent, in percent compared with untreated control, n=3, *$P \leq 0.01$). (**B**) Cell amount of HPDLF cells exposed to extraction products of different P11-SAP hydrogels (after 24 hours, 1, 5, and 10 mg/mL, in percent compared with untreated control, n=3, *$P \leq 0.01$, determined by crystal violet staining) and (**C**) LDH release of HPDLF cells exposed to extraction products of P11-SAP hydrogels (after 24 hours, 1, 5, and 10 mg/mL, in percent compared with untreated control, n=3, *$P \leq 0.01$, measured with LDH cytotoxicity test kit).

Abbreviations: HPDLF, human periodontal ligament fibroblast; LDH, lactate dehydrogenase; P11-SAP, 11-amino acid self-assembling peptide.

was investigated for the self-assembled state (ie, as hydrogels) (Figure 3B and C). For this purpose, extracts of the P11-SAP hydrogels were obtained in cell culture medium and HPDLF and HCO were exposed for 24 hours with extracts prepared at 1, 5, and 10 mg/mL and then analyzed for the cell number and cytotoxicity. The extracts did not affect the cell number except for the extracts of the P11-SAP hydrogel P11-4 (10 mg/mL), which showed a slight but statistically significant increase of HPDLF cell numbers to 124.6%±19.9% (Figure 3B); in HCO, no significant differences were detectable (Figure S1B). To investigate the potential of highly charged P11-SAP hydrogels to interact with and to disrupt cell membranes, an LDH cytotoxicity assay was performed. Cytotoxicity of the P11-SAP hydrogel extracts was examined indirectly by the quantification of the LDH release of HPDLF and HCO after the extract exposure. There was no deviation identified in comparison with the untreated control (Figures 3C and S1C).

Cell morphology on SAP hydrogels

Furthermore, the cells were brought into direct contact with the four P11-SAP hydrogels. P11-SAP concentrations of 15 mg/mL for P11-4 and P11-8 and 10 mg/mL for P11-13/14 and P11-28/29 were chosen for stability and handling reasons. The cell phenotypes were analyzed by actin cytoskeleton staining with phalloidin-TRITC (tetramethylrhodamine), 24 hours after seeding HPDLF and HCO onto P11-SAP hydrogels in the presence of 10% calf serum in cell culture medium. Nuclear staining could not be executed, as P11-SAP hydrogels possess highly intrinsic autofluorescence (Figure S2). Cells cultured on the control surface (cell culture-adequate SPL glass slides) displayed a spindle-shaped, spread phenotype with long actin fibers. The growth of HPDLF and HCO on P11-4 and P11-8 hydrogels resulted in spindle-shaped, outspread cell phenotypes (Figure 4A). In contrast, HPDLF and HCO in contact with P11-13/14 hydrogels developed a roundish, nonspread phenotype.

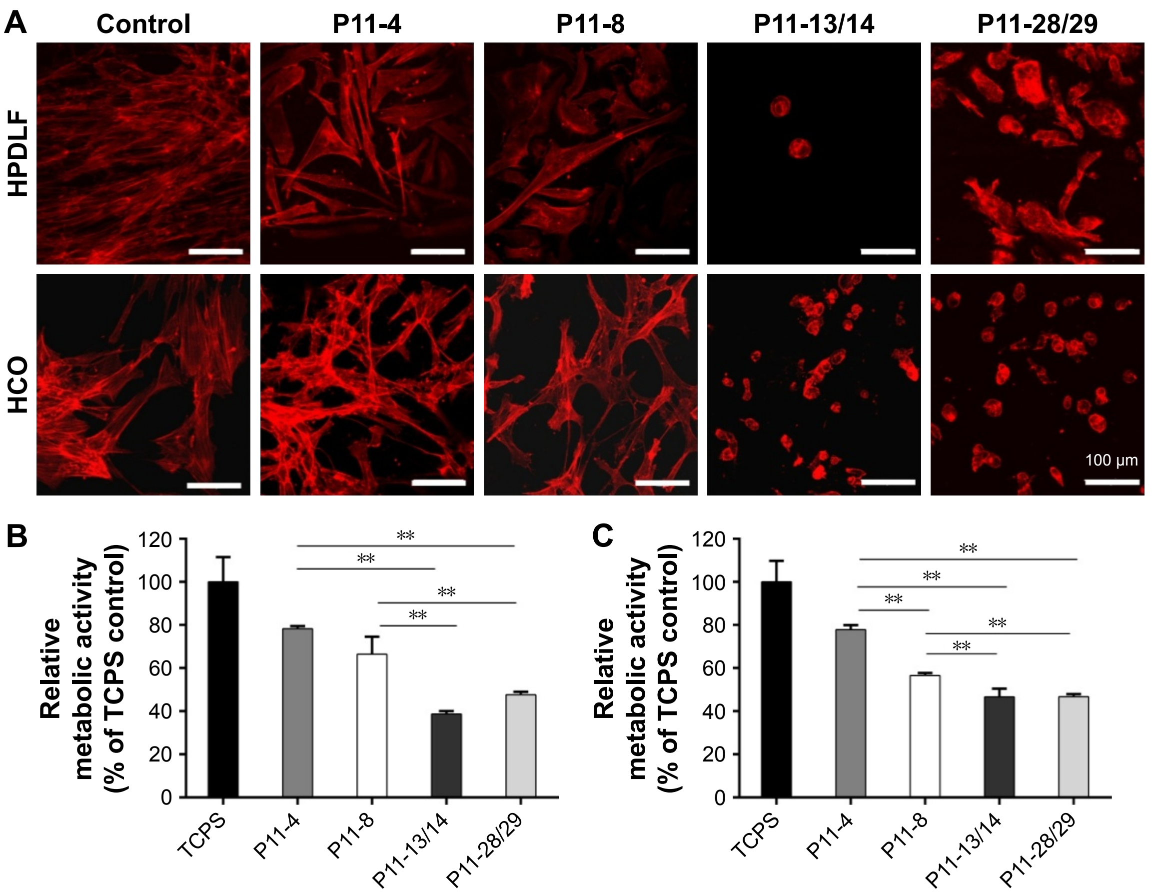

Figure 4 Cellular phenotype and metabolic activity of HPDLF and HCO on P11-SAP hydrogels in the presence of bovine serum (10%).

Notes: (**A**) Fluorescent depiction of the actin cytoskeleton in HPDLF and HCO (after 24 hours, scale bar 100 µm, n=6). (**B**) Metabolic activity of HPDLF and (**C**) HCO (PrestoBlue® assay performed after 24 hours, % to TCPS control, n=3, ***P*≤0.001).

Abbreviations: HCO, human calvarial osteoblasts; HPDLF, human periodontal ligament fibroblast; P11-SAP, 11-amino acid self-assembling peptide; TCPS, tissue culture polystyrene.

The phenotype of HPDLF on P11-28/29 was more heterogeneous with parallel existing roundish and spindle-shaped cells. HCO grown on P11-28/29 hydrogels developed only roundish, nonspread phenotypes (Figure 4A).

The overall metabolic activity of the attached HPDLF and HCO population was quantified at the same time (24 hours after seeding). In both cell types, the overall metabolic activity was found to be lower on all P11-SAP hydrogels compared with the control on TCPS. The highest metabolic activity of HPDLF was observed on P11-4 (78.2% of TCPS control) followed by P11-8 with 66.4% (Figure 4B). The metabolic activity of HPDLF was even lower on P11-13/14 (38.7%) and P11-28/29 hydrogels (47.6%). However, the comparison of the complementary P11-SAP hydrogels revealed that HPDLF metabolic activity was higher on P11-28/29 than on P11-13/14. A similar metabolic activity pattern was shown for HCO, although there was no difference detected between P11-13/14 and P11-28/29 hydrogels (Figure 4C). The reduced overall metabolic activity of the cells in direct contact with the P11-SAP hydrogels implies a lower cell attachment, as in the TCPS control, confirming the optical impression estimated by the microscopic phenotype analysis.

Fibronectin adsorption to SAP hydrogels

The phenotype of cells in contact with P11-SAP hydrogels was also tested under serum-free conditions and in the presence of fibronectin. HPDLF and HCO phenotypes were not spread in contact with P11-SAP hydrogels under serum-free and noncoating conditions. The precoating of P11-SAP hydrogels with fibronectin (300 µg/mL) prior to cell seeding induced outspread, spindle-shaped HPDLF with long actin fibers (Figure 5A) on P11-4, P11-8, and P11-28/29 hydrogels. Only on P11-13/14 hydrogels did the cells not spread at all. Seeding of HCO on fibronectin-coated surface resulted in a roundish, nonspread phenotype on P11-13/14 and P11-28/29 (Figure S3). To attain a deeper understanding of the varying cellular reactions after fibronectin coating,

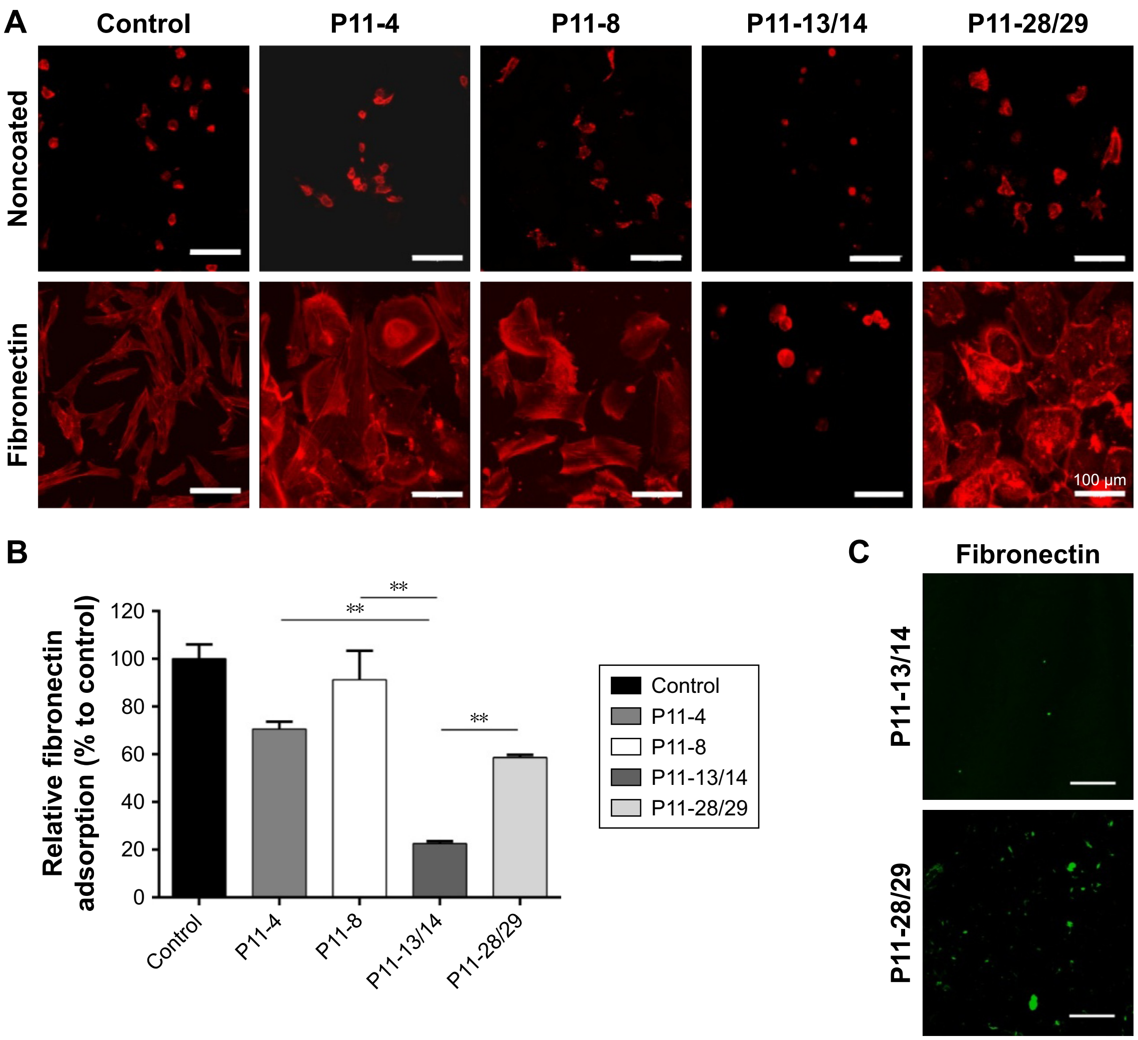

Figure 5 Fibronectin coating of P11-SAP hydrogels.

Notes: (**A**) Fluorescent depiction of the actin cytoskeleton of HPDLF cultured for 24 hours on P11-SAP hydrogels under noncoated/serum-free conditions or precoated with fibronectin (confocal microscopy, fibronectin concentration 300 µg/mL, scale bar 100 µm). (**B**) Quantification of fibronectin adsorption on P11-SAP hydrogels after 1-hour incubation with fibronectin-supplemented PBS (300 µg/mL, n=3, $^{**}P\leq 0.001$). (**C**) Immunostaining of bound fibronectin on P11-13/14 and P11-28/29 hydrogels (confocal microscopy, scale bar 100 µm).

Abbreviations: HPDLF, human periodontal ligament fibroblast; P11-SAP, 11-amino acid self-assembling peptide.

we analyzed the fibronectin adsorption after 1 hour of incubation on P11-SAP hydrogels (Figure 5B). Protein adsorption on TCPS surfaces was taken as a control and set to 100%. Fibronectin adsorption was highest on the single-component systems P11-8 (91.2%) and P11-4 (58.9%) compared with the complementary P11-SAP hydrogels P11-28/29 at 58.9% and P11-13/14 at 22.5%. Moreover, the immunofluorescent, microscopic analysis of fibronectin adsorption confirmed the higher adsorption degree on P11-28/29 hydrogels compared with P11-13/14 hydrogels (Figure 5C).

To evaluate whether the cellular phenotype was affected by the P11-SAP hydrogel stiffness, different P11-SAP concentrations were tested. The adjusted hydrogel stiffnesses, obtained by changing the peptide concentration from 10 to 5 mg/mL, was G′=6.8 and 1.0 kPa for P11-13/14 and G′=1.2 and 0.4 kPa for P11-28/29 (Figure 6A). For both complementary P11-SAP hydrogels P11-13/14 and P11-28/29, the lower peptide concentrations and thus induced lower stiffnesses impaired cell spreading, resulting in roundish cells. Thus, different hydrogel stiffness could not change the cellular phenotypes toward a spread morphology (Figure 6B). Hence, neither protein adsorption (Figure 5) nor peptide concentration and thus hydrogel stiffness (Figure 6) led to a change of HCO phenotype on P11-13/14 and P11-28/29 hydrogels after 24 hours.

Osteogenic differentiation on SAP hydrogels

Finally, we investigated the capacity of P11-SAP hydrogels regarding the growth and osteogenic differentiation of HCO in long-term experiments. For this purpose, HCOs were

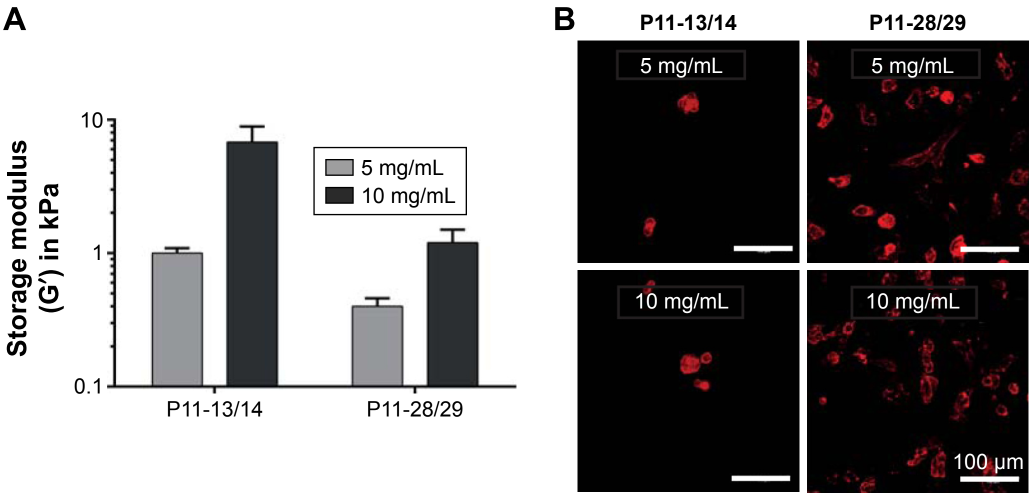

Figure 6 Hydrogel stiffness and phenotype of HCO in contact with P11-SAP hydrogels of different concentrations.
Notes: (**A**) Hydrogel stiffness displayed as storage modulus of P11-13/14 and P11-28/29 hydrogels (at 5 and 10 mg/mL). (**B**) HCO phenotypes were assessed on P11-13/14 and P11-28/29 hydrogels (5 and 10 mg/mL, after 24 hours) by staining the actin cytoskeleton (scale bar 100 µm).
Abbreviations: HCO, human calvarial osteoblasts; P11-SAP, 11-amino acid self-assembling peptide.

cultivated for up to 30 days and the metabolic activity was analyzed as an indirect measure for the development of the cell number over time. Metabolic activity of the TCPS control on day 1 was taken as 100%. The highest metabolic activity (189.3%) and thus an indication for the highest cell number were found after 14 days of cultivation of HCO on P11-4 hydrogels (Figure 7A). HCO cultivation on the complementary P11-SAP hydrogels, P11-13/14 and P11-28/29 resulted in metabolic activity rates of 31.7% and 16.7%, respectively, indicating low cell numbers. Long-term cultivation of HPDLF on P11-SAP hydrogels (data not shown) revealed high metabolic activity rates for P11-4 (182.4%) and P11-8 (145.5%) after 14 days.

Because the P11-4 and P11-8 hydrogels allowed the highest rates of cell adhesion and cell amount, we selected them for further osteogenic differentiation experiments with HCO. To this end, we quantified ALP activity as a marker for osteogenic differentiation (Figure 7B). ALP activity after 7 and 14 days was increased in HCO cultured on TCPS. However, HCO in contact with P11-4 and P11-8 hydrogels showed significantly increased ALP activity after 7 and 14 days cultivation compared with the TCPS control. ALP activity was found to be three times higher for P11-4 after 14 days and four times higher for P11-8 compared with TCPS control surfaces. Moreover, ALP activity at day 14 was significantly higher (by a factor of 1.5) on P11-8 than on P11-4 hydrogels.

The osteogenic marker OPG was analyzed after osteogenic stimulation of HCO on TCPS and P11-SAP hydrogels (Figure 7C). A significantly higher OPG concentration was measured for HCO cultured for 14 days on TCPS compared with P11-4 and P11-8 hydrogels. For P11-SAP hydrogels, OPG levels in cell lysates were found to be significantly higher on P11-8 than on P11-4 hydrogels. As a further marker for osteogenic differentiation, extracellular calcium deposition was measured after 30 days in HCO under osteogenic stimulation (Figure 7D). Already after 1 day, significant calcium amounts were detectable on P11-4 and P11-8 hydrogels. Moreover, calcium deposition was found to be significantly higher (factor of 1.4) after 30 days of incubation on P11-4 and P11-8 hydrogels compared with HCO grown on TCPS.

Discussion

In the present study, we analyzed four β-sheet forming P11-SAP hydrogels (P11-4, P11-8, P11-13/14, and P11-28/29) regarding their physicochemical properties and capacities to act as scaffolds for periodontal therapy by means of in vitro testing with cells involved in periodontal tissue regeneration.

As SAPs can be rationally designed to yield tailored hydrogel stiffness and meet specific tissue elasticities, they are promising materials in biomedical applications, eg, for periodontal therapy.[28] SAPs are shown to have compatible fiber diameters similar to extracellular matrix (ECM) molecules.[12,29] In previous studies, it was demonstrated that each individual SAP composition will affect the hydrogel characteristics regarding fiber morphology, surface charge, and stiffness. Therefore, we analyzed the nanofibrillar architecture, surface charge, and swelling ratio of the four P11-SAP hydrogels. The mean fibril diameters of all assembled nanofibrillar P11-SAP hydrogels (36.8–44.5 nm) were found to be in a range similar to that reported for the naturally

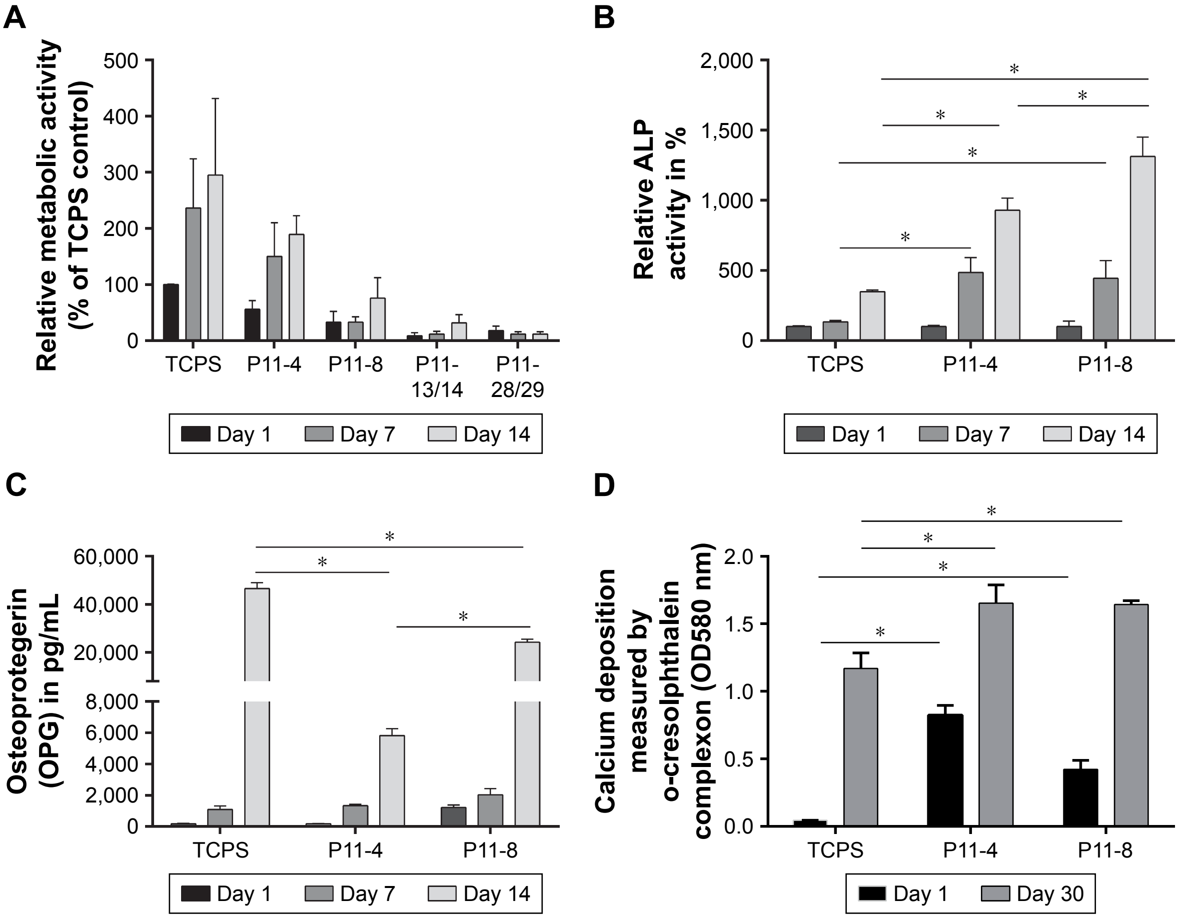

Figure 7 Analysis of metabolic activity and osteogenic differentiation capacities of HCO on P11-SAP hydrogels in long-term culture.

Notes: (**A**) Metabolic activity of HCO on TCPS or P11-4/P11-8 hydrogels (assessed after 1, 7, and 14 days by PrestoBlue® assay, % of TCPS control on day 1, n=3, 15 mg/mL peptide concentration). (**B**) ALP activity (% of TCPS control on day 1, assessed on days 1, 7 and 14, n=3), (**C**) amount of OPG on days 1, 7, and 14 (n=3), (**D**) calcium deposition (measured on days 1 and 30) (all data were normalized to metabolic activity, $^{*}P \leq 0.01$).

Abbreviations: HCO, human calvarial osteoblasts; P11-SAP, 11-amino acid self-assembling peptide; TCPS, tissue culture polystyrene.

occurring ECM proteins, ie, collagen fibrils in the range of 30–300 nm in diameter[30] or fibrillin, which forms microfibrils of about 10 nm.[31]

In our analyses, the nanofibrillar network architecture of the single-component systems (P11-4, P11-8) was found to be different compared with the two-component P11-SAP systems (P11-13/14, P11-28/29) regarding their intersection density and pore size. The discrepancy between the two P11-SAP systems cannot be explained directly by different hydrogel stiffnesses because the hydrogels with the higher intersection density had lower hydrogel stiffness, as was analyzed in a previous study.[17] Because, for example, the P11-28/29 hydrogels revealed the highest intersection density but lowest hydrogel stiffness, we conclude that the individual fiber strength affects the final hydrogel stiffness of the P11-SAP systems rather than the intersection density due to a denser packaging of a fibril. This phenomenon has also been described in a previous study that investigated the effect of increased ionic strength on the elastic modulus of peptide hydrogels.[32]

It is known that hydrogel stiffness can influence cellular responses, and thus, it is a crucial parameter to address a tissue regeneration purpose.[4,5] Engler et al[33] showed that nondifferentiated MSC specify lineage and commit to phenotypes with extreme sensitivity to the corresponding tissue-level elasticity. They could show that very soft matrices mimicking brain tissue induced neurogenic differentiation, whereas stiffer matrices induced myogenic differentiation and comparatively rigid matrices induced osteogenic differentiation. The mechanical properties of tissue niches vary from 0.1 kPa of soft brain tissue to >30 kPa of rigid calcifying bone. The hydrogel stiffness of the four P11-SAP systems was reported by Koch et al[17] to be in the range of 1.7–31.5 kPa and thus matches soft to hard tissue elasticities.

One prerequisite for the application of a biomaterial is its cytocompatibility. The cytocompatibility of the four selected P11-SAPs was tested in vitro in human fibroblasts and osteoblasts of the periodont because these cell types are essential for the periodontal regeneration process. The P11-SAP monomers as well as P11-SAP hydrogel extracts cultured with HPDLF and HCO did not show cytotoxic reactions and can thus be classified as cytocompatible. The slight reduction of the metabolic activity for HPDLF induced by P11-13 and P11-28 monomers at high monomer concentrations (5 mg/mL) might be explained by the release of the counterions of P11-13 (78.5%; ammonium salt) and P11-28 (70.7%; TFA). TFA has been shown to impair the proliferation of L929 fibroblasts.[23] Previous reports have already shown the biocompatibility of P11-SAP hydrogels on human dermal fibroblasts and murine cells.[11,34]

The process of periodontal regeneration induced by implanted or injected biomaterials is highly complex and involves several characteristic events such as cell proliferation, migration differentiation, and tissue maturation.[35] An early step in the cascade of tissue regeneration after the implantation of a biomaterial is the adhesion of cells to the biomaterial.[5] The cell adhesion characteristics influence the capacity of the cells to proliferate and differentiate. The cellular phenotype is known to be controlled by the adsorption of soluble proteins from blood or the surrounding wound fluid and is closely related to the biomaterials topography, chemistry, or surface charge.[36] Fibronectin is a major component of the ECM that regulates cell adhesion and ECM interactions.[37,38] Furthermore, fibronectin binds to a variety of different artificial materials and can potentially influence cellular responses rather than the material surface itself.[38,39] Thus, we decided to investigate the effect of fibronectin adsorption on P11-SAP hydrogels and subsequently on the cellular phenotype.

In previous studies, it has already been shown that fibronectin adsorbs rather on a hydrophobic than on hydrophilic surfaces.[40,41] The isoelectric point of fibronectin is about 5.5–6.3 and is thus negatively charged under physiological conditions.[42,43] As fibronectin consists of acidic as well as of basic surface residues, it can bind to positively or negatively charged biomaterials, but with different protein conformation.[44,45] In the present study, fibronectin bound to all P11-SAP hydrogels tested, but preferably to P11-4 and P11-8. As all four P11-SAP systems contain several polar amino acid residues (ie, Gln, Glu, Orn), they display similar hydrophilic surfaces. Although the theoretical calculated net surface charges (+2/–2) are similar for all P11-SAPs tested, their surface charge measured by zeta potential was different for positive (P11-8, P11-28/29) and negative (P11-4, P11-13/14) P11-SAP fibrils. Thus, the reduced fibronectin adsorption on P11-13/14 hydrogels can be explained by the high zeta potential of P11-13/14 fibrils (–49.5±2.5 mV) compared with P11-4 (–31.9±1.8 mV), resulting in a higher repulsion of fibronectin and thus lower protein adsorption. Similar effects were reported by Cai et al[46] in their study of fibrinogen binding on titanium films displaying COOH functional surface groups. These authors observed that a lower zeta potential of a substrate leads to higher charge repulsion and thus lower fibrinogen adsorption.

The adsorption of fibronectin to four P11-SAP hydrogels was found to be reflected by variable cell adhesion characteristics and morphologic appearance of both cell types tested. HPDLF was extensively spread on the hydrogels with the high fibronectin adsorption properties (P11-4 and P11-8 hydrogels), whereas the cells were not spread on hydrogels with low fibronectin adsorption, such as on P11-13/14 hydrogels. Similar effects were shown for cellular spreading in the presence of FBS. Because cell adhesion and spreading are important in the first phase of tissue–biomaterial interaction after implantation in vivo, and because cell adhesion and spreading depends on the protein-binding capacity of a material, we assumed that P11-4 and P11-8 hydrogels are the most suitable candidates to study long-term cultivation and cellular differentiation.

Cell proliferation is another key parameter in the process of tissue regeneration.[47] We could show that the amounts of HPDLF and HCO on P11-SAP hydrogels were highest on P11-4 and P11-8. Because these hydrogels also showed high fibronectin adsorption, we assumed a direct connection between high fibronectin adsorption, initial cell adhesion, and high proliferation rates. Based on these results, P11-4 and P11-8 hydrogels were again chosen as the best candidates for the differentiation study with HCO.

Periodontal regeneration of the alveolar bone or the periodontal cementum is accompanied by hard tissue formation, ie, bone and cementum. To evaluate the osteogenic potential of P11-4 and P11-8 hydrogels, we induced HCO for osteogenic differentiation in contact with the hydrogels. HCO differentiation was measured by ALP activity, OPG expression, and calcium amount of the ECM. After 14 days of culture, ALP activity and OPG were significantly increased on P11-8 hydrogels compared with P11-4 hydrogels. The high osteogenic differentiation potential of P11-8 hydrogels might be based on its surface chemistry. P11-8 contains three positively charged ornithines, whereas P11-4 contains three negatively charged glutamic acids. It was already shown in the study of Griffin et al[7] that adipose-derived mesenchymal stem cells can react to modifications of plasma-modified scaffolds using NH_2 and COOH residues by changes in ALP activity and osteogenic gene expressions. Thus, our results are in good alignment to the study of Griffin et al,[7] demonstrating a higher osteogenic differentiation potential on NH_2 than on COOH-modified surfaces. The initial degree of calcium deposition after 1 day of culture was distinctly higher on P11-4 compared with P11-8 hydrogels. This difference in initial calcium deposition may be explained by the diverging peptide sequences of P11-4 and P11-8, resulting in either a negative or a positive surface charge. As described previously by Thomson et al,[48] the calcium-binding site of the SAP is made up of four central glutamic acid residues (two from each strand). Due to the negatively charged surface of P11-4 by glutamic acid residues, the binding of the divalent calcium ions causes a high mineral deposition. In contrast, the peptide sequence of P11-8 contains ornithine residues that lead to an overall positive surface charge, which cannot bind the positive calcium ions. However, after 30 days of culture, calcium deposition on P11-4 and P11-8 hydrogels no longer differed. Thus, the mineralization deposited by the cells seemed to have a greater effect in the long run than the mineralization due to the hydrogels' surface charge.

In summary, the present study demonstrates that the four different P11-SAP hydrogels tested possess specific physicochemical characteristics that lead to variations in protein adsorption and thus to different cellular reactions. Based on the present study, P11-SAP hydrogels, especially P11-4 and P11-8, are suitable candidates as scaffolds in periodontal therapy, as they provide ECM-mimetic fibrillar architecture and favorable cellular reactions regarding the proliferation and osteogenic differentiation of important periodontal cells.

Conclusion

In this study, we demonstrated that the single-component P11-SAP systems P11-4 and P11-8 have suitable and adjustable nanofibrillar architectural and physicochemical properties that enable HPDLF and HCO cell adhesion, growth, and differentiation, which might be suitable for soft-to-hard tissue formation in regenerative periodontal therapy. Thus, these peptides should be further investigated regarding their in vivo potential, eg, as drug delivery systems for the application of antimicrobial agents in a microbial-rich environment like the periodontal pocket.

Acknowledgments

The authors would like to thank Michael Hug and Dominik Lysek (credentis AG) for funding and supporting this work and for the valuable discussions.

Disclosure

The authors report no conflicts of interest in this work.

References

1. Grzesik WJ, Narayanan AS. Cementum and periodontal wound healing and regeneration. *Crit Rev Oral Biol Med*. 2002;13(6):474–484.
2. Kim J, Amar S. Periodontal disease and systemic conditions: a bidirectional relationship. *Odontology*. 2006;94(1):10–21.
3. Wang HL, Cooke J. Periodontal regeneration techniques for treatment of periodontal diseases. *Dent Clin North Am*. 2005;49(3):637–659.
4. Thevenot P, Hu W, Tang L. Surface chemistry influences implant biocompatibility. *Curr Top Med Chem*. 2008;8(4):270–280.
5. Anselme K. Osteoblast adhesion on biomaterials. *Biomaterials*. 2000; 21(7):667–681.
6. Keselowsky BG, Collard DM, García AJ. Surface chemistry modulates fibronectin conformation and directs integrin binding and specificity to control cell adhesion. *J Biomed Mater Res A*. 2003;66(2):247–259.
7. Griffin MF, Ibrahim A, Seifalian AM, Butler PEM, Kalaskar DM, Ferretti P. Chemical group-dependent plasma polymerisation preferentially directs adipose stem cell differentiation towards osteogenic or chondrogenic lineages. *Acta Biomater*. 2017;50:450–461.
8. Ge S, Zhao N, Wang L, et al. Bone repair by periodontal ligament stem cell seeded nanohydroxyapatite-chitosan scaffold. *Int J Nanomedicine*. 2012;7:5405.
9. Ni P, Fu S, Fan M, et al. Preparation of poly(ethylene glycol)/polylactide hybrid fibrous scaffolds for bone tissue engineering. *Int J Nanomedicine*. 2011;6:3065.
10. Koutsopoulos S. Self-assembling peptide nanofiber hydrogels in tissue engineering and regenerative medicine: progress, design guidelines, and applications. *J Biomed Mater Res A*. 2016;104(4):1002–1016.
11. Maude S, Ingham E, Aggeli A. Biomimetic self-assembling peptides as scaffolds for soft tissue engineering. *Nanomedicine*. 2013;8(5): 823–847.
12. Kumada Y, Zhang S. Significant type I and type III collagen production from human periodontal ligament fibroblasts in 3D peptide scaffolds without extra growth factors. *PLoS One*. 2010;5(4):e10305.
13. Takeuchi T, Bizenjima T, Ishii Y, et al. Enhanced healing of surgical periodontal defects in rats following application of a self-assembling peptide nanofibre hydrogel. *J Clin Periodontol*. 2016;43(3):279–288.
14. Firth A, Aggeli A, Burke JL, Yang X, Kirkham J. Biomimetic self-assembling peptides as injectable scaffolds for hard tissue engineering. *Nanomedicine*. 2006;1(2):189–199.
15. Kind L, Stevanovic S, Wuttig S, et al. Biomimetic remineralization of carious lesions by self-assembling peptide. *J Dent Res*. 2017;96(7): 790–797.
16. Kirkham J, Firth A, Vernals D, et al. Self-assembling peptide scaffolds promote enamel remineralization. *J Dent Res*. 2007;86(5):426–430.
17. Koch F, Müller M, König F, et al. Mechanical characteristics of beta sheet-forming peptide hydrogels are dependent on peptide sequence, concentration and buffer composition. *R Soc Open Sci*. 2018; 5(3):171562.
18. Aggeli A, Nyrkova IA, Bell M, et al. Hierarchical self-assembly of chiral rod-like molecules as a model for peptide beta-sheet tapes, ribbons, fibrils, and fibers. *Proc Natl Acad Sci U S A*. 2001;98(21):11857–11862.
19. Carrick LM, Aggeli A, Boden N, Fisher J, Ingham E, Waigh TA. Effect of ionic strength on the self-assembly, morphology and gelation of pH responsive β-sheet tape-forming peptides. *Tetrahedron*. 2007;63(31):7457–7467.
20. Aggeli A, Bell M, Carrick LM, et al. pH as a trigger of peptide beta-sheet self-assembly and reversible switching between nematic and isotropic phases. *J Am Chem Soc*. 2003;125(32):9619–9628.
21. Wilshaw SP, Aggeli A, Fisher J, Ingham E. The biocompatibility and immunogenicity of self-assembling peptides for use in tissue engineering and regenerative application. *Tissue Eng Part A*. 2008;14(5):785.
22. Kyle S, Felton SH, Mcpherson MJ, Aggeli A, Ingham E. Rational molecular design of complementary self-assembling peptide hydrogels. *Adv Healthc Mater*. 2012;1(5):640–645.

23. Maude S, Miles DE, Felton SH, et al. De novo designed positively charged tape-forming peptides: self-assembly and gelation in physiological solutions and their evaluation as 3D matrices for cell growth. *Soft Matter*. 2011;7(18):8085.
24. Bell CJ, Carrick LM, Katta J, et al. Self-assembling peptides as injectable lubricants for osteoarthritis. *J Biomed Mater Res A*. 2006;78(2):236–246.
25. Kyle S, Felton SH, Mcpherson MJ, Aggeli A, Ingham E. Rational molecular design of complementary self-assembling peptide hydrogels. *Adv Healthc Mater*. 2012;1(5):640–645.
26. Hotaling NA, Bharti K, Kriel H, Simon CG. DiameterJ: a validated open source nanofiber diameter measurement tool. *Biomaterials*. 2015;61:327–338.
27. Park H, Guo X, Temenoff JS, et al. Effect of swelling ratio of injectable hydrogel composites on chondrogenic differentiation of encapsulated rabbit marrow mesenchymal stem cells in vitro. *Biomacromolecules*. 2009;10(3):541–546.
28. Sieminski AL, Was AS, Kim G, Gong H, Kamm RD. The stiffness of three-dimensional ionic self-assembling peptide gels affects the extent of capillary-like network formation. *Cell Biochem Biophys*. 2007;49(2):73–83.
29. Cunha C, Panseri S, Villa O, Silva D, Gelain F. 3D culture of adult mouse neural stem cells within functionalized self-assembling peptide scaffolds. *Int J Nanomedicine*. 2011;6:943.
30. Ushiki T. The three-dimensional ultrastructure of the collagen fibers, reticular fibers and elastic fibers: a review. *Kaibogaku Zasshi*. 1992;67(3):186–199.
31. Sakai LY, Keene DR, Engvall E, Fibrillin EE. Fibrillin, a new 350-kD glycoprotein, is a component of extracellular microfibrils. *J Cell Biol*. 1986;103(6 Pt 1):2499–2509.
32. Feng Y, Taraban M, Yu YB. The effect of ionic strength on the mechanical, structural and transport properties of peptide hydrogels. *Soft Matter*. 2012;8(46):11723–11731.
33. Engler AJ, Sen S, Sweeney HL, Discher DE. Matrix elasticity directs stem cell lineage specification. *Cell*. 2006;126(4):677–689.
34. Kyle S, Aggeli A, Ingham E, Mcpherson MJ. Recombinant self-assembling peptides as biomaterials for tissue engineering. *Biomaterials*. 2010;31(36):9395–9405.
35. Polimeni G, Xiropaidis AV, Wikesjö UM. Biology and principles of periodontal wound healing/regeneration. *Periodontol*. 2006;41(1):30–47.
36. Castner DG, Ratner BD. Biomedical surface science: foundations to frontiers. *Surf Sci*. 2002;500(1–3):28–60.
37. Macdonald DE, Markovic B, Boskey AL, Somasundaran P. Physico-chemical properties of human plasma fibronectin binding to well characterized titanium dioxide. *Colloids Surf B Biointerfaces*. 1998;11(3):131–139.
38. Guo C, Wu C, Chen M, Zheng T, Chen N, Cummings PT. Molecular modeling of fibronectin adsorption on topographically nanostructured rutile (110) surfaces. *Appl Surf Sci*. 2016;384:36–44.
39. Wilson CJ, Clegg RE, Leavesley DI, Pearcy MJ. Mediation of biomaterial-cell interactions by adsorbed proteins: a review. *Tissue Eng*. 2005;11(1–2):1–18.
40. Wu CS, Chen GC. Adsorption of proteins onto glass surfaces and its effect on the intensity of circular dichroism spectra. *Anal Biochem*. 1989;177(1):178–182.
41. Jönsson U, Ivarsson B, Lundström I, Berghem L. Adsorption behavior of fibronectin on well-characterized silica surfaces. *J Colloid Interface Sci*. 1982;90(1):148–163.
42. Paul JI, Hynes RO. Multiple fibronectin subunits and their post-translational modifications. *J Biol Chem*. 1984;259(21):13477–13487.
43. Vuento M, Wrann M, Ruoslahti E. Similarity of fibronectins isolated from human plasma and spent fibroblast culture medium. *FEBS Lett*. 1977;82(2):227–231.
44. Richter H, Hörmann H. Early and late cathepsin D-derived fragments of fibronectin containing the C-terminal interchain disulfide cross-link. *Hoppe Seylers Z Physiol Chem*. 1982;363(4):351–364.
45. Sekiguchi K, Hakomori S. Topological arrangement of four functionally distinct domains in hamster plasma fibronectin: a study with combination of S-cyanylation and limited proteolysis. *Biochemistry*. 1983;22(6):1415–1422.
46. Cai K, Frant M, Bossert J, Hildebrand G, Liefeith K, Jandt KD. Surface functionalized titanium thin films: zeta-potential, protein adsorption and cell proliferation. *Colloids Surf B Biointerfaces*. 2006;50(1):1–8.
47. Ghasemi-Mobarakeh L, Prabhakaran MP, Tian L, Shamirzaei-Jeshvaghani E, Dehghani L, Ramakrishna S. Structural properties of scaffolds: crucial parameters towards stem cells differentiation. *World J Stem Cells*. 2015;7(4):728.
48. Thomson BM, Hardaker L, Davies RPW, et al. P11-15 (NNRFEWEFENN): a biocompatible, self-assembling peptide with potential to promote enamel remineralisation. Abstract 47. *Caries Res*. 2014;48(411):405.

4.3 Studie III

A versatile biocompatible antibiotic delivery system based on self-assembling peptides with antimicrobial and regenerative potential

Koch F, Ekat K, Kilian D, Hettich T, Germershaus O, Lang H, Peters K, Kreikemeyer B.
Journal of Advanced Healthcare Materials. 2019, 1900167

Zusammenfassung

Das hohe Aufkommen verschiedener Bakterienspezies in der Mundhöhle zusammen mit den anspruchsvollen Gewebeschnittstellen (Weich/Hartgewebe), macht die parodontale Regeneration sehr kompliziert. Daher wurden in Studie III die intrinsische antimikrobielle Aktivität, das regenerative Potential und die Fähigkeit, Antibiotika in SSP-Hydrogelen zu inkorporieren, untersucht. Dabei konnte eine signifikante antibakterielle Wirkung von positiv geladenen SSP-Hydrogelen auf den pathogenen Bakterienspezies *Porphyromonas gingivalis* beobachtet werden. Im Gegensatz dazu zeigten negativ geladene SSP-Hydrogele keinen signifikanten antimikrobiellen Effekt. Die hohe metabolische Aktivitätsrate von menschlichen Zahnfollikelstammzellen (DFSC) kultiviert auf negativ geladenen SSP-Hydrogelen kann auf ein gesteigertes Regenerationspotential hindeuten. Positiv geladene SSP-Hydrogele resultierten im Vergleich zu negativ geladenen SSP-Hydrogelen in einer niedrigeren metabolischen Aktivität. Bemerkenswerterweise verstärken beide SSP-Hydrogele die osteogene Differenzierung von DFSC im Vergleich zur Kontrolle. Der Einbau von verschiedenen Antibiotika beeinflusste die Fibrillenbildung beider SSP-Hydrogele nicht und führte zu einer günstigen Freisetzungskinetik bis zu 5 Tagen. Zusammenfassend zeigt diese Studie, dass P11-SSP-Hydrogele viele vorteilhafte Eigenschaften kombinieren, die für eine neuartige Parodontaltherapie erforderlich sind.

A Versatile Biocompatible Antibiotic Delivery System Based on Self-Assembling Peptides with Antimicrobial and Regenerative Potential

*Franziska Koch, Katharina Ekat, David Kilian, Timm Hettich, Oliver Germershaus, Herrmann Lang, Kirsten Peters, and Bernd Kreikemeyer**

Periodontitis is a chronic inflammatory and tissue-destructive disease. Since the polymicrobiome in the oral cavity makes it difficult to treat, novel therapeutic strategies are required. Hydrogels based on self-assembling peptides (SAP) can be suitable candidates for periodontal therapy due to their injectability, biocompatibility, cargo-loading capacity, and tunable physicochemical and mechanical properties. In this study, two SAP hydrogels (P11-4 and P11-28/29) are examined for their intrinsic antimicrobial activity, regenerative potential, and antibiotic delivery capacity. A significant antibacterial effect of P11-28/29 hydrogels on the periodontal pathogen *Porphyromonas gingivalis* and a less pronounced effect for P11-4 hydrogels is demonstrated. The metabolic activity rates of human dental follicle stem cells (DFSCs), which reflect cell viability and may thus indicate the regenerative capacity, are similar on tissue culture polystyrene (TCPS) and on P11-4 hydrogels after 14 days of culture. Noticeably, both SAP hydrogels strengthen the osteogenic differentiation of DFSCs compared with TCPS. The incorporation of tetracycline, ciprofloxacin, and doxycycline does not affect fibril formation of either SAP hydrogel and results in favorable release kinetics up to 120 h. In summary, this study reveals that P11-SAP hydrogels combine many favorable properties required to make them applicable as prospective novel treatment strategy for periodontal therapy.

1. Introduction

Periodontal disease (PD) is characterized by complex inflammatory conditions inside the oral cavity, involving tooth supporting structures such as the cementum, the periodontal ligament and the alveolar bone. PD is caused by the colonization of oral polymicrobial pathogens and the shift of the composition inside the microbiological plaque from nonmobile coccoid cells and rods toward a mix of anaerobic Gram-negative bacteria.[1] If not treated properly, PD will progress further and result in chronic inflammation, destruction of adjacent connective tissue structures and tooth loss.[2] Thus, the aim of periodontal therapy is to eliminate the pathogenic bacterial plaque from the tooth surface and the subgingival structures and to re-establish a healthy microbiota.[3] For this purpose, mechanical scaling and root planning as well as surgical interventions are indicated.[1] However, it is known that these techniques often fail to remove pathogenic plaque effectively.[4] Thus, the application of antimicrobial agents as an additive therapy to pure mechanical treatment can be valuable in preventing a recolonization of pathogenic bacteria.[5] Antimicrobial agents, such as antibiotics, can be applied systemically (i.e., oral route) or by local drug delivery. Systemic administration of antimicrobial agents is associated with side effects such as hypersensitivity, gastrointestinal intolerance, and the development of bacterial resistance.[6,7] Moreover, some studies have reported

---

F. Koch, D. Kilian, T. Hettich
School of Life Sciences
Institute for Chemistry and Bioanalytics
University of Applied Sciences and Arts Northwestern Switzerland
4132 Muttenz, Switzerland

F. Koch, Dr. K. Ekat, Prof. B. Kreikemeyer
Institute of Medical Microbiology
Virology and Hygiene
University Medicine Rostock
18057 Rostock, Germany
E-mail: bernd.kreikemeyer@med.uni.rostock.de

The ORCID identification number(s) for the author(s) of this article can be found under https://doi.org/10.1002/adhm.201900167.

DOI: 10.1002/adhm.201900167

F. Koch, Dr. K. Ekat, K. Peters
Department of Cell Biology
University Medicine Rostock
18057 Rostock, Germany

Dr. K. Ekat, Prof. H. Lang
Clinic for Restorative Dentistry and Periodontology
University Medicine Rostock
18057 Rostock, Germany

Prof. O. Germershaus
School of Life Sciences
Institute of Pharma Technology
University of Applied Sciences and Arts Northwestern Switzerland
4132 Muttenz, Switzerland

an inability of systemically administered antimicrobial agents to reach adequate antibacterial concentrations for a sufficient period of time at the site of action.[8] These disadvantages may be bypassed by local drug application. For example, the local drug concentration within the tissue can be increased if antimicrobial agents were released from controlled drug delivery systems applied directly into the periodontal pocket. Today, several common local drug delivery systems based on polymeric materials, applied as fibers, gels, films, microspheres, and nanoparticles, are known. These materials can encapsulate antimicrobial agents and are applied in periodontal therapy.[9]

Polymeric systems have to fulfill certain biophysical and chemical requirements, among them (1) syringability, (2) adhesion of the drug delivery system to the tooth surface to prevent removal from the periodontal pocket, (3) biodegradability, (4) noncytotoxicity, (5) superior molecule encapsulation ability at high concentrations of load, (6) prolonged and controlled release, and finally (7) enabling of guided tissue regeneration (GTR).[10]

One class of biomaterial that fulfills all of the fundamental requirements are self-assembling peptides (SAP).[11–15] Besides the direct incorporation of drugs at high concentrations during the self-assembling process, SAP offer the advantage of being applied into a defect site in a minimally invasive manner, and they lack the toxic residual substances from polymerization.[16] Moreover, their rationally designed physicochemical properties and their tunable mechanical characteristics allow for a high variety of encapsulated drugs.[17] The release of small molecules from SAP is mostly governed by their molecular weight, charge, and the hydrophobicity of the encapsulated drug, but also by their peptide characteristics such as peptide sequence, concentration, and peptide hydrogel pore size.[18] In previous reports, several SAP hydrogels have been used as drug delivery systems for small hydrophilic and hydrophobic drugs.[19,20] Moreover, SAP hydrogels could become attractive candidates in the future for periodontal therapy due to their intrinsic antimicrobial activity.[21] As an example, Veiga et al.[22] demonstrated an inhibitory effect of an arginine-rich SAP system on the growth of *Escherichia coli* and *Staphylococcus aureus*.

However, novel therapeutic strategies for the treatment of periodontal disease should not only include the control of local inflammation by, e.g., antimicrobial activity, but also need to ensure the regeneration of new periodontal tissues, such as alveolar bone and periodontal ligament.[23] The periodontium is known to contain various stem cell sources from dental pulp, dental follicle, dental papilla, and periodontal ligament, as well as in exfoliated deciduous teeth.[24] As these dental stem cells are able to differentiate into hard and soft tissue, the periodontium possesses a high intrinsic regenerative capacity that can be leveraged for GTR.[25] As demonstrated in previous studies, diverse SAP hydrogels can act as fibrillar scaffolds for dental pulp stem cells promoting cellular growth and osteogenic differentiation in vitro.[26–28] Taken together, the application of SAP hydrogels could evolve as attractive treatment strategy to combat periodontal disease.

To our knowledge, SAP hydrogels have not yet been evaluated in vitro in the context of the three potentials defined in periodontal therapy: antimicrobial activity, drug delivery potential, and regenerative capacity. Thus, we selected two different β-sheet forming SAP hydrogels, consisting of 11-amino acids (named P11-4 and P11-28/29), from a well described P11-library developed by the group of Aggeli and co-workers,[29,30] that were reported recently to be injectable, biocompatible, and noncytotoxic for periodontal tissue cells[31] and obtained variable physicochemical characteristics.[32]

In this study, we evaluated the two selected P11-SAP hydrogels with respect to (1) their antimicrobial activity using Gram-positive (*Streptococcus sanguinis* (*S. sanguinis*)) and Gram-negative (*Porphyromonas gingivalis* (*P. gingivalis*)) bacteria, (2) their ability to act as a scaffold for human dental follicle stem cells (DFSCs), and finally (3) their drug delivery potential using a set of common antimicrobial agents (see **Figure 1**). To test the drug delivery potential of P11-SAP hydrogels, commonly

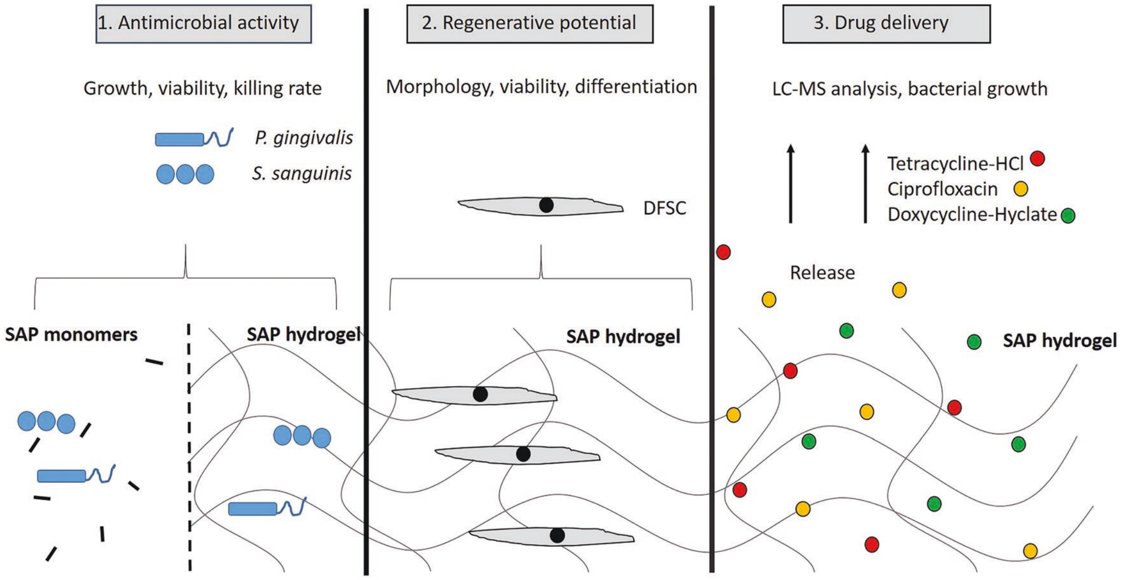

Figure 1. Illustration of the study design. The investigation focuses on the capacity of SAP hydrogel with regards to antimicrobial activity, regenerative potential, and drug delivery.

clinical applied antibiotics such as tetracycline hydrochloride (TC) and doxycycline-hyclate (DH) have been chosen as broad spectrum, bacteriostatic antibiotic. Moreover, ciprofloxacin (CX), a member of the fluorquinolones, has been further selected based on its efficiency in the treatment of periodontal superinfections.[3]

2. Results

2.1. Antimicrobial Properties of P11-SAP Monomers

As a first step in this study we investigated whether monomeric SAPs possess intrinsic antimicrobial activity. Initially, we examined whether P11-SAP in their monomeric state affect the growth behavior of *P. gingivalis* and *S. sanguinis*. As shown in **Table 1**, all SAP monomers increased the generation time of *P. gingivalis*, reaching significance for P11-4 and P11-29. This growth inhibitory effect is also reflected by a decrease in the growth rate, suggesting that monomeric SAPs have a suppressive influence on *P. gingivalis* growth. In contrast to the Gram-negative pathobiont species *P. gingivalis*, SAP do not significantly influence the growth rate and generation times of the Gram-positive oral commensal species *S. sanguinis*.

Next, we tested the effects of monomeric SAP on resting bacterial cells, thereby assessing a potential influence on bacterial killing. Monomeric SAP were incubated together with a fixed number (colony forming unit, CFU) of late stationary phase bacteria, which were not allowed to actively grow due to incubation in phosphate buffered saline (PBS). The temporal development of the bacterial CFU was monitored in direct comparison to untreated controls. None of the tested SAP showed any effect on the rate at which *P. gingivalis* and *S. sanguinis* died (Figure S3, Supporting Information).

Taken together, we conclude that monomeric SAP exhibit species- and peptide-specific antimicrobial activity exclusively on actively growing bacteria.

2.2. Antimicrobial Effect of Polymerized P11-SAP Hydrogels

Next, we investigated potential effects of assembled SAP hydrogels in direct contact with *P. gingivalis* and *S. sanguinis*. This is an approach resembling the in vivo situation in a periodontal pocket, where SAP hydrogels will come into direct contact with pathogenic bacteria. Different methods to determine bacterial viability and proliferation were used to approach this aspect. First, polymerized P11-SAP hydrogels were overlaid with a brain–heart-infusion (BHI) medium suspension containing 10^7 CFU mL^{-1} viable bacteria and the bacterial vitality was visually inspected using a fluorescence microscope after live/dead staining at 48 h postinoculation (Figure 1A–D). As displayed by a majority of vital and thus green fluorescent bacteria in the microscopic pictures, contact of *P. gingivalis* and *S. sanguinis* with P11-4 hydrogels, which have a negative surface charge, did not lead to bactericidal effects (**Figure 2**A,C). However, the positively charged surface of P11-28/29 hydrogels led to substantial numbers of red fluorescent and thus dead bacterial cells for both species after 48 h of coincubation (Figure 2B,D).

Second, as an independent and more quantitative test, we further investigated the relative bacterial growth in BHI medium of *P. gingivalis* and *S. sanguinis* suspensions on P11-4 and P11-28/29 hydrogels in comparison with growth on tissue culture polystyrene (TCPS) (Figure 2E,F). After 24 h, *P. gingivalis* growth was significantly reduced in contact with P11-28/29, which was even more pronounced after 48 h of coincubation (Figure 2E). Compared to TCPS surfaces, which allowed noninhibited growth of *P. gingivalis*, P11-4 suppressed the growth of *P. gingivalis* exclusively after 48 h of coincubation. Growth of *S. sanguinis* on both hydrogel surfaces was unaffected after 24 h of coincubation and only slightly, but significantly decreased on the gels after 48 h.

In summary, both polymerized gels influenced bacterial growth, in a time- and species-specific manner. Overall, *P. gingivalis* was more susceptible to these antimicrobial hydrogel features.

2.3. Viability and Osteogenic Differentiation Capability of DFSCs on P11-SAP Hydrogels

As a subsequent step, the effects of P11-SAP hydrogels on the viability and osteogenic differentiation of DFSCs were tested. For this purpose, the cellular phenotype, the metabolic activity and the osteogenic differentiation were analyzed in vitro. It should be noted that the visualization of cells in contact with the hydrogel samples was technically challenging due to their intrinsic fluorescence, especially in the UV range. Hence, the cells were not stained for cell nuclei, since most of the nuclear dyes are dependent on UV excitation. The staining of the F-actin in DFSCs in the red excitation range was feasible and after 24 h of cultivation on P11-4 hydrogels, the cells demonstrated a spread phenotype with stretched actin filaments (**Figure 3**A). DFSCs on P11-28/29 hydrogels did not spread and remained round in shape (Figure 3B).

Table 1. Generation time (*g*) and growth rates (μ) of *P. gingivalis* and *S. sanguinis* in BHI medium after 24 h incubation with SAP monomers (1.5 mg mL^{-1}). Data represent mean values ± SD. A two-way ANOVA test was performed, followed by a Turkey's multiple comparison post hoc test. A **p*-value of ≤0.01 was considered significant.

Bacteria	Generation times (*g*) and growth rates (μ)	Untreated	P11-4	P11-28	P11-29
P. gingivalis	*g* [h]	0.65 ± 0.01	0.75 ± 0.02*	0.71 ± 0.03	0.75 ± 0.03*
	μ [h^{-1}]	0.14 ± 0.01	0.06 ± 0.02*	0.06 ± 0.03*	0.06 ± 0.02*
S. sanguinis	*g* [h]	1.12 ± 0.01	1.13 ± 0.01	1.19 ± 0.01	1.20 ± 0.01
	μ [h^{-1}]	0.11 ± 0.02	0.09 ± 0.01	0.10 ± 0.01	0.11 ± 0.01

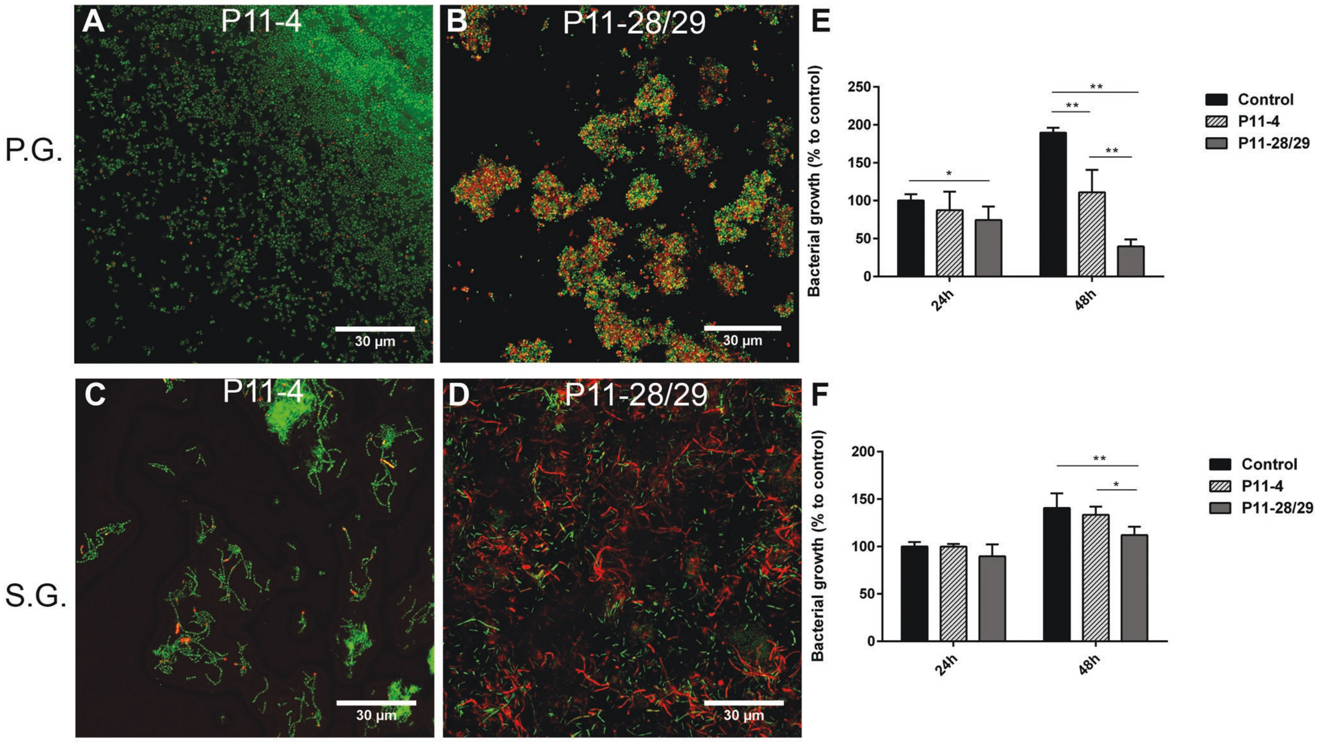

Figure 2. Bacterial growth and viability on P11-SAP hydrogels. A–D) Live/dead staining of *P. gingivalis* (A and B) and *S. sanguinis* (C and D) after 48 h incubation on P11-4 and P11-28/29 hydrogels. Green color indicates uptake of only SYTO 9, red color indicates membrane permeability for propidium iodide. Scale bar corresponds to 30 µm. Growth rate of E) *P. gingivalis* and F) *S. sanguinis* on P11-4 (15 mg mL^{-1}) and P11-28/29 (10 mg mL^{-1}) after 24 and 48 h in BHI medium. Bacteria cultured in BHI were taken as control. Data represent mean values ± SD ($n = 3$ biological replicates and 3 technical replicates). A two-way ANOVA test was performed, followed by a Turkey's multiple comparison post hoc test with *p-value ≤ 0.01, **p-value ≤ 0.001.

Furthermore, we assessed long-term metabolic activity rates of DFSCs on P11-SAP hydrogels. The cells were cultured up to 14 days on P11-4 and P11-28/29 hydrogels and measured for their metabolic activity at day 1, 3, 7, and 14 (Figure 3C). As a control, cells were grown on TCPS. On day 1, the initial metabolic activity of DFSCs on TCPS, P11-4, and P11-28/29 varied significantly (Figure S2, Supporting Information), which indicated a different cell attachment capacity of TCPS and P11-SAP hydrogels. To compare the metabolic activity rates over the time span without the inclusion of the variable attachment capacities, the initial metabolic activity for every sample was set to 1. Over a period of 14 days, TCPS and P11-4 hydrogels revealed similar metabolic activities (5.89 ± 0.71 for TCPS and 4.60 ± 0.30 for P11-4, Figure 3C). It is noteworthy that four times lower metabolic activities were detected for P11-28/29 compared with TCPS and P11-4 hydrogels. As the increase of metabolic activity can be used as an indication for cell proliferation, the PrestoBlueViability assay revealed high cell proliferation rates of DFSCs on TCPS and P11-4, and lower proliferation rates on P11-28/29 hydrogels.

The osteogenic differentiation capacity of DFSCs on P11-SAP hydrogels was analyzed after 21 days by detection of their collagen I expression, alkaline phophatase activity (ALP) activity, osteocalcin (OC), and osteoprotegerin (OPG) expression levels (Figure 3D–G). Cells cultured on TCPS in osteogenic medium were taken as a control. Significantly high expression levels of collagen type I were measured after 7 days of culture on P11-4 (256.0 ± 3.1 ng mL^{-1}), followed by P11-28/29 (211.3 ± 1.7 ng mL^{-1}) and TCPS control (173.0 ± 3.2 ng mL^{-1}). Overall, the DFSCs culture on P11-SAP hydrogels resulted in a statistically significant higher collagen type I expression, compared with the TCPS control. In contrast to the collagen expression, similar ALP activity levels of DFSCs were found for TCPS compared with P11-SAP hydrogels. However, after 14 days of culture ALP activity was found to be significantly lower for P11-28/29 hydrogels than for cells grown on TCPS. Expression of osteogenic markers such as OC and OPG reached similar levels after 14 and 21 days of DFSCs culture on TCPS, P11-4, and P11-28/29 hydrogels. Exclusively on day 7, DFSCs expressed significantly lower amounts of OC (by twofold) and OPG (fourfold) after the incubation of P11-SAP hydrogels compared with TCPS. In summary, a largely similar and thus unaffected degree of osteogenic differentiation was shown for DFSCs grown on P11-SAP hydrogel and TCPS.

2.4. Hemolytic Activity of P11-SAP Monomers and Hydrogels

To approach the aspect of biocompatibility and toxicity, P11-4 and P11-28/29 monomers and hydrogels were co-incubated with human red blood cells (hRBCs). TCPS was used as a control surface. The treatment of hRBCs with 1% TritonX 100 was normalized to 100%, as this led to complete cell lysis. In comparison to TCPS, the hemolytic activity of hRBCs

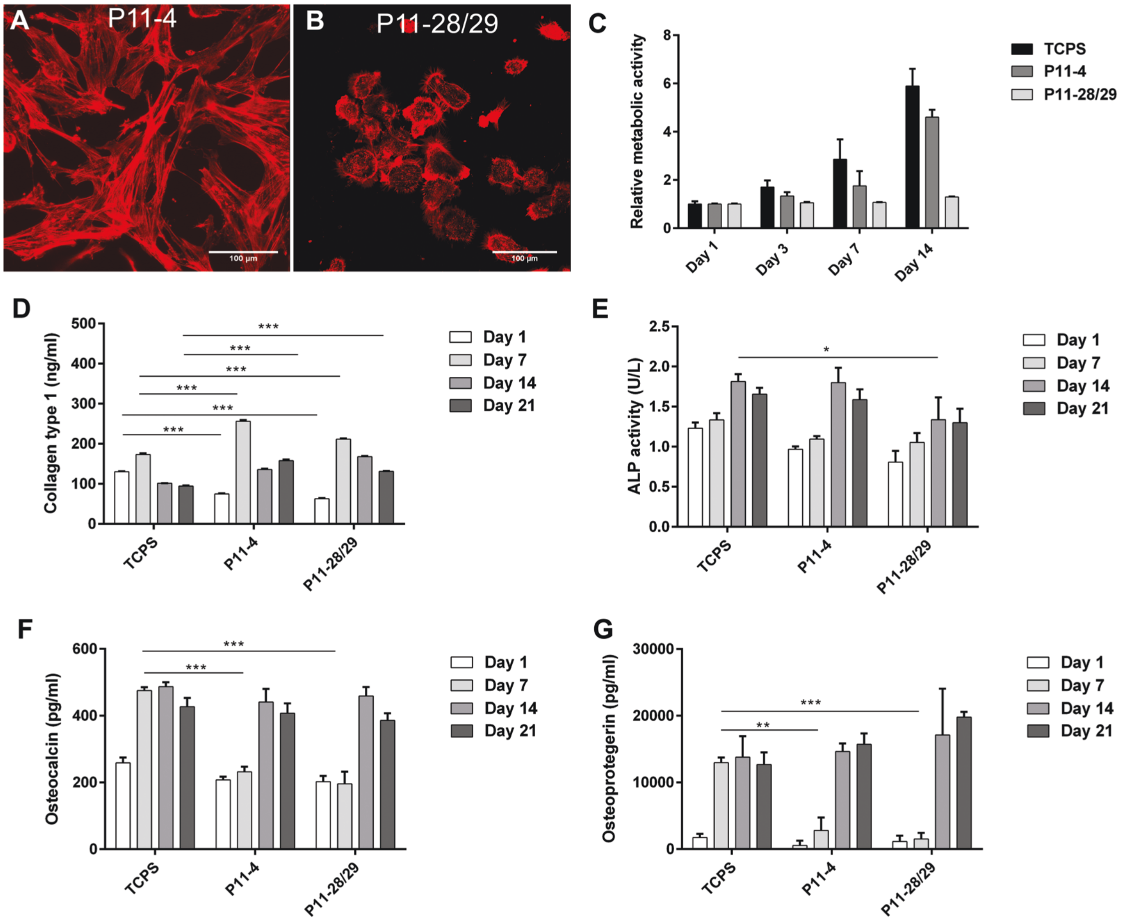

Figure 3. Cellular behavior of DFSCs in contact to P11-SAP hydrogels. Phenotypic characterization by the depiction of the F-actin cytoskeleton in DFSCs on A) P11-4 and B) P11-28/29 hydrogels after 24 h (scale bar: 100 µm, n = 3). C) Relative metabolic activity of DFSCs on P11-4 and P11-28/29 hydrogels (PrestoBlue assay performed after 24 h, % to TCPS control, data represent mean ± SD, n = 3). D–G) DFSCs osteogenic differentiation capacities on P11-SAP hydrogels. (D) Collagen I expression of DFSCs on TCPS or P11-4/P11-28/29 hydrogels (assessed after 1, 7, 14, 21 days by ELISA, n = 3) and (E) ALP activity (U/L, n = 3) were measured as early osteogenic markers. The amount of (F) osteocalcin (OC) and (G) osteoprotegerin (OPG) were measured as late phase osteogenic markers, (pg mL^{-1}, n = 3 biological replicates and 3 technical replicates). A two-way ANOVA test was performed, followed by a Dunnetts's multiple comparison post hoc test with *p-value ≤ 0.01, **p-value ≤ 0.001, ***p-value ≤ 0.0001).

exposed to P11-4 and P11-28 monomers was found to be similar. However, for P11-29 monomers, the hemolytic activity increased approximately by twofold (**Figure** 4A). In contrast to P11-SAP monomers, no increased hemolytic activity was detected for P11-4 and P11-28/29 hydrogels, compared to the TCPS control (Figure 4B). Taken together, these preliminary results characterize the SAP monomers and hydrogels tested to be biocompatible and nontoxic to human cells.

2.5. Incorporation of Antibiotics in P11-SAP Hydrogels

2.5.1. Fibrillar formation after CX Incorporation

To investigate the ability of P11-SAP assembly into fibrillar structures after CX incorporation, transmission electron microscopy (TEM) studies were conducted (**Figure** 5). Nanofibrillar formation was observed for P11-4 and P11-28/29 hydrogels with and without incorporation of CX. Moreover, the added incorporation of TC and doxycycline hyclate (DH) in P11-4 and P11-28/29 resulted in fibrillar hydrogel formation (Figure S3, Supporting Information). Thus, we conclude that incorporation of those three antibiotics at a concentration of 150 mg L^{-1} had no effect on fiber and hydrogel formation.

2.5.2. Evaluation of Controlled Release of TC, CX, and DH from P11-SAP Hydrogels

As a consequent next step, the release of TC, CX, and DH from P11-SAP hydrogels was monitored by liquid chromatography mass spectrometry (LC-MS) analysis. The cumulative release profiles (%) of the incorporated antibiotics are presented in **Figure** 6. The initially incorporated antibiotic concentration of 150 mg L^{-1} was set to 100%. Generally, P11-4 and P11-28/29 hydrogels evoked an antibiotic release up to 120 h (5 days). The release kinetics were characterized by a rapid release rate within the first 48 h, before slowly plateauing between 48 and

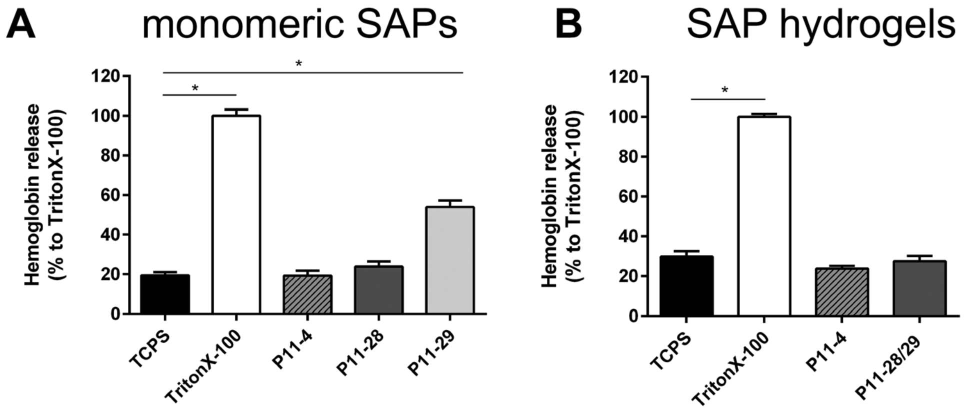

Figure 4. Hemolytic activity of P11-SAP on red blood cells (RBCs). Hemoglobin release was measured after 1 h exposure to A) monomeric P11-SAP (1.5 mg mL^{-1}) and B) P11-SAP hydrogels (P11-4 with 15 mg mL^{-1} and P11-28/29 with 10 mg mL^{-1}). Hemoglobin release after treatment with the membrane disrupting agent Triton-X100 (1% solution in PBS) was considered as 100%. RBCs on TCPS were taken as a control. Data represent the mean ± SD, $n = 3$ technical replicates. A one-way ANOVA test was performed, followed by a Dunnetts's multiple comparison post hoc test with $*p$-value ≤ 0.01.

120 h (Figure 6A,C). Remarkably, for P11-4 hydrogels with incorporated TC and CX, no plateau was reached after 120 h, suggesting an ongoing release for an extended time period. Among the tested substances, the highest amount of antibiotic was calculated for CX released from P11-4 hydrogels (98.5% ± 2.1%) and from P11-28/29 hydrogels (84.7% ± 7.6%). After 120 h, a final antibiotic release of 50.1% ± 1.6% was reached for TC- and DH-supplemented P11-28/29 hydrogels. In comparison to P11-28/29 hydrogels, P11-4 hydrogels demonstrated a 1.6-fold higher release of TC (84.4% ± 1.5%) and a 1.2-fold higher release of DH (62.6% ± 1.2%).

From the therapeutic point of view, high antibiotic burst releases with levels equal to or higher than the minimal inhibitory concentrations (MICs) are essential for an immediate and sustained effect. Thus, the burst release after initial contact ($t = 0$ h) was calculated for TC-, CX-, and DH-incorporated P11-4 and P11-28/29 hydrogels (Figure 6B,D). For P11-4 hydrogels, the highest burst release was obtained for TC (7.9 ± 0.2 mg L^{-1}), followed by CX (6.3 ± 1.4 mg L^{-1}) and DH (5.9 ± 0.9 mg L^{-1}). By contrast, the lowest antibiotic level upon placement of P11-28/29 hydrogels in PBS was observed for TC (0.3 ± 0.1 mg L^{-1}). However, in comparison with P11-4 hydrogels, similar burst release profiles

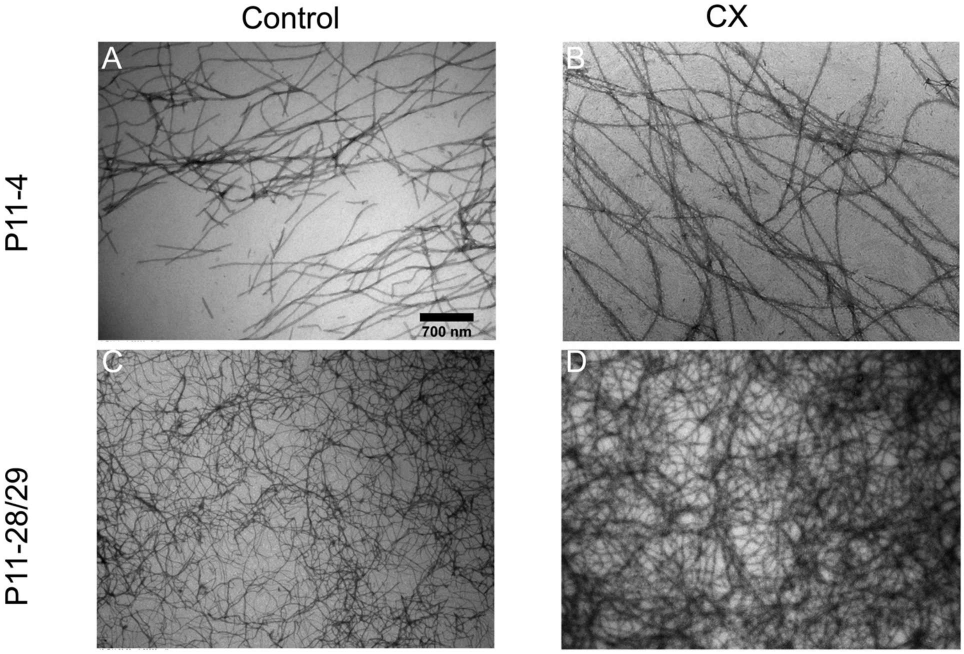

Figure 5. Nanofibrillar structures of assembled P11-SAP. Proof of concept study on the fibrillation of A,B) P11-4 (15 mg mL^{-1}) and C,D) P11-28/29 (10 mg mL^{-1}) with (B and D) and without (A and C) incorporation of CX (150 mg L^{-1}). Fibrils are visualized by transmission electron microscopy (TEM). Scale bar in panel A corresponds to 700 nm and applies to all images.

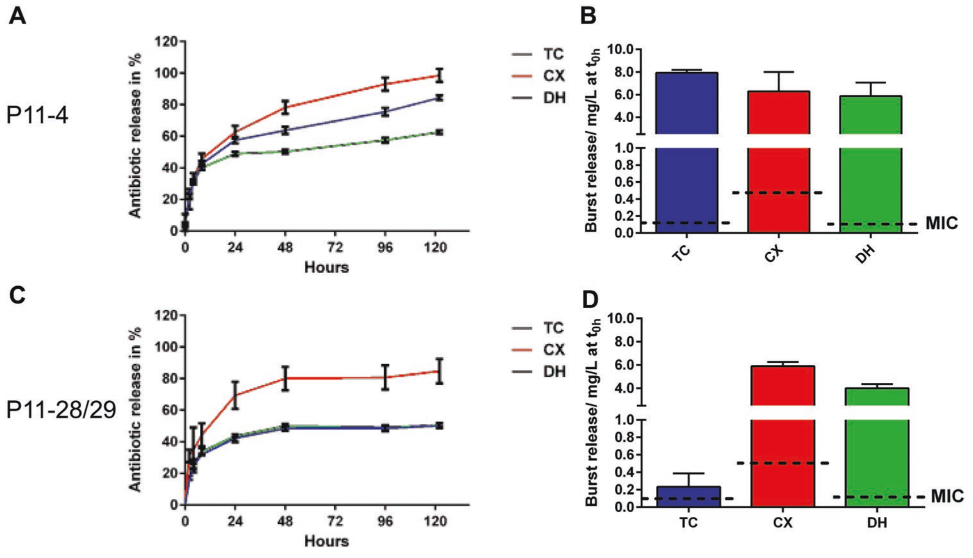

Figure 6. Cumulative release profiles of antibiotic-incorporated P11-SAP hydrogels. Release profile of incorporated TC, CX, and DH from A,B) P11-4 hydrogels (15 mg mL^{-1}) and C,D) P11-28/29 hydrogels (10 mg mL^{-1}). Samples were incubated in PBS and analyzed after 1, 2, 4, 8, 24, 48, 72, 96, and 120 h. B,D) Burst release of TC, CX, and DH (in mg L^{-1}) after initial contact with PBS ($t = 0$ h). Data represent the mean values ± SD, $n = 3$ technical replicates.

were detected for P11-28/29 hydrogels with CX (5.9 ± 0.2 mg L^{-1}) and DH (4.0 ± 0.3 mg L^{-1}) incorporation. In summary, the data revealed antibiotic levels after burst release of P11-SAP hydrogels above the determined MICs (Figure S4, Supporting Information) for *P. gingivalis* and *S. sanguinis*.

2.6. Antibacterial Activity of Antibiotic Extracts Released from P11-SAP Hydrogels

After confirmation that P11-SAP hydrogels provide a favorable burst as well as a long-term sustained release profile of the tested antibiotics, we next investigated their in vitro efficacy as antibacterial delivery systems. Extracts of TC-, CX-, and DH-loaded P11-SAP hydrogels placed in BHI medium were collected over a period of 120 h and examined for their inhibitory effect on *P. gingivalis* and *S. sanguinis* (**Figure 7**). Bacteria cultured in BHI medium on TCPS were taken as a control. As a measure of bacterial growth, the optical density (OD) was monitored at a wavelength of 600 nm. An OD of 1.0 was set to 100%. *P. gingivalis* and *S. sanguinis*, grown for 24 h in BHI medium without the addition of antibiotic extracts, achieved a relative bacterial growth of 71.2% ± 9.5% and 72.3% ± 4.1%, respectively. The lowest relative growth of *S. sanguinis* was detected for DH extracts from P11-4 hydrogels (2–5%, Figure 7C), DH extracts from P11-28/29 hydrogels (2–10%, Figure 7F), and CX-loaded P11-28-29 hydrogels (2–10%, Figure 7E). Hence, these antibiotic-hydrogel compositions achieved an inhibitory effect of 90–98%. Higher relative growth values of about 10–20% (which correspond to an inhibitory effect of 80–90%) were calculated for TC- and CX-loaded P11-4 hydrogels (Figure 7A,B) as well as for TC-loaded P11-28/29 hydrogels (Figure 7D). Similar growth profiles were obtained for *P. gingivalis*. Relative growth values of 10% were observed for DH-loaded P11-4 (Figure 7C) and P11-28/29 (Figure 7F) hydrogels as well as for CX-loaded P11-28/29 hydrogels (Figure 7E). Thus, a maximum inhibitory effect of 90% was achieved for *P. gingivalis* grown with antibiotic extracts of P11-SAP hydrogels. The highest relative growth values of *P. gingivalis* (20–50%) were measured for TC-loaded P11-4 hydrogels (Figure 7A). In summary, these experiments proved that SAP hydrogels release therapeutically relevant doses of active antibiotics.

2.7. DFSCs Response after the Treatment with TC, CX, and DH Solutions

In order to define the antibiotic concentration level which could cause a cytotoxic effect on DFSCs, TC, CX, and DH solutions were prepared at concentrations of 5, 50, and 150 mg L^{-1} in a maintenance medium and cultured for 24 h. As a first qualitative analysis, live/dead staining was performed after 24 h of DFSCs exposure to antibiotic solutions. Viable cells are highlighted in green (SYTO9) and dead cells are visualized in red (propidium iodide) (**Figure 8**A). Viable and spread DFSCs were observed for TC, CX, and DH solutions prepared at 5 and 50 mg L^{-1}. Cells treated with 150 mg L^{-1} antibiotic solutions exhibit an attenuated morphology and round shape. However, dead cells (indicated in red) were exclusively observed for CX at 150 mg L^{-1}. As a subsequent step, cells were also analyzed in a quantitative manner using crystal violet staining to quantify the cell amount (Figure 8B) and an MTS assay (Figure 8C) to investigate their metabolic activity after treatment with a TC, CX, and DH solution. As a control, DFSCs were cultured on TCPS for 24 h in maintenance medium. As observed for

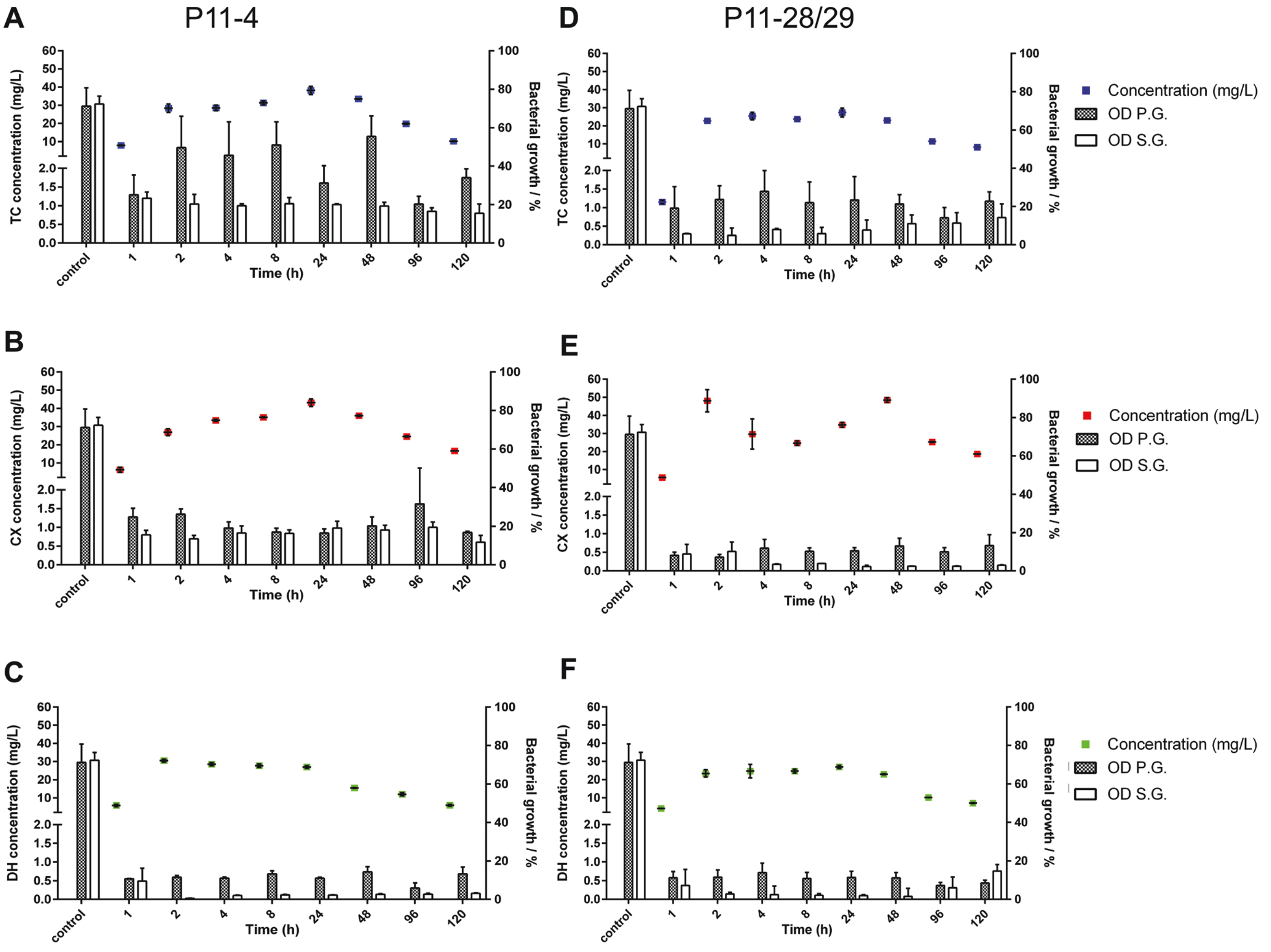

Figure 7. Bacterial growth after treatment with antibiotic extracts. Extracts of A,D) TC, B,E) CX, and C,F) DH were taken after 1, 2, 4, 8, 24, 48, 96, and 122 h incubation of antibiotic-incorporated (150 mg L^{-1}) P11-4 (15 mg mL^{-1}) and P11-28/29 (10 mg mL^{-1}) with BHI medium at 37 °C. Antibiotic concentrations (mg L^{-1}) are shown at the left *y*-axis. Growth rates (turbidity measurements at 600 nm, right *y*-axis) of *P. gingivalis* (P.G. gray bars) and *S. sanguinis* (S.G., white bars) were analyzed after 24 h incubation with antibiotic extracts. As a control, bacteria were grown on TCPS in BHI medium. Data represent the mean values ± SD, *n* = 3 biological and 3 technical replicates.

the live/dead staining, the CX solution (150 mg L^{-1}) affected an DFSCs response and resulted in a significantly reduced cell amount (68.4% ± 3.7%), compared with the TCPS control (Figure 8B). In contrast to the cell amount, the metabolic activity of DFSCs after antibiotic exposure was more severely affected (Figure 8C). Reduced metabolic activity in comparison with the TCPS control was observed for TC (78.6% ± 13.1% at 50 mg L^{-1} and 82.5% ± 5.1% at 150 mg L^{-1}) and for CX (40.4% ± 3.1%, 150 mg L^{-1}) solutions. However, treatment with DH at any concentrations showed no effect on the number of cells or on their metabolic activity.

3. Discussion

In this study, we investigated two β-sheet forming SAPs and their respective hydrogels (P11-4, P11-28/29) with the focus on their antimicrobial activity, cytotoxicity, regenerative capacity, support for osteogenic differentiation and drug delivery potential.

The antimicrobial activity of SAP hydrogels is a key feature for periodontal therapy, as it prevents the invasion of pathogenic bacteria into the hydrogel after injecting it into the periodontal pocket and is therefore essential for a successful treatment. The antimicrobial activity of SAP hydrogels is mostly driven by side chain functionality of the charge residues (e.g., lysine or arginine), charge density, charge accessibility, and amphiphilicity.[33] Veiga et al.[22] proved that the antimicrobial activity of another closely related SAP class is based on the cationic surface engaging the negatively charged, phospho-rich surface of the bacterial membrane, which leads to membrane disruption and consequently to cell death. Several groups have presented SAP hydrogels with a broad-spectrum antimicrobial activity combined with minimum cytotoxicity to eukaryotic cells.[22,34,35] For example MAX1, a 20-residue peptide consisting of valine and lysine amino acids, showed antimicrobial activity after direct contact with Gram-positive (*Staphylococcus epidermidis*, *Staphylococcus aureus*, and *Streptococcus pyogenes*) and Gram-negative (*Klebsiella pneumoniae* and *Escherichia coli*) bacteria on its hydrogel surface.[33]

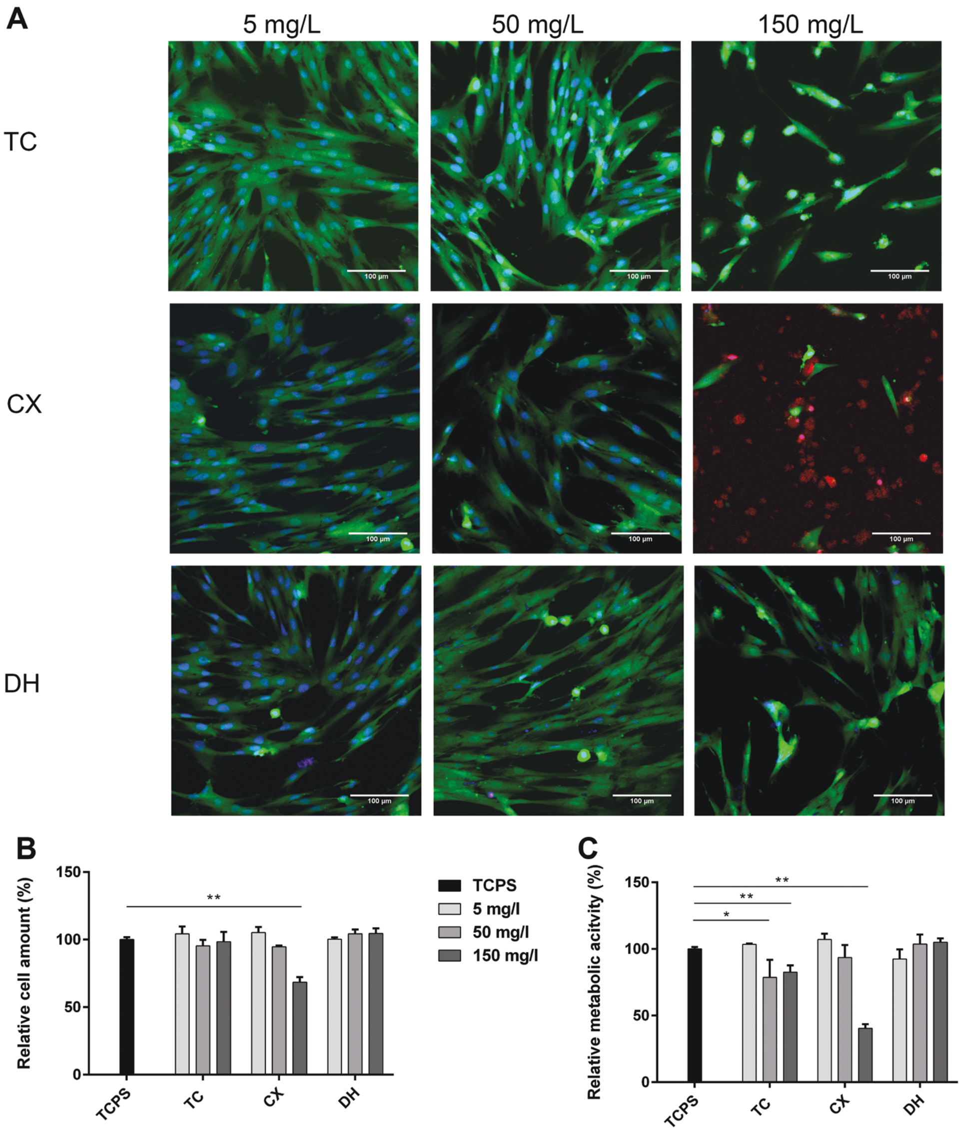

Figure 8. Analysis of viability and relative cell number of DFSCs after antibiotic treatment. A) Live/dead staining after 24 h incubation (in green: viable cells; in red: nuclei of dead cells, the scale bar corresponds to 100 µm). B) Relative cell number of DFSCs after 24 h incubation with different concentrations of TC, CX, and DH (5, 50, and 150 mg L^{-1}). C) Metabolic activity of DFSCs after 24 h incubation with different concentrations of TC, CX, and DH (DFSCs grown on TCPS were taken as a 100% control, $n = 3$ biological replicates and 3 technical replicates). A two-way ANOVA test was performed, followed by a Dunnetts's multiple comparison post hoc test with *p-value ≤ 0.01, **p-value ≤ 0.001).

In this study, no antimicrobial activity was observed for P11-4 hydrogels. This phenomenon can be explained by the overall negative net charge of P11-4 (QQRFEWEFEQQ), due to glutamic acid residues. In contrast to P11-4, P11-28/29 hydrogels showed antimicrobial activity, as proved by live/dead staining and turbidity measurements (Figure 2). The antimicrobial effect of P11-28/29 is based on the highly positive charge of P11-28 (OQOFOWOFOQO) due to the high number of ornithine residues and its structural similarity to lysine, which has previously been reported to possess an antimicrobial effect. Of note, *P. gingivalis* vitality and growth was more severely affected after culture on P11-28/29 hydrogels compared with the commensal bacterial species *S. sanguinis*. This result is most likely explained by the vast differences in membrane composition of Gram-positive and Gram-negative bacteria, but needs to be studied in more detail in the future. Overall this selectivity would be beneficial and promising for treatment, since many commensal species are Gram-positive and could survive. Monomers of P11-4, P11-28, and P11-29 neither affected bacterial growth nor contributed to the killing rate compared with the BHI control (Table S2 and Figure S5, Supporting Information). Therefore, we concluded that the charge density on SAP in its monomeric state is too low to cause a bactericidal effect.

In addition to the antimicrobial activity of SAP hydrogels, the membrane disruptive effect and regenerative capacity are important functional parameters and quality measures to be monitored. As reported in previous studies for other SAP systems, such as MAX1, no disruptive effect on eukaryotic membranes (e.g., red blood cells) was detected for the SAP P11-4 and P11-28/29, neither in the monomeric nor in the polymerized state (hydrogels). The cell selectivity (bacteria vs eukaryotic) in membrane disruption is mainly caused by the difference in membrane composition, as mammalian cells lack anionic lipids such as lipopolysaccharides or lipoteichoic acid that can interact with the cationic hydrogels.

To test the ability of P11-4 and P11-28/29 hydrogels to act as a scaffold for dental stem cells, cell morphology, growth, and osteogenic differentiation were studied. DFSCs were used as a stem cell model system as they have the potential to undergo osteogenic, adipogenic, and neurogenic differentiation in vitro.[36–38] DFSCs cultured on P11-4 hydrogels showed an evenly spread phenotype, whereas on P11-28/29, hydrogels cells were round in shape. These observations were in line with the cellular growth rates measured, showing an ≈4 times lower growth rate of P11-28/29 compared with P11-4 and TCPS. As reported in our previous study,[31] the difference in cell morphology and cell growth can result from the discrepancy in protein adsorption of SAP hydrogels, as absorbed extracellular matrix proteins such as fibronectin can act as anchorage points for the cellular adherence to the scaffold. The lack of such anchor points can thus in turn have negative effects on cell morphology and cell growth.

Furthermore, osteogenic differentiation of DFSCs on TCPS, P11-4 and P11-28/29 was monitored up to 21 days via osteogenic markers such as ALP activity, and protein amounts of collagen type I OC and OPG. The levels of all osteogenic markers in DFSCs in contact with P11-4 and P11-28/29 were similar to the TCPS control (after osteogenic stimulation of DFSCs), suggesting that both SAP hydrogels do not interrupt osteogenic differentiation of DFSCs. However, the level of osteogenic differentiation varied between P11-4 and P11-28/29 hydrogels. This effect can be explained by the different surface chemistry of the SAP, as evaluated recently.[31]

Overall, these results are in good agreement with previous reports, demonstrating a high degree of osteogenic differentiation of mesenchymal stem cells on various nanofibrillar SAP hydrogels.[39,40]

To sustain a regenerative environment where cells are able to form new tissue structures, the high microbial load and the diverse spectrum of bacteria within the subgingival fluid has to be countered. As the intrinsic antimicrobial activity of SAP hydrogels may not be sufficient by itself to reduce the microbial invasion from subgingival reservoirs, encapsulation of antibiotics with subsequent temporal release would be beneficial. As a proof of concept, we incorporated three classes of antibiotics (TC, CX, and DH) at a concentration of 150 mg L^{-1} into P11-4 and P11-28/29 hydrogels and tested their sustained drug delivery potential. First, we proved that encapsulation does not disturb self-assembly by the interaction of the SAP monomers with TC, CX, and DH. TEM studies and tubing tests revealed no disturbance of fiber formation and no inhibition of hydrogelation for P11-4 or for P11-28/29 in the presence of the antibiotics.

Afterward, the release properties of antibiotics from P11-4 and P11-28/29 hydrogels were studied, since sustained, therapeutically effective levels of antibiotics could be beneficial to avoid a revivification of the inflammation. TC, CX, and DH concentrations in the range of 5.7–48.1, 4.2–30.5, and 7.9–38.1 mg L^{-1} were constantly released for up to 120 h, respectively. Moreover, concentrations of TC, CX, and DH released from P11-SAP hydrogels were similar to or even higher than the concentrations reached in the gingival crevicular fluid after oral dosing of CX (2.39 ± 0.09 µg mL^{-1}, 500 mg twice a day[41]), DH (3–10 µg mL^{-1}, 100 mg once a day[42]), and TC (0.61 µg mL^{-1}, 250 mg once[43]). Furthermore, the antibiotic concentrations after release from P11-4 and P11-28/29 did not only exceed the determined MIC values, but also the minimal bactericidal concentrations, which are reported to be several times higher.[41] These promising kinetic release values were confirmed by bacterial growth experiments, demonstrating the high bactericidal effect of TC, CX, and DH extracts on *P. gingivalis* and *S. sanguinis*. No cytotoxic effects of these antibiotic concentrations were found in DFSCs. To proof that the release of TC, CX, and DH from P11-4 and P11-28/29 hydrogel will be therapeutically sufficient, further in vivo animal experiments are needed.

4. Conclusion

In summary, our results support the applicability of the SAP hydrogels as drug delivery systems and thus their potential future usefulness in periodontal therapy. P11-4 demonstrated no antimicrobial activity, a sustained release delivery for TC, CX, and DH, and a good regenerative capacity in different in vitro model systems. On the other hand, P11-28/29 showed antimicrobial activity against Gram-negative bacteria as well as Gram-positive bacteria, intermediate regeneration capacity (low cellular growth rates but good osteogenic differentiation achieved) and long-term release of incorporated TC, CX, and DH. In the event that the delivery of one antibiotic will be sufficient to combat the periodontal inflammation, P11-4 with the incorporation of one antibiotic may be favorable. However, if two or more antibiotics are required to treat pathogenic bacteria with differential sensitivity to antimicrobials,[3] the complementary P11-28/29 system may be used as a multidrug delivery system by diluting one antibiotic to a P11-28 and the other antibiotic to a P11-29 monomer solution, before mixing and assembling them to form the P11-28/29 hydrogel. Based on these in vitro results regarding release properties, the bacterial growth inhibition and the absence of cytotoxicity, DH might be favorable for antibiotic incorporation into P11-SAP hydrogels. As a next step, SAP hydrogels will be evaluated in animal models of periodontitis, which have been recently established in our lab.[44]

5. Experimental Section

SAP and SAP Preparation: The SAP P11-4 (sequence: CH_3CO-QQRFEWEFEQQ-NH_2, peptide content 95%, ammonium salt), P11-28 (sequence: CH_3CO-OQOFOWOFOQO-NH_2, peptide content 70.7%, TFA salt), and P11-29 (sequence: CH_3CO-QQEFEWEFEQQ-NH_2, peptide content 89.0%, ammonium salt) were purchased from CS Bio Co, USA. Quality control was done by high performance liquid chromatography (HPLC) and MS.

The monomer solutions of P11-4, P11-28, and P11-29 were prepared at a concentration of 1.5 mg mL^{-1} in either BHI medium (Oxoid, UK) to study bacterial growth, or 1× PBS (Sigma-Aldrich, Germany) to evaluate the time dependent killing rate of bacteria and red blood cell (RBC) membrane disruption.

For the assessment of bacterial growth, bacterial vitality, RBC membrane disruption, DFSCs metabolic activity, and DFSCs osteogenic differentiation, P11-SAP hydrogels were prepared in either 24- or 96-well plates, as previously described.[31]

For the incorporation of antibiotics into P11-SAP hydrogels, stock solutions of 1000 mg L^{-1} were prepared for TC (Sigma-Aldrich, Germany), CX (Sigma-Aldrich, Germany), and DH (Sigma-Aldrich, Germany) in water, and sterile filtered with a syringe filter (pore size: 0.22 µm; Braun Sterifix, B. Braun Melsungen AG, Germany). For CX, the stock solution was adjusted to a pH of 5 using 0.1 м HCl for it to fully dissolve. For all antibiotics, a final concentration of 150 mg L^{-1} was achieved in 100 µL of P11-SAP hydrogel by dissolving, for example, 1.5 mg of P11-4 with 35 µL of buffer A (55×10^{-3} м Tris, Sigma-Aldrich, Germany, pH 8) followed by the addition of 15 µL of antibiotic stock solution. To achieve a final concentration of 15 mg mL^{-1} P11-4 and 150 mg L^{-1} antibiotic concentration, 50 µL of buffer B (55×10^{-3} м Tris, 192×10^{-3} м NaCl, pH 6.8) was added. After antibiotic incorporation, P11-SAP hydrogels were incubated overnight at 37 °C to ensure full assembly.

Fibrillar Microstructure after Antibiotic Incorporation: To confirm fibril formation after encapsulation of TC, CX, and DH during the self-assembling process of P11-4 and P11-28/29, SAP hydrogels were prepared according to the description given in "SAP and SAP Preparation" and assembled overnight at room temperature. Afterward, SAP hydrogels were diluted with water (1:64). 10 µL of the solution was added to a TEM copper grid (Electron Microscopy Sciences, USA) and incubated for 7 min at room temperature. The residual sample was removed from the grid. Negative staining of the fibrils was achieved by adding 10 µL of uranyl acetate (2%, Electron Microscopy Sciences, USA) to parafilm and dipping the grid into the solution for 30 s. To remove residual uranyl acetate, the grid was washed two times with water prior to drying the sample for 1 h. Images were taken with a transmission electron microscope (Zeiss EM900, Germany), equipped with an AMT XR280 sCMOS camera (AMT- Advanced Microscopy Techniques, USA) and an AMT Image Capture Engine V700 software (AMT- Advanced Microscopy Techniques, USA).

Bacteria and Culture Conditions: P. gingivalis W83 was kindly provided by Potempa and co-workers[45] and cultured on Columbia blood agar plates (5% sheep blood, Becton Dickinson, Germany). *P. gingivalis* cultures were maintained by weekly subculture for up to 5 weeks. Liquid cultures were prepared by inoculation of bacterial colonies from blood agar plates into 10 mL BHI medium (Oxoid, UK) and subsequent incubation for 24 h under anaerobic conditions (10%, CO_2, 10% H_2, 80% N_2) at 37 °C in a Don Whitley Scientific anaerobic cabinet (Meintrup DWS Laborgeräte GmbH, Germany). *Streptococcus sanguinis (S. sanguinis)* (DSM 20567) was purchased from the Leibniz Institute DSMZ (German collection of microorganisms and cell cultures, Germany) and maintained on BHI agar plates (1.5% Agar technical No 3, Oxoid, UK). For all experiments, *S. sanguinis* was inoculated into 30 mL of freshly prepared BHI medium from BHI agar plates and incubated overnight at 37 °C under aerobic conditions (5% CO_2).

DFSCs Cultivation: DFSCs were isolated and characterized as described by Chatzivasileiou et al.[46] Cells were maintained and expanded in 75 cm^2 culture flasks (CELLSTAR, Greiner bio-one, Germany) in maintenance medium consisting of Dulbecco's modified Eagle medium (DMEM containing 4.5 g L^{-1} D-Glucose GlutaMAX, Invitrogen, Germany) and 10% fetal bovine serum (FBS, Invitrogen, Germany). Every 2–3 days, the maintenance medium was replaced. Upon 80–90% confluency, the cells were detached with 0.05% trypsin (Gibco Life Technologies, Germany) and transferred into a new 75 cm^2 culture flask. For all subsequent in vitro experiments, DFSCs from passages 4 to 6 were used.

In Vitro Assays Determining Bacterial Growth, Killing Rate, and Vitality: Bacterial Generation Times and Growth Rates: To evaluate the growth of *P. gingivalis* and *S. sanguinis* in contact with P11-SAP monomers, hydrogels and antibiotic extracts, bacteria were grown to the stationary phase in BHI medium under either anaerobic or aerobic conditions at 37 °C. Bacteria were harvested by centrifugation at 4000× rpm for 10 min at 5 °C. Sedimented bacteria were washed in PBS by centrifugation for 5 min at 4000 rpm, 5 °C. Subsequently, bacteria were diluted to their strain-specific optical density at 600 nm (OD_{600}) to obtain 1×10^8 CFU mL^{-1}. For further experiments, *P. gingivalis* and *S. sanguinis* were diluted tenfold in BHI medium to obtain a living bacterial count of 1×10^7 CFU mL^{-1}. Optical densities were measured with a SpectraMax M2 microplate reader (Molecular Devices, USA), to follow any increase in turbidity. Measurements were done at 0, 1, 2, 4, 8, and 24 h after cultivation with P11-SAP monomers and at 24 and 48 h after cultivation with P11-SAP hydrogels. As a control, bacteria were cultured in BHI without the addition of SAP monomers. To determine the growth rate (μ) and the generation time (g) after cultivation with P11-SAP monomers, the following equations were used as described by Cappuccino & Sherman[47]

$$\mu = \left[\left(\log_{10} N - \log_{10} \ N_0 \right) * \left(\frac{2.303}{t - t_0} \right) \right] \tag{1}$$

$$g = \frac{\log_{10} N - \log_{10} N_0}{\log_{10} 2} \tag{2}$$

Bacterial growth (in %) after exposure to P11-SAP hydrogels was calculated with the following equation

$$\begin{aligned} &\% \ \text{bacterial growth (hydrogel)} \\ &= \frac{\left(\text{OD}\,(\text{matrix} + \text{bacteria}) - \text{OD}\,(\text{matrix})\right) + \text{OD}\,(\text{supernatant})}{\text{OD}\,(\text{control})} * 100 \end{aligned} \tag{3}$$

Optical density of bacteria grown in pure BHI was normalized to 100%.

Bacterial Time-Dependent Killing Assay: A killing assay was performed to investigate the bactericidal effect of P11-SAP monomers on vital *P. gingivalis* and *S. sanguinis* in comparison with the untreated control. The bacteria were prepared as described in "In Vitro Assays Determining Bacterial Growth, Killing Rate, and Vitality: Bacterial Generation Times and Growth Rates" in PBS. For the quantification of living bacterial counts after cultivation for 2, 4, and 24 h, bacterial suspensions were serially diluted in PBS and plated on blood agar plates (*P. gingivalis*) or BHI agar plates (*S. sanguinis*), respectively. Agar plates were cultivated for at least 24 h at 37 °C under either anaerobic or aerobic conditions. Finally, living bacteria were quantified by counting CFU on agar plates (CFU mL^{-1}). As a positive control, bacteria were suspended in PBS without the addition of P11-SAP.

Bacterial Vitality Visualized by Live/Dead Staining: Qualitative analysis of the antimicrobial activity of P11-4 and P11-28/29 hydrogels was performed by microscopic evaluation. SAP hydrogels were prepared on glass coverslips (Sigma-Aldrich, Germany) in a 24-well plate (Greiner bio-one, Germany) cultured with *P. gingivalis* and *S. sanguinis* in BHI medium as described in "In Vitro Assays Determining Bacterial Growth, Killing Rate, and Vitality: Bacterial Generation Times and Growth Rates." After 48 h of incubation, supernatants were removed and bacteria were fixed with 4% paraformaldehyde solution (Sigma-Aldrich, Germany) for 1 h. Samples were washed twice with PBS before staining with a bacterial live/dead staining kit (LIVE/DEAD BacLight Bacterial Viability Kit, Thermo Fisher Scientific, Germany) containing SYTO9 (1:1000 in PBS) and propidium iodide (PI) (1:1000 in PBS) for 20 min at 37 °C under either anaerobic or aerobic conditions. Finally, the glass coverslips were washed twice with PBS and transferred with a tweezer in an ibidi slide (Ibidi, Germany). Samples were inspected with a confocal laser-scanning microscope (LSM 780, Zeiss, Germany) using 60× objective. Representative pictures were taken and stored with the accompanying Zeiss Zen software (Zeiss, Germany).

Determination of MICs: The MICs of TC, CX, and DH on *P. gingivalis* and *S. sanguinis* were assessed by performing a conventional agar dilution method described by Ericsson and Sherris.[48] In addition, the susceptibility of an antibiotic dilution range on *P. gingivalis* and *S. sanguinis* was determined by measuring the turbidity at an OD of 600 nm as described by Andrew.[49] Stock solutions of the three antibiotics were prepared at 1000 mg L^{-1} in water and further diluted to 128, 32, 8, 2, 0.5, 0.125, and 0.03 mg L^{-1} in BHI medium. Bacterial suspensions were prepared as described in "In Vitro Assays Determining Bacterial Growth, Killing Rate, and Vitality: Bacterial Generation Times and Growth Rates" by inoculation of the diluted antibiotic solutions with 1 × 10^{7} CFU mL^{-1} and incubated at 37 °C for 24 h under anaerobic (*P. gingivalis*) and aerobic conditions (*S. sanguinis*). Bacteria grown in BHI medium served as a control. After 24 h, the turbidity of the samples was measured at 600 nm with a SpectraMax M2 microplate reader (Molecular Devices, USA) and samples plated on BHI agar plates or blood agar plates to determine the CFU mL^{-1}.

Hemolytic Activity of P11-SAP Monomers and Hydrogels: As a sensitive surrogate experiment for cytotoxicity, the hemolytic activities of P11-4, P11-28, and P11-29 in a monomeric state and as SAP hydrogels were determined using hRBCs. Blood was obtained from the Institute for Transfusion Medicine, University Medical Center Rostock. The preparation of hRBCs was done according to Veiga et al.[22] Briefly, SAP monomers were dissolved in bis-tris propane buffer (BTP, Sigma-Aldrich, Germany) and were added to hRBC stock solution, resulting in a final hRBC concentration of 0.08% (v/v). For P11-4 and P11-28/29 hydrogels, the hRBCs stock solution was mixed with BTP buffer and placed on top of the hydrogels. Samples were then incubated at 37 °C for 1 h. To determine the release of hemoglobin due to membrane disruption, supernatants of the SAP hydrogels were removed and centrifuged at 14 000 rpm for 10 min at 4 °C. SAP monomer samples were directly centrifuged. The amount of hemoglobin released in the supernatants was determined photometrically at 415 nm (Beckmann Anthos Microplate Reader, Germany). BTP buffer was used as a 0% control (no hemolysis detectable), whereas 100% hemolysis was defined by the addition of 1% Triton X-100 solution to the hRBC solution.

DFSCs Viability Assays: Cell Mass Determined by Crystal Violet Staining: Crystal violet staining on DFSCs was performed according to Feoktistova et al.[50] after 1 and 4 days of treatment with freshly prepared TC, CX, and DH solutions (5, 50, and 150 mg L^{-1} in maintenance medium). DFSCs were seeded at a density of 6 × 10^{3} cells per well in a 96-well plate. Briefly, cells were washed twice with PBS before they were fixed with isopropanol (SERVA Electrophoresis GmbH, Germany). After fixation, cells were washed three times with PBS/0.05% Tween prior to staining with 0.1% crystal violet solution (Sigma-Aldrich, Germany). To excavate crystal violet from the attached cells, acetic acid (33%) was added. As a final step, the supernatant was transferred to a new 96-well plate (Greiner bio-one, Germany) and absorption was measured at 450 nm with a spectrophotometer (Beckmann Anthos Microplate Reader, Germany). DFSCs cultured in an expansion medium on TCPS were used as an untreated control.

Quantification of Metabolic Activity: As a second independent cell viability parameter, the metabolic activity of DFSCs was assessed after 1 and 4 days of incubation with TC, CX, and DH solutions at concentrations of 5, 50, and 150 mg L^{-1} by performing a CellTiter96 Aqueous One Solution Cell Proliferation MTS test (MTS, Promega, Germany). The protocol was followed according to Herzmann et al.[51] Cells were seeded at a density of 6 × 10^{3} cells per well in a 96-well plate.

Based on the intrinsic autofluorescence of the P11-SAP, another reagent with an excitation wavelength above 490 nm was selected. For this purpose, the metabolic activity of DFSCs (6 × 10^{3} cells per well, 96-well plate) in contact with P11-SAP hydrogels was analyzed after 1, 3, 7, and 14 days by using the PrestoBlue Viability Reagent (Thermo Fisher Scientific, Germany) as previously described.[31] Prior to the analysis, supernatants were transferred into a new 96-well plate and fluorescence was measured at an emission wavelength of 590 nm with excitation at 560 nm using a fluorescence microplate reader (TECAN, Germany). As a control, DFSCs were cultured on TCPS in expansion medium.

Live/Dead Staining: In addition, DFSCs (2 × 10^{4} cells per well, 24-well plate) were stained with live/dead stain using calcein AM (0.3 µg mL^{-1} in DMEM, Becton Dickinson, Germany), PI (1 µg mL^{-1} in DMEM, Becton Dickinson, Germany) and nuclear dye Hoechst 33342 bisbenzimide (5 µg mL^{-1}, Sigma-Aldrich, Germany) after 1 day and 4 days of antibiotic treatment. Stained cells were incubated for 15 min at 37 °C. Prior to imaging with a Zeiss confocal microscope LSM780 (Zeiss, Germany), the media was removed and replaced by maintenance media. As a control, DFSCs were cultured in maintenance medium.

Staining for Cell Morphology: To evaluate DFSCs morphology after 24 h of exposure on P11-SAP hydrogels (prepared in chamber slides, SPL Life Sciences, Korea), cells (1 × 10^{4} per well) were stained for actin cytoskeleton using Rhodamine-conjugated phalloidin (1:40 in DPBS, Thermo Fisher Scientific, Switzerland). The staining protocol was previously described.[31] Visualization was achieved using a confocal laser-scanning microscope (LSM 780, Zeiss, Germany).

Osteogenic Differentiation: DFSCs (1 × 10^{4} per well) were seeded on top of P11-4 and P11-28/29 hydrogels prepared in chamber slides (SPL Life Sciences, Korea). The osteogenic differentiation medium contained DMEM 10% FBS, 1% penicillin/streptomycin (Sigma-Aldrich, Germany), 1 × 10^{-6} M dexamethasone (Sigma-Aldrich, Germany), 250 µg mL^{-1} ascorbate (Sigma-Aldrich, Germany), and 10 × 10^{-3} M β-glycerophosphate (Sigma-Aldrich, Germany) to induce DFSCs osteogenic differentiation. Cells were cultured at 37 °C and 5% CO$_2$ atmosphere up to 21 days with fresh medium replacement every 2–3 days. After 1, 7, 14, and 21 days the supernatant was removed and osteogenic markers (OC and OPG) were quantified by a Milliplex MAP Human Bone Magnetic Bead Kit (Merck Milipore, Germany) according to the manufacturer's protocol. Data were collected with a Bio-Plex 200 system (Bio-Rad, Germany).

Antibiotic Release Profiles Determined by HPLC-MS: To study the in vitro release profile of TC, CX, and DH-based P11-SAP hydrogels, (prepared in 1.5 mL protein low binding tubes, Eppendorf, Germany, as described in "SAP and SAP Preparation"), 100 µL of PBS was added on top of the hydrogels. After 0, 2, 4, 8, 24, 48, 72, 96, and 120 h incubation at 37 °C, 50 µL samples were collected in 1.5 mL protein low-binding tubes (Eppendorf, Germany) and frozen at −20 °C. To imitate a constant flow rate over time, 50 µL of fresh PBS was added at each time point where supernatants had been taken for analysis. Prior to the analysis by HPLC-MS (Agilent Technologies, Switzerland), collected samples were thawed at room temperature and centrifuged (12 500 rpm, 30 min, Spectrafuge 24D, Labnet International Inc, USA) to remove residual fibril fragments. Detailed information about the HPLC procedure is provided in Figure S1 of the Supporting Information.

The release of TC, CX, and DH based on the applied protocol was calculated as an example with the following equation for $t = 8$ h

$$\text{Cumulative concentration}\left(t_{8\text{h}}\right) = \left(\text{concentration}_{t(8\text{h})} - \left(\frac{\text{concentration}_{t(4\text{h})}}{2}\right)\right) + \text{cumulativ concentration}_{t(4\text{h})} \tag{4}$$

$$\text{Cumulative concentration in \%} = (\text{cumulative concentration}_{(\text{tx})} * 100)/15 \tag{5}$$

Statistical Analysis: For bacterial experiments (Table 1, Figures 2E,F and 7) as well for the cell experiments (Figures 3C–G and 8B,C) at least three biological and three technical triplicates have been measured. The hemolytic activity (Figure 4) and the cumulative release of antibiotics (Figure 6) have been measured in triplicates. Data from the named figures above are presented as mean values ± standard deviation. All statistics were performed using the program GraphPad Prism 6. To test for significant differences between the control and test groups as well as between all groups, a one-way (Figure 4) or two-way ANOVA (Table 1, and Figures 2E,F and 8B,D) followed by Dunnett's (Figures 3D–G, 4, and 8B,D) or Tukey's (Table 1, Figure 2E,F) multiple comparison post hoc test was performed. A p-value of ≤ 0.01 was considered significant.

Supporting Information

Supporting Information is available from the Wiley Online Library or from the author.

Acknowledgements

This work was funded and supported by credentis AG (Windisch, Switzerland) and the Forschungsfond Aargau (Project No. 20150831_11, Windisch, Switzerland). The authors would like to thank Michael Hug and Dominik Lysek (credentis AG) for funding and supporting this work and for the valuable discussions.

Conflict of Interest

The authors declare no conflict of interest.

Keywords

antibiotic delivery, antimicrobial activity, dental stem cells, periodontal disease, self-assembling peptides

Received: February 7, 2019
Revised: March 20, 2019

[1] K. Schwach-Abdellaoui, N. Vivien-Castioni, R. Gurny, *Eur. J. Pharm. Biopharm.* **2000**, *50*, 83.
[2] K. Y. How, K. P. Song, K. G. Chan, *Front. Microbiol.* **2016**, *7*, 53.
[3] A. Aurer, D. PlanEak, *Acta Stomatol. Croat.* **2004**, *38*, 67.
[4] J. Slots, M. Ting, *Periodontology* **2002**, *28*, 106.
[5] J. Gordon, C. Walker, I. Lamster, T. West, S. Socransky, M. Seiger, R. Fasciano, *J. Periodontol.* **1985**, *56*, 75.
[6] A. L. Dumitrescu, *Antibiotics and Antiseptics in Periodontal Therapy*, Springer, Berlin, Germany **2011**.
[7] C. M. Bollen, M. Quirynen, *J. Periodontol.* **1996**, *67*, 1143.
[8] B. N. Vandekerckhove, M. Quirynen, D. van Steenberghe, *J. Periodontol.* **1997**, *68*, 353.
[9] N. Jain, G. K. Jain, S. Javed, Z. Iqbal, S. Talegaonkar, F. J. Ahmad, R. K. Khar, *Drug Discovery Today* **2008**, *13*, 932.
[10] L. Xu, X. Sun, J. Bai, L. Jiang, S. Wang, J. Zhao, L. Xia, X. Zhang, J. Wen, G. Li, *Clin. Implant Dent. Relat. Res.* **2016**, *18*, 379.
[11] Y. Loo, M. Goktas, A. B. Tekinay, M. O. Guler, C. A. E. Hauser, A. Mitraki, *Adv. Healthcare Mater.* **2015**, *4*, 2557.
[12] L. Collins, A. L. Parker, J. D. Gehman, L. Eckley, M. A. Perugini, F. Separovic, J. W. Fabre, *ACS Nano* **2010**, *4*, 2856.
[13] K. Rajagopal, J. P. Schneider, *Curr. Opin. Struct. Biol.* **2004**, *14*, 480.
[14] H. Santana, C.L. Avila, I. Cabrera, R. Páez, V. Falcón, A. Pessoa, N. Ventosa, J. Veciana, R. Itri, L. R. S. Barbosa, *Soft Matter* **2014**, *10*, 9260.
[15] L. Sun, C. Zheng, T. J. Webster, *Int. J. Nanomed.* **2017**, *12*, 73.
[16] M. C. Branco, J. P. Schneider, *Acta Biomater.* **2009**, *5*, 817.
[17] J. Gao, C. Tang, M. A. Elsawy, A. M. Smith, A. F. Miller, A. Saiani, *Biomacromolecules* **2017**, *18*, 826.
[18] R. Pawar, A. Ben-Ari, A. J. Domb, *Expert Opin. Biol. Ther.* **2004**, *4*, 1203.
[19] M. J. Webber, J. B. Matson, V. K. Tamboli, S. I. Stupp, *Biomaterials* **2012**, *33*, 6823.
[20] S. Marchesan, Y. Qu, L. J. Waddington, C. D. Easton, V. Glattauer, T. J. Lithgow, K. M. McLean, J. S. Forsythe, P. G. Hartley, *Biomaterials* **2013**, *34*, 3678.
[21] L. Zhou, T. Qiu, F. Lv, L. Liu, J. Ying, S. Wang, *Adv. Healthcare Mater.* **2018**, *7*, 1800670.
[22] A. S. Veiga, C. Sinthuvanich, D. Gaspar, H. G. Franquelim, M. A. Castanho, J. P. Schneider, *Biomaterials* **2012**, *33*, 8907.
[23] L. Liu, L. Wang, W. Liu, Q. Li, Z. Jin, Y. Jin, *PLoS One* **2014**, *9*, e108752.
[24] L. A. Aly, *World J. Stem Cells* **2015**, *7*, 1047.
[25] B. C. Kim, H. Bae, I. K. Kwon, E. J. Lee, J. H. Park, A. Khademhosseini, Y. S. Hwang, *Tissue Eng., Part B* **2012**, *18*, 235.
[26] S. Koutsopoulos, *J. Biomed. Mater. Res., Part A* **2016**, *104*, 1002.
[27] K. M. Galler, A. Cavender, V. Yuwono, H. Dong, S. Shi, G. Schmalz, J. D. Hartgerink, R. N. D'Souza, *Tissue Eng., Part A* **2008**, *14*, 2051.
[28] J. Tsukamoto, K. Naruse, Y. Nagai, S. Kan, N. Nakamura, M. Hata, M. Omi, T. Hayashi, T. Kawai, T. Matsubara, *Tissue Eng., Part A* **2017**, *23*, 1394.
[29] A. Aggeli, N. Boden, S. Zhang, *Self-Assembling Peptide Systems in Biology, Medicine, and Engineering*, Springer, Dordrecht, NL **2001**.
[30] S. Kyle, S. H. Felton, M. J. McPherson, A. Aggeli, E. Ingham, *Adv. Healthcare Mater.* **2012**, *1*, 640.
[31] F. Koch, A. Wolff, S. Mathes, U. Pieles, S. Saxer, B. Kreikemeyer, K. Peters, *Int. J. Nanomed.* **2018**, *13*, 6717.
[32] F. Koch, M. Müller, F. König, N. Meyer, J. Gattlen, U. Pieles, K. Peters, B. Kreikemeyer, S. Mathes, S. Saxer, *R. Soc. Open Sci.* **2018**, *5*, 171562.
[33] D. A. Salick, J. K. Kretsinger, D. J. Pochan, J. P. Schneider, *J. Am. Chem. Soc.* **2007**, *129*, 14793.
[34] L. Schnaider, S. Brahmachari, N. W. Schmidt, B. Mensa, S. Shaham-Niv, D. Bychenko, L. Adler-Abramovich, L. J. W. Shimon, S. Kolusheva, W. F. DeGrado, E. Gazit, *Nat. Commun.* **2017**, *8*, 1365.
[35] G. Laverty, A. P. McCloskey, B. F. Gilmore, D. S. Jones, J. Zhou, B. Xu, *Biomacromolecules* **2014**, *15*, 3429.
[36] C. Morsczeck, W. Götz, J. Schierholz, F. Zeilhofer, U. Kühn, C. Möhl, C. Sippel, K. Hoffmann, *Matrix Biol.* **2005**, *24*, 155.
[37] F. Völlner, W. Ernst, O. Driemel, C. Morsczeck, *Differentiation* **2009**, *77*, 433.
[38] S. Yao, F. Pan, V. Prpic, G. Wise, *J. Dental Res.* **2008**, *87*, 767.
[39] L. A. Castillo Diaz, M. Elsawy, A. Saiani, J. E. Gough, A. F. Miller, *J.Tissue Eng.* **2016**, *7*, 204173141664978.
[40] C. R. Nuttelman, D. S. Benoit, M. C. Tripodi, K. S. Anseth, *Biomaterials* **2006**, *27*, 1377.
[41] M. Alamanda, S. K. Denthumdas, U. Wadgave, P. M. Pharne, S. J. Patil, S. Kondreddi, P. Deshpande, R. S. Koppikar, *J. Clin. Diagn. Res.* **2016**, *10*, ZC47.
[42] D. Pascale, J. Gordon, I. Lamster, P. Mann, M. Seiger, W. Arndt, *J. Clin. Periodontol.* **1986**, *13*, 841.
[43] J. Gordon, C. Walker, J. Murphy, J. Goodson, S. Socransky, *J. Periodontol.* **1981**, *52*, 609.
[44] M. Ebbers, P. M. Lübcke, J. Volzke, K. Kriebel, C. Hieke, R. Engelmann, H. Lang, B. Kreikemeyer, B. Müller-Hilke, *Sci. Rep.* **2018**, *8*, 15129.
[45] N. Wegner, R. Wait, A. Sroka, S. Eick, K. A. Nguyen, K. Lundberg, A. Kinloch, S. Culshaw, J. Potempa, P. J. Venables, *Arthritis Rheum.* **2010**, *62*, 2662.
[46] K. Chatzivasileiou, C. A. Lux, G. Steinhoff, H. Lang, *J. Cell. Mol. Med.* **2013**, *17*, 766.
[47] J. G. Cappuccino, N. Sherman, *Microbiology: A Laboratory Manual*, 7th ed., Pearson Int, Ontario, Canada **2005**.
[48] H. M. Ericsson, J. C. Sherris, *Acta Pathol. Microbiol. Scand.* **1971**, *217*, Suppl 217:1+.
[49] J. M. Andrews, *J. Antimicrob. Chemother.* **2001**, *48*, 5.
[50] M. Feoktistova, P. Geserick, M. Leverkus, *Crystal Violet Assay for Determining Viability of Cultured Cells*, Cold Spring Harbor Protocols, NY, USA **2016**.
[51] N. Herzmann, A. Salamon, T. Fiedler, K. Peters, *Exp. Cell Res.* **2016**, *342*, 95.

5 Diskussion

Die hohe bakterielle Belastung mit verschiedenen Bakterienspezies und der Verlust von Weich - und Hartgewebe während des Verlaufs einer Parodontitis führt zu einer komplexen Situation in der gebildeten Zahntasche. Diese Komplexität im parodontalen Defektbereich macht die Anforderungen an ein regenerativ wirksames Biomaterial sehr hoch [41].

Daher sollten die 4 ausgewählten SSP-Hydrogele anhand von *in vitro*-Modell-Systemen auf die Eigenschaften Zellverträglichkeit, antimikrobielle Eigenschaft und Antibiotika-Freisetzungskapazität untersucht werden. Im Rahmen der durchgeführten Studien sollte evaluiert werden, ob SSP-Hydrogele die Anforderungen als innovatives Biomaterial für eine mögliche Behandlung von Parodontitis erfüllen können. Diese Promotionsarbeit bildet daher die Grundlage für die Produktentwicklung und weiterführende *in vivo* Studien.

5.1 SSP-Hydrogele und ihr Effekt auf parodontale Gewebezellen

Aus früheren Untersuchungen ist bekannt, dass die physikalisch-chemischen Eigenschaften, wie Architektur, Oberflächenchemie und Ladung eines synthetischen Gerüsts, die zellulären Reaktionen und damit die Geweberegeneration positiv beeinflussen können [42-44].

Wie in der Veröffentlichung von Baker et al. [45] beschrieben, ist die fibrilläre Netzwerk-Architektur eines Biomaterials ein wichtiger Parameter, der das regenerative Potential beeinflussen kann. Eine flexible Netzwerkarchitektur ermöglicht den Zellen, mit den Fasern aus ihrer Umgebung in Kontakt zu treten und diese durch intrazelluläre mechanische Kräfte umzustrukturieren [46]. Die Adhäsion der Zelle an eine fibrilläre Matrixstruktur geht dabei einher mit einer Veränderung der Zellmorphologie. Diese Morphologieveränderung kann über das Aktin-Zytoskelett der Zelle Einfluss auf die Signaltransduktion nehmen und somit zugleich zu Veränderungen im Proliferationsverhalten führen [47].

Mittels REM-Analyse konnte in Studie I und II nachgewiesen werden, dass die untersuchten komplementären Peptidsysteme dichte Netzwerkstrukturen mit kleinen Maschenweiten und hohem Vernetzungsgrad ausbildeten, während die Einkomponenten-Systeme offene Netzwerke mit großen Maschenweiten und kleinen Vernetzungsgrad bildeten. Durch die flexible und offene Netzwerkstruktur der Einkomponenten-Systeme bildeten die Zellen einen ausgebreiteten Phänotyp aus und zeigten eine erhöhte Zellproliferation. Baker et al. [45] haben ein vergleichbares Phänomen bei der Testung von mesenchymalen Stammzellen auf weichen offen-porösen Dextran Methacrylat Fasern nachweisen können.

Auch die Oberflächenchemie und die Ladung eines Biomaterials spielen eine wichtige Rolle in der Kontrolle zellulärer Reaktionen, indem beide Parameter die Adsorptionskapazität von EZM-Proteinen, wie z. B. Fibronektin, an das Biomaterial beeinflussen können [48]. Da EZM-Proteine Zelladhäsionsmotive beinhalten, kann z. B. eine hohe Fibronektin-Adsorption zu einer gesteigerten Zelladhäsion und durch die Aktivierung intrazellulärer Signalkaskaden auch zu einer erhöhten Zellproliferation führen [45]. Wie in den Studien von Richter et al. [49] gezeigt, kann ein EZM-Protein, wie z. B. Fibronektin, durch seinen amphiphilen Charakter sowohl an positiv als auch negativ geladene Biomaterialien binden. Hingegen kann eine starke negative Ladung des Biomaterials zu einer erhöhten Abstossungsreaktion von Fibronektin führen [50]. Eine mögliche Assoziation zwischen Oberflächenladung, Proteinadsorptionskapazität und zellulärer Adhäsion und Proliferation konnte auch in Studie II beschrieben werden. Hier zeigte das Einkomponenten-System P11-4, welches ein Zeta-Potential von -30 mV aufweist, eine hohe Fibronektin-Adsorption, während das Komplementär-System P11-13/14 mit einer doppelt so hohen negativen Ladung (-60 mV) eine niedrigere Fibronektin-Adsorption aufwies. Die unterschiedlichen Proteinadsorptionskapazitäten scheinen sich auch in den entstehenden Zellmorphologien und der Zellproliferation widerzuspiegeln. Aufgrund dessen nehmen wir an, dass die Oberflächenchemie, respektive die Oberflächenladung eines SSP-Systems, ein kritischer Faktor ist, welcher die zelluläre Reaktion signifikant beeinflussen kann.

Darüber hinaus spielt die Oberflächenchemie eines Biomaterials eine entscheidende Rolle hinsichtlich der Zelldifferenzierung [51]. So ist z. B. aus einer Studie von Griffin et al. [52] bekannt, dass es einen Zusammenhang zwischen der Präsentation funktioneller Gruppen, wie z. B. der Aminogruppe (-NH_2), und einem gesteigerten Grad der osteogenen Differenzierung gibt. Ein vergleichbarer Effekt konnte auch in Studie II demonstriert werden: hier konnte ein höherer osteogener Differenzierungsgrad humaner Osteoblasten auf den SSP-Hydrogelen mit einem höheren Anteil von Aminogruppen erreicht werden (Verhältnis $NH_2 \geq COOH$).

Zusammenfassend lässt sich sagen, dass die Netzwerkarchitektur, die Oberflächenchemie und die Oberflächenladung wesentliche Parameter sind, die die Eignung von SSP-Sequenzen für den Einsatz als synthetische Gerüste für die Parodontaltherapie bestimmen können.

5.2 Intrinsische antimikrobielle Aktivität von P11-SSP Sequenzen

Wie in der Studie von Veiga et al. [53] berichtet, basiert die intrinsische antimikrobielle Aktivität der SSP auf der kationischen Oberfläche, die mit der negativ geladenen, phosphorreichen Oberfläche der Bakterienmembran interagieren kann und dadurch zu einer Zerstörung der Membran bis hin zum Zelltod führt.

In Studie III konnte eine signifikante bakterizide Wirkung von P11-28/29 Hydrogelen auf Gram-negative Bakterien (*P. gingivalis*) und eine weniger proklamierte Wirkung auf Gram-positive Bakterien (*S. sanguinis*) beobachtet werden. Der unterschiedliche Effekt bei Gram-positiven und Gram-negativen Bakterien lässt sich aus der variablen Membranzusammensetzung ableiten. Bei Gram-positiven Bakterien kann die negative Ladung aus Teichonsäuren abgeleitet werden, die entweder mit dem Peptidoglykan (Zellwand) oder mit der darunter liegenden Plasmamembran verbunden sind. Bei Gram-negativen Bakterien ist die Außenmembran mit Phospholipiden und Lipopolysacchariden bedeckt, die der Oberfläche eine stark negative Ladung verleihen [54]. Basierend auf diesen Fakten gehen wir davon aus, dass die positiv geladenen P11-28/29-Fasern, welche einen hohen Ornithingehalt besitzen, stark mit den negativ geladenen Phosphat- und KDO-Gruppen (2-Keto-Desoxyocturonsäure) der Lipopolysaccharide von Gram-negativen Bakterien interagieren. Weiterhin wurde in der Studie von Veiga et al. [53] nachgewiesen, dass eine hohe Menge an Arginin statt Lysin innerhalb der Peptidsequenz zu einem erhöhten antimikrobiellen Potenzial der SSP-Systeme führt.

Da die Aminosäure Ornithin (vorhanden in den SSP-Sequenzen der vorliegenden Studie) strukturähnlich zu Lysin ist, könnte es für eine zukünftige Studie interessant sein herauszufinden, ob die antimikrobielle Aktivität von P11-28/29 durch den Austausch von Ornithin gegen Arginin noch verstärkt werden kann. Dennoch kann nicht vorausgesagt werden wie sich ein solcher Austausch auf die Ausbildung von β-Faltblattstrukturen auswirken wird.

5.3 Die SSP-Sequenz und ihr Einfluss auf die Antibiotika-Freisetzung

Für eine lokale Antibiotika Therapie ist eine schnelle initiale Freisetzung der Wirkstoffe mit Konzentrationen oberhalb der minimalen Hemm-Konzentration der Bakterien wichtig, um eine bakterielle Infektion innerhalb der gebildeten Zahntasche zu stoppen und somit die Regeneration von neuem Gewebe zu gewährleisten.

Die Konzentration der getesteten Antibiotika (TC, CX und DH) nach initialer Freisetzung übertraf, wie in Studie III gezeigt, nicht nur die ermittelten MIC-Werte, sondern auch die Minimal Bakterizide Konzentration (MBK), für *P. gingivalis* und *S. sanguinis*, welche einem Vielfachen der MIC entspricht [55]. Diese vielversprechende initiale Freisetzung der Antibiotika aus P11-SSP-Hydrogelen konnte zusätzlich durch Bakterienwachstumsexperimente bestätigt werden, welche die hohe bakterizide Wirkung von Antibiotika-Extrakten auf *P. gingivalis* und *S. sanguinis* belegten. Da die gebildete Zahntasche ein perfektes Reservoir für Bakterien bildet, ist es wichtig eine konstante Antibiotika Freisetzung oberhalb der MIC über mehrere Tage zu halten, da es sonst zu einer nicht vollständigen Eradikation der Bakterien und dadurch zu einer potentiellen Rekurrenz der bakteriellen Infektion kommen kann. Die verzögerte/kontrollierte Freisetzung von Antibiotika wird hauptsächlich durch das Molekulargewicht, die Ladung und die Hydrophobizität des Antibiotikums bestimmt, aber zugleich auch durch die Peptid-Hydrogel Merkmale, wie die Oberflächenchemie, Ladung, Peptidkonzentration und Hydrogel-Porengröße [56]. Wie auch schon in der Studie von Nultsch & Germershaus [57] beschrieben, kann eine verzögerte kontrollierte Freisetzung durch die elektrostatische Interaktion und Komplexbildung eines positiv geladenen Wirkstoffes mit einem negativ geladenen Trägermaterial erreicht werden.

Diese Beobachtung stimmt mit unseren Ergebnissen aus Studie III überein. Zum Beispiel wurden die negativ geladenen Antibiotika Tetracyclin [58] und Doxycyclin [59] (pH 7) nur langsam und unvollständig (bis maximal 40 % nach 5 Tagen) aus dem positiv geladenen SSP-Komplementär-System freigesetzt. Dies kann auf eine Interaktion der Antibiotika aufgrund der physikochemischen Eigenschaften der fibrillären SSP-Hydrogele hindeuten. Trotz des simulierten Sulkus-Flüssigkeitsflusses und der verzögerten Freisetzung über 5 Tage wurden therapeutisch effektive Antibiotika Konzentrationen gemessen, welche eine antibakterielle Wirkung zeigten. Die freigesetzten Antibiotika-Konzentrationen aus SSP-Hydrogelen waren dabei vergleichbar mit der Konzentration der Antibiotika, welche oral verabreicht wurden und in der gingivalen Sulkusflüssigkeit gemessen wurden [55, 60, 61].

5.4 Eignung von P11-SSP-Hydrogelen

Die Untersuchung der P11-SSP-Hydrogele anhand von *in vitro*-Modell-Systemen ergab, dass die Einkomponenten-Systeme (wie z. B. P11-4) Eigenschaften besitzen, welche eine Weich- und Hartgewebe-Regeneration sowie eine Antibiotika-Freisetzung ermöglichen aber keine intrinsische antimikrobielle Aktivität aufweisen. Die Komplementär-Systeme (wie z. B. P11-28/29) hingegen besitzen eine intrinsische antimikrobielle Aktivität, dennoch aber ein geringeres Proliferations- und Differenzierungspotential *in vitro*. Die unterschiedlichen Proliferations-und Differenzierungspotentiale sowie die intrinsische antimikrobielle Aktivität können vermutlich auf die variable Aminosäurezusammensetzung der SSP zurückgeführt werden, welche die Eigenschaften der SSP-Hydrogele bestimmt. Somit bringen SSP-Hydrogele eine Reihe von Eigenschaften mit, die sie als innovatives Biomaterial für die parodontale Regeneration geeignet erscheinen lassen. Aufgrund dieser Ergebnislage können die SSP-Hydrogele weiterentwickelt und in prä-klinischen Studien getestet werden.

6 Zusammenfassung

Die Parodontitis ist eine komplexe entzündliche Erkrankung, die zur Zerstörung des Zahnhalteapparates führen kann. Das hohe Aufkommen verschiedener Bakterienspezies in der Mundhöhle sowie der Gewebedefekt von Weich- und Hartgewebe machen die Behandlung von Parodontitis sehr anspruchsvoll. Daher sind neuartige therapeutische Strategien erforderlich.

Hydrogele auf der Basis von selbststrukturierenden Peptiden (SSP) könnten aufgrund ihrer minimal-invasiven Applizierbarkeit, ihrer Biokompatibilität, ihrer Wirkstoff-Beladbarkeit und ihren einstellbaren physikalisch-chemischen und mechanischen Eigenschaften geeignete Kandidaten für die Parodontaltherapie sein. Im Rahmen dieser Promotionsarbeit wurden zwei Einkomponenten- und zwei komplementäre β-Faltblatt-bildende SSP-Systeme auf ihre Hydrogeleigenschaften, ihren Einfluss auf die Zellreaktion, ihre intrinsische antimikrobielle Aktivität und ihr Antibiotika-Freisetzungspotential untersucht.

Alle SSP-Hydrogele zeigten eine nanofibrilläre Netzwerkarchitektur, die mit nativen EZM-Strukturen vergleichbar war. Durch die Variation der Peptidkonzentration und der Pufferzusammensetzung konnten Steifigkeiten erzielt werden, die den Steifigkeiten von Weich- bis Hartgewebe entsprechen. Zellkulturexperimente zeigten eine höhere Zelladhäsion und ein gesteigertes Zellwachstum der Einkomponenten-Systeme im Vergleich zu den Komplementär-Systemen. Darüber hinaus wurde bei den Einkomponenten-Systemen ein signifikant erhöhter osteogener Differenzierungsgrad humaner Osteoblasten nachgewiesen. Für das positiv geladene Komplementär-System konnte eine signifikante intrinsische antibakterielle Wirkung auf *Porphyromonas gingivalis* nachgewiesen werden. Die Einarbeitung von Antibiotika hatte keinen Einfluss auf die Fibrillenbildung von SSP-Hydrogelen und führte zu einer Wirkstofffreisetzung von bis zu 5 Tagen, welche für eine lokale Antibiotikatherapie geeignet ist.

Insgesamt ergab diese Promotionsarbeit, dass P11-SSP-Hydrogele eine Reihe von Eigenschaften besitzen, welche erforderlich sind, um sie zu potentiellen Kandidaten im Rahmen neuartiger therapeutischer Strategien für die Behandlung der Parodontitis weiterzuentwickeln.

7 Summary

Periodontal disease (PD) is characterized by complex inflammatory conditions inside the oral cavity, leading to the destruction of tooth supporting structures. The high polymicrobiome in the oral cavity together with the destruction of soft and hard tissue, make periodontitis difficult to treat. Thus, novel therapeutic strategies are required.

Hydrogels based on self-assembling peptides (SAP) can be suitable candidates for periodontal therapy due to their injectability, biocompatibility, cargo-loading capacity and tunable physicochemical and mechanical properties. Within this PhD project, two single-component and two complementary β-sheet forming SAP systems were studied. The four SAP systems were investigated for their hydrogel properties, their influence on cell response, their intrinsic antimicrobial activity and their antibiotic delivery potential.

All SAP hydrogels provided a nanofibrillar network formation under physiological conditions, which were comparable to the architecture of native extracellular matrix structures. The stiffnesses of the four SAP hydrogels were similar to stiffnesses of soft and hard tissue. SAP hydrogel stiffness were found to be mostly affected by the peptide sequence, peptide concentration and buffer composition. Cell culture experiments revealed a significant increase in cell adhesion and cellular growth of the single component systems compared with the complementary systems. Moreover, for the single component systems, significantly enhanced osteogenic differentiation of human osteoblasts was detected. Microbiological studies revealed a significant intrinsic antibacterial effect only for the positive charged complementary SAP system on the periodontal pathogen *Porphyromonas gingivalis*. The incorporation of various antibiotics did not affect fibril formation of SAP hydrogels and resulted in release kinetics up to 5 days, which will be favorable for a local antibiotic therapy.

Overall, this thesis showed that P11-SAP hydrogels possess a number of properties that are necessary to develop them into potential candidates in novel therapeutic strategies for the treatment of periodontitis.

8 Referenzen

[1] Nazir MA. Prevalence of periodontal disease, its association with systemic diseases and prevention. International journal of health sciences 2017;11:72-80.

[2] Kim J, Amar S. Periodontal disease and systemic conditions: a bidirectional relationship. Odontology 2006;94:10-21.

[3] Bartold PM, Shi S, Gronthos S. Stem cells and periodontal regeneration. Periodontology 2000 2006;40:164-72.

[4] Polimeni G, Xiropaidis AV, Wikesjö UM. Biology and principles of periodontal wound healing/regeneration. Periodontology 2000 2006;41:30-47.

[5] Lira-Junior R, Figueredo CM. Periodontal and inflammatory bowel diseases: Is there evidence of complex pathogenic interactions? World journal of gastroenterology 2016;22:7963-72.

[6] Stabholz A, Soskolne WA, Shapira L. Genetic and environmental risk factors for chronic periodontitis and aggressive periodontitis. Periodontology 2000 2010;53:138-53.

[7] Lindroth AM, Park YJ. Epigenetic biomarkers: a step forward for understanding periodontitis. Journal of periodontal & implant science 2013;43:111-20.

[8] Hajishengallis G. Immunomicrobial pathogenesis of periodontitis: keystones, pathobionts, and host response. Trends in immunology 2014;35:3-11.

[9] Pelletier M, Maggi L, Micheletti A, Lazzeri E, Tamassia N, Costantini C, et al. Evidence for a cross-talk between human neutrophils and Th17 cells. Blood 2010;115:335-43.

[10] Nussbaum G, Shapira L. How has neutrophil research improved our understanding of periodontal pathogenesis? Journal of Clinical Periodontology 2011;38:49-59.

[11] Ryder MI. Comparison of neutrophil functions in aggressive and chronic periodontitis. Periodontology 2000 2010;53:124-37.

[12] Beklen A, Ainola M, Hukkanen M, Gürgan C, Sorsa T, Konttinen Y. MMPs, IL-1, and TNF are regulated by IL-17 in periodontitis. Journal of dental research 2007;86:347-51.

[13] Lee Y. The role of interleukin-17 in bone metabolism and inflammatory skeletal diseases. BMB reports 2013;46:479.

[14] Leivadaros E, Van der Velden U, Bizzarro S, ten Heggeler JM, Gerdes VE, Hoek FJ, et al. A pilot study into measurements of markers of atherosclerosis in periodontitis. Journal of periodontology 2005;76:121-8.

[15] Prabhu A, Michalowicz BS, Mathur A. Detection of local and systemic cytokines in adult periodontitis. Journal of periodontology 1996;67:515-22.

[16] Scannapieco FA, Bush RB, Paju S. Associations between periodontal disease and risk for atherosclerosis, cardiovascular disease, and stroke. A systematic review. Annals of Periodontology 2003;8:38-53.

[17] Tariq M, Iqbal Z, Ali J, Baboota S, Talegaonkar S, Ahmad Z, et al. Treatment modalities and evaluation models for periodontitis. International journal of pharmaceutical investigation 2012;2:106.

[18] Bhavsar A, Parween S, Varadhan K, Prabhuji M. Critical Issues in Periodontal Regeneration-A Review. J Oral Health Dent 2018;2:204.

[19] Sheikh Z, Hamdan N, Ikeda Y, Grynpas M, Ganss B, Glogauer M. Natural graft tissues and synthetic biomaterials for periodontal and alveolar bone reconstructive applications: a review. Biomaterials research 2017;21:9.

[20] Sheikh Z, Najeeb S, Khurshid Z, Verma V, Rashid H, Glogauer M. Biodegradable materials for bone repair and tissue engineering applications. Materials 2015;8:5744-94.

[21] Chai Q, Jiao Y, Yu X. Hydrogels for biomedical applications: their characteristics and the mechanisms behind them. Gels 2017;3:6.

[22] Gunatillake PA, Adhikari R. Biodegradable synthetic polymers for tissue engineering. Eur Cell Mater 2003;5:1-16.

[23] Mishra M, Mishra P, Shambharkar V, Raut A. Scaffolds in Periodontal Regeneration2016.

[24] Matson JB, Stupp SI. Self-assembling peptide scaffolds for regenerative medicine. Chemical communications 2012;48:26-33.

[25] Aggeli A, Boden N, Zhang S. Self-assembling peptide systems in biology, medicine, and engineering: Springer; 2001.

[26] Kyle S, Felton SH, McPherson MJ, Aggeli A, Ingham E. Rational Molecular Design of Complementary Self-Assembling Peptide Hydrogels. Advanced Healthcare Materials 2012;1:640-5.

[27] Laurenti M, Abdallah M-N. Natural and synthetic hydrogels for periodontal tissue regeneration. International Dental Journal of Student's Research, January–March 2015: 3 (2) 2015:46.

[28] Sun L, Zheng C, Webster TJ. Self-assembled peptide nanomaterials for biomedical applications: promises and pitfalls. International journal of nanomedicine 2017;12:73.

[29] Tu RS, Tirrell M. Bottom-up design of biomimetic assemblies. Advanced drug delivery reviews 2004;56:1537-63.

[30] Shi J, Xu B. Nanoscale assemblies of small molecules control the fate of cells. Nano Today 2015;10:615-30.

[31] Aggeli A, Bell M, Carrick LM, Fishwick CW, Harding R, Mawer PJ, et al. pH as a trigger of peptide β-sheet self-assembly and reversible switching between nematic and isotropic phases. Journal of the American Chemical Society 2003;125:9619-28.

[32] Carrick LM, Aggeli A, Boden N, Fisher J, Ingham E, Waigh TA. Effect of ionic strength on the self-assembly, morphology and gelation of pH responsive β-sheet tape-forming peptides. Tetrahedron 2007;63:7457-67.

[33] Aggeli bA, Bell M, Boden N, Keen J, Knowles P, McLeish T, et al. Responsive gels formed by the spontaneous self-assembly of peptides into polymeric β-sheet tapes. Nature 1997;386:259.

[34] Bell CJ, Carrick LM, Katta J, Jin Z, Ingham E, Aggeli A, et al. Self-assembling peptides as injectable lubricants for osteoarthritis. Journal of Biomedical Materials Research Part A 2006;78:236-46.

[35] Maude S, Ingham E, Aggeli A. Biomimetic self-assembling peptides as scaffolds for soft tissue engineering. Nanomedicine 2013;8:823-47.

[36] Kyle S, Aggeli A, Ingham E, McPherson MJ. Production of self-assembling biomaterials for tissue engineering. Trends in biotechnology 2009;27:423-33.

[37] Firth A, Aggeli A, Burke JL, Yang X, Kirkham J. Biomimetic self-assembling peptides as injectable scaffolds for hard tissue engineering. Nanomedicine 2006;1:189-99.

[38] Kirkham J, Firth A, Vernals D, Boden N, Robinson C, Shore R, et al. Self-assembling peptide scaffolds promote enamel remineralization. Journal of dental research 2007;86:426-30.

[39] Chatzivasileiou K, Lux CA, Steinhoff G, Lang H. Dental follicle progenitor cells responses to Porphyromonas gingivalis LPS. Journal of cellular and molecular medicine 2013;17:766-73.

[40] Wegner N, Wait R, Sroka A, Eick S, Nguyen KA, Lundberg K, et al. Peptidylarginine deiminase from Porphyromonas gingivalis citrullinates human fibrinogen and α-enolase: Implications for autoimmunity in rheumatoid arthritis. Arthritis & Rheumatism 2010;62:2662-72.

[41] Shue L, Yufeng Z, Mony U. Biomaterials for periodontal regeneration: a review of ceramics and polymers. Biomatter 2012;2:271-7.

[42] Tang L, Thevenot P, Hu W. Surface chemistry influences implant biocompatibility. Current topics in medicinal chemistry 2008;8:270-80.

[43] Anselme K. Osteoblast adhesion on biomaterials. Biomaterials 2000;21:667-81.

[44] Keselowsky BG, Collard DM, García AJ. Surface chemistry modulates fibronectin conformation and directs integrin binding and specificity to control cell adhesion. Journal of Biomedical Materials Research Part A 2003;66:247-59.

[45] Baker BM, Trappmann B, Wang WY, Sakar MS, Kim IL, Shenoy VB, et al. Cell-mediated fibre recruitment drives extracellular matrix mechanosensing in engineered fibrillar microenvironments. Nature materials 2015;14:1262.

[46] Yang MT, Sniadecki NJ, Chen CS. Geometric considerations of micro-to nanoscale elastomeric post arrays to study cellular traction forces. Advanced Materials 2007;19:3119-23.

[47] Pasapera AM, Schneider IC, Rericha E, Schlaepfer DD, Waterman CM. Myosin II activity regulates vinculin recruitment to focal adhesions through FAK-mediated paxillin phosphorylation. The Journal of cell biology 2010;188:877-90.

[48] Castner DG, Ratner BD. Biomedical surface science: Foundations to frontiers. Surface Science 2002;500:28-60.

[49] Richter H, Hormann H. Early and late cathepsin D-derived fragments of fibronectin containing the C-terminal interchain disulfide cross-link. Hoppe-Seyler's Zeitschrift fur physiologische Chemie 1982;363:351-64.

[50] Cai K, Frant M, Bossert J, Hildebrand G, Liefeith K, Jandt KD. Surface functionalized titanium thin films: zeta-potential, protein adsorption and cell proliferation. Colloids and Surfaces B: Biointerfaces 2006;50:1-8.

[51] Keselowsky BG, Collard DM, García AJ. Integrin binding specificity regulates biomaterial surface chemistry effects on cell differentiation. Proceedings of the National Academy of Sciences 2005;102:5953-7.

[52] Griffin M, Ibrahim A, Seifalian A, Butler P, Kalaskar D, Ferretti P. Chemical group-dependent plasma polymerisation preferentially directs adipose stem cell differentiation towards osteogenic or chondrogenic lineages. Acta biomaterialia 2017;50:450-61.

[53] Veiga AS, Sinthuvanich C, Gaspar D, Franquelim HG, Castanho MA, Schneider JP. Arginine-rich self-assembling peptides as potent antibacterial gels. Biomaterials 2012;33:8907-16.

[54] Baron EJ, Chang RS, Howard DH, Miller JN, Turner JA. Medical microbiology: a short course: Wiley-Liss; 1994.

[55] Alamanda M, Denthumdas SK, Wadgave U, Pharne PM, Patil SJ, Kondreddi S, et al. Comparative Evaluation of Ciprofloxacin Levels in GCF and Plasma of Chronic Periodontitis Patients: Quasi Experimental Study. Journal of clinical and diagnostic research: JCDR 2016;10:ZC47.

[56] Loo Y, Goktas M, Tekinay AB, Guler MO, Hauser CAE, Mitraki A. Self-Assembled Proteins and Peptides as Scaffolds for Tissue Regeneration. Advanced Healthcare Materials 2015;4:2557-86.

[57] Nultsch K, Germershaus O. Silk fibroin degumming affects scaffold structure and release of macromolecular drugs. European Journal of Pharmaceutical Sciences 2017;106:254-61.

[58] Chang P-H, Jiang W-T, Li Z, Jean J-S, Kuo C-Y. Antibiotic tetracycline in the environments—a review. Research & Reviews: Journal of Pharmaceutical Analysis 2015;4:86-111.

[59] Kogawa AC, Salgado HRN. Doxycycline hyclate: a review of properties, applications and analytical methods. Int J Life Sci Pharma Res 2012;2:11-25.

[60] Pascale D, Gordon J, Lamster I, Mann P, Seiger M, Arndt W. Concentration of doxycycline in human gingival fluid. Journal of clinical periodontology 1986;13:841-4.

[61] Gordon J, Walker C, Murphy J, Goodson J, Socransky S. Tetracycline: Levels Achievable in Gingival Crevice Fluid and in Vitro Effect on Subgingival Organisms: Part I. Concentrations in Crevicular Fluid After Repeated Doses. Journal of periodontology 1981;52:609-12.

9 Abkürzungen

ALP	Alkalische Phosphatase
BHI	Brain-Heart Infusion/ Gehirn-Herz-Infusionsmedium
CFU	Colony-Forming Units / Kolonie-Bildende Einheit
CX	Ciprofloxacin
DC	Dendritische Zellen
DH	Doxycyclin Hyclat
EZM	Extrazelluläre Matrix
FBS	Fetale Bovine Serum / fetales Rinderserum
HPDLF	Humane Periodontal Ligament Fibroblasten
HCO	Human Calvarial Osteoblast/ Humane Kalvaria Osteoblasten
HDFSC	Human dental follicle stem cells/ humane Zahnfollikel Stammzellen
HIV	Humanes Immundefizienz-Virus
IL	Interleukin
KDO	Keto-Desoxyocturonsäure
HPLC	High performance liquid chromatography/ Hochleistungsflüssigkeitschromatographie
LDH	Laktat Dehydrogenase
LPS	Lipopolysaccharid
MBK	Minimale Bakterizide Konzentration
MMP	Matrix-Metalloproteinase

MIC	Minimal inhibitory concentration/ Minimale Hemm-Konzentration
MS	Massenspektroskopie
MSC	Mesenchymale Stammzellen
OD	Optische Dichte
OCL	Osteoklasten
OCP	Osteoklasten Vorläuferzellen
P. gingivalis	Porphyromonas Gingivalis
ROS	Reaktive Oxygen/Sauerstoff Spezies
RGD	Aminosäuresequenz (Arginin, Glycin, Asparaginsäure)
RT	Raumtemperatur
REM	Rasterelektronenmikroskopie
RANKL	Rezeptor Aktivator von NF-κB Ligand
S. sanguinis	Streptococcus Sanguinis
SSP	Selbst-Strukturierende Peptide
TC	Tetracyclin
TCPS	Tissue Culture Polystysrene/Gewebekultur Polystyrol
TNF	Tumor-Nekrose-Faktor
Th	T-Helferzellen
TEM	Transmission-Elektronen-Mikroskopie
WHO	World Health Organization/Weltgesundheitsorganisation

Danksagung

Meinen tief empfundenen Dank möchte ich meiner Doktormutter, PD Dr. Kirsten Peters, für ihre enorme Unterstützung und Betreuung während meiner ganzen Dissertation aussprechen. Ich hätte mir nie eine bessere Doktormutter vorstellen können, welche geduldiger und mitfühlender mit ihrer Doktorandin umgegangen ist. Vielen Dank, dass du mir geholfen hast, meine rote Linie in jeder Veröffentlichung und für jede Experimentreihe zu finden. Ich schätzte am meisten unsere wertvollen und effizienten Gespräche, die mich meiner Verteidigung schrittweise immer wieder ein Stück näher gebracht haben und mich auch in schlechten Zeiten immer wieder weiter motiviert haben.

Mein herzlicher Dank gilt auch meinem zweiten Betreuer Prof. Dr. Bernd Kreikemeyer, der mich auf meinem steinigen Doktoratsweg jederzeit mit Herzblut beraten, unterstützt und motiviert hat. Ohne unser schönes Flipchart Diagramm hätte ich meine mikrobiologischen Experimente nie so schnell, strukturiert und zielführend durchführen können. Vielen Dank, dass du mich immer mit deinem Team und deinen Ressourcen bestmöglich unterstützt hast.

Ich möchte mich auch bei meiner dritten Betreuerin Dr. Sina Saxer herzlichst bedanken, die immer an mich geglaubt hat und mich gelehrt hat, eine gute Wissenschaftlerin und eine starke Frau zu werden. Ich werde nie vergessen wie man eine Wendy-Geschichte in eine wissenschaftliche Publikation umschreibt :)

Vielen Dank auch an Prof. Dr. Uwe Pieles, der mir die Möglichkeit gab, an einem so wertvollen und erfolgreichen Projekt mitzuwirken und mich anhand dieses Projektes persönlich als auch fachlich stark weiterzuentwickeln. Vielen Dank, dass ich ein Mitglied der liebevollen Nanoteam-Familie sein durfte.

Ich möchte mich auch zu tiefst bei all meinen lieben Kolleginnen und Kollegen aus der Rostocker Zellbiologie-Gruppe (Anne Wolff, Katharina Ekat, Juliane Meyer, Nina Gehm, Olga Hahn, Susanne Stählke, Caroline Mörke, Henrike Rebl, Petra Müller, Petra Seidel, Claudia Bergemann) für ihre Freundschaft, ihren Rat und ihre Hilfsbereitschaft im Labor bedanken.

Danke auch, dass ihr mich als Vollmitglied in eurer freundlichen Gruppe aufgenommen habt und mir die schöne Seite von Rostock gezeigt habt. Vielen Dank auch für die vielen tollen und lustigen privaten Stunden, welche wir zusammen verbracht haben. Jetzt weiss ich was es bedeutet, einen "Sturmsack" zu essen, einen "Pfeffi-Schnaps" zu trinken und welche Vorteile der Studentenkeller haben kann :).

Vielen Dank auch an meine großartigen Kollegen aus der Nanotechnologie-Gruppe in Muttenz (Lucy Kind, Theodor Bühler, Lena Mungenast, Joachim Köser, Markus Waser, Christelle Retard-Jarcot, Floriana Burgio) für die technische und emotionale Unterstützung in jeder Situation. Vielen Dank für das freundliche Arbeitsklima, aber auch für die wertvollen Gespräche und die Unterstützung bei unseren Laborbesprechungen.

Ein grosses und herzliches Dankeschön gilt auch dem Credentis-Team, insbesondere Michael Hug und Dominik Lysek, welche mich seit Tag 1 meines PhD's in jeder Lebenslage begleitet und unterstützt haben. Ich hätte mir nie vorstellen können, dass ein Industrie-Partner mit so viel Leidenschaft, Hilfsbereitschaft und Freundschaft einen PhD Studenten betreuen kann. Vielen Dank, dass ihr immer für mich da wart und ich euch zu jederzeit anrufen konnte.

Last but not least ein großes Dankeschön an meine grossartige Familie, insbesondere an meine geliebten Eltern. Vielen Dank für ihre Liebe, Unterstützung, Energie, offene Arme und Ohren zu jederzeit und an jedem Ort. Ohne euch hätte ich die Besteigung des «PhD» Mount Everest bis an die Spitze des Berges nicht erreicht. Mein aufrichtiger und tiefster Dank gilt auch meinem Ehemann Marko Rudi Koch, der mich immer in allen Höhen und Tiefen in dieser Zeit begleitet hat und mich nie aufgeben liess mein Ziel zu erreichen. Ich danke dir für all die Liebe die du in mein Leben gebracht hast. Du bist mein Fels in der Brandung. Ich freue mich riesig auf unsere neue Herausforderung als Eltern und auf die gemeinsame Zeit mit unserer Tochter.

Lebenslauf

Persönliche Daten

Name	Franziska Koch
Geburtsdatum	02.05.1988
Staatsbürgerschaft	Deutsch
Familienstand	Verheiratet

Berufliche Tätigkeit

03.2019 – heute	**Gleichstellungsbeauftragte** Fachhochschule Nordwestschweiz, Hochschule für Life Sciences
01.2018 – heute	**Wissenschaftliche Mitarbeiterin** Fachhochschule Nordwestschweiz (FHNW Muttenz) Hochschule für Life Sciences, Institut für Chemie und Bioanalytik, Abteilung für Nanomaterialien und Oberflächen

Ausbildung

09/2013 – heute	**Promotionsstudentin der Medizinwissenschaft** Universitätsmedizin Rostock, AB Zellbiologie
09/2015 – 08/2017	**Diplom-Studiengang für Pharmazeutische Wissenschaften** Europäisches Zentrum für Pharmazeutische Wissenschaften, Universität Basel
09/2011 – 06/2013	**Master Studium mit Schwerpunkt in Molekularer Technologie** Fachhochschule Nordwestschweiz (CH) Abschluss: Master of Science **Masterarbeit an der Universität in Bern (Vetsuisse Fakultät)** Thema: Zytotoxizität und Verteilung von Nanopartikel in neuronalen Zellen und im Rattengehirn

04/2011 – 05/2011	**Innovations-und Networking Workshop in Amerika** Business Management School der FHNW, Olten
09/2008 – 08/2011	**Bachelor Studium mit Schwerpunkt in molekulare Bioanalytik** Fachhochschule Nordwestschweiz (CH) Abschluss: Bachelor of Molecular Life Science

Veröffentlichungen

An in vitro toxicity evaluation of gold-, PLLA- and PCL-coated silica nanoparticles in neuronal cells for nanoparticle-assisted laser-tissue soldering

Toxicology in Vitro. 2014;28(5):990-8

Franziska Koch, Anja M. Möller, Martin Frenz, Uwe Pieles, Kathrin Kuehni Boghenbor, Meike Mevissen

Self-assembling peptide hydrogels with adjustable physical properties for tissue specific microenvironments

Royal Society Open Science. 2018; 5(3):171562

Franziska Koch, Michael Müller, Finja König, Nina Meyer, Jasmin Gattlen, Uwe Pieles, Kirsten Peters, Bernd Kreikemeyer, Stephanie Mathes, Sina Saxer

Amino acid composition of nanofibrillar self-assembling peptide hydrogels scaffolds affects responses of periodontal tissue cells in vitro

Journal of International Nanomedicine. 2018;13: 6717-6733

Franziska Koch, Anne Wolff, Stephanie Mathes, Uwe Pieles, Sina Saxer, Bernd Kreikemeyer, Kirsten Peters

A versatile biocompatible antibiotic delivery system based on self-assembling peptides with antimicrobial and regenerative potential

Journal of Advanced Healthcare Materials. 2019, 1900167

Franziska Koch, Katharina Ekat, David Kilian, Timm Hettich, Oliver Germershaus, Stephanie Mathes, Uwe Pieles, Sina Saxer, Bernd Kreikemeyer, Kirsten Peters

An organotypic in vitro model of the periodontal ligament for the evaluation of viscous biomaterials

Submitted to Journal of BMC oral health

Franziska Koch, Nina Meyer, Silvio Valdec, Ronald E. Jung, Stephanie Mathes

Patent: Composition comprising self-assembling peptides for use in treatment of gingivitis, periodontitis and/or peri-implantitis

Inventors: Michael Hug, Dominik Lysek, Franziska Koch, Uwe Pieles, Nina Meyer, Stephanie Mathes, Ronald Jung

Konferenzen

10/2015	**WCRM (world conference of regenerative medicine) Leipzig** Presentation: A new light comes up in periodontal therapy- Self-assembling-peptides and their physicochemical impact on hard and soft tissue cells

08/2015	**ESB (European society of Biomaterials) Krakow** Poster: Matrix design of self-assembled peptide hydrogels for hard and soft tissue engineering
06/2015	**SSB (Swiss Society of Biomaterials) Lausanne** Poster: Controlled matrix stiffness through self-assembled peptides and their effect on osteoblast like cell morphology and proliferation
09/2014	**ESB (European society of Biomaterials) Liverpool** Poster: Characterization of network and self-assembling process of a short sequence peptide for biomimetic therapy

Weitere Kenntnisse

Fremdsprachen	Deutsch (Muttersprache), Englisch (First Certificate, Cambridge)
Software	MS-Office, Adobe Photoshop/ Indesign/Illustrator, Graphpad

Basel, 22.07.2019

Ort, Datum Unterschrift